

Impact of the sea surface temperature in the north-eastern tropical Atlantic on precipitation over Senegal

Mamadou Thiam¹, Ludivine Oruba², Gaelle De Coetlogon³, Malick Wade¹, Bouya Diop¹, and Abdou Karim Farota¹

¹Université Gaston Berger

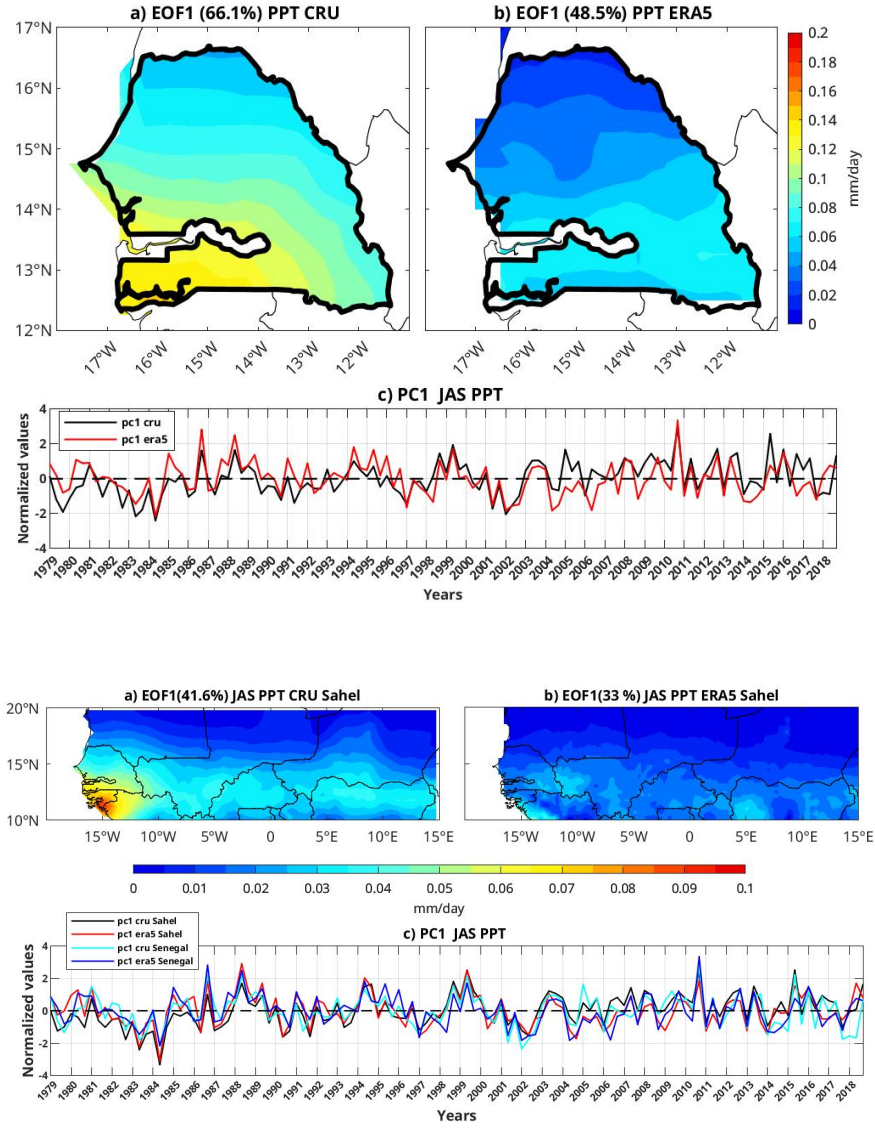
²Sorbonne Université

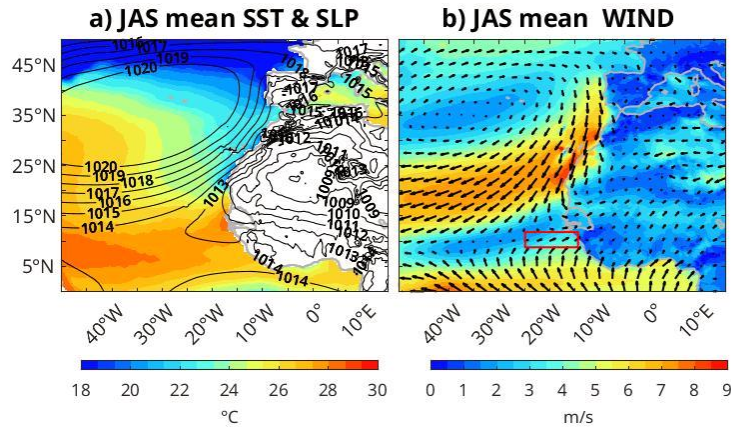
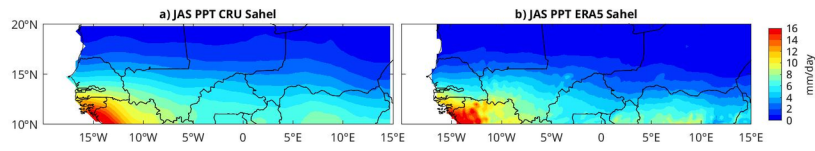
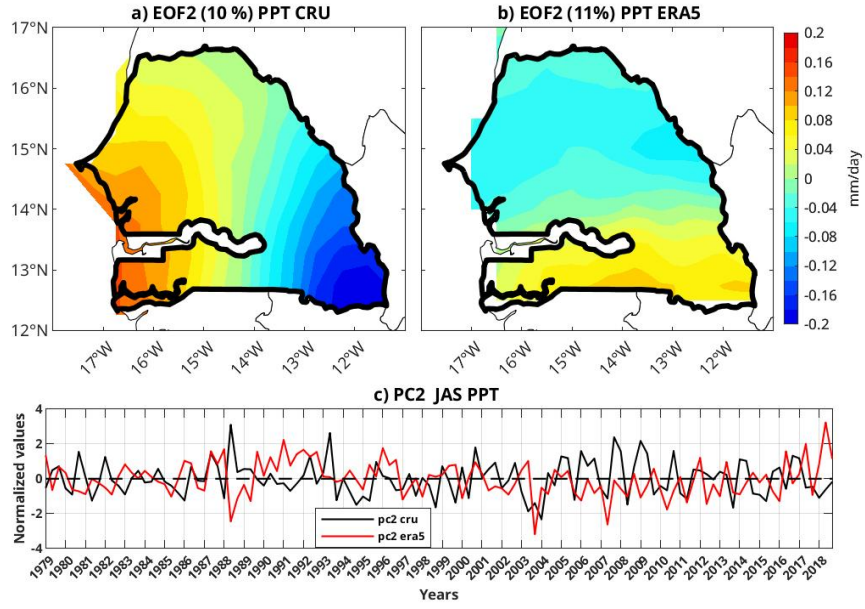
³Sorbonne Université

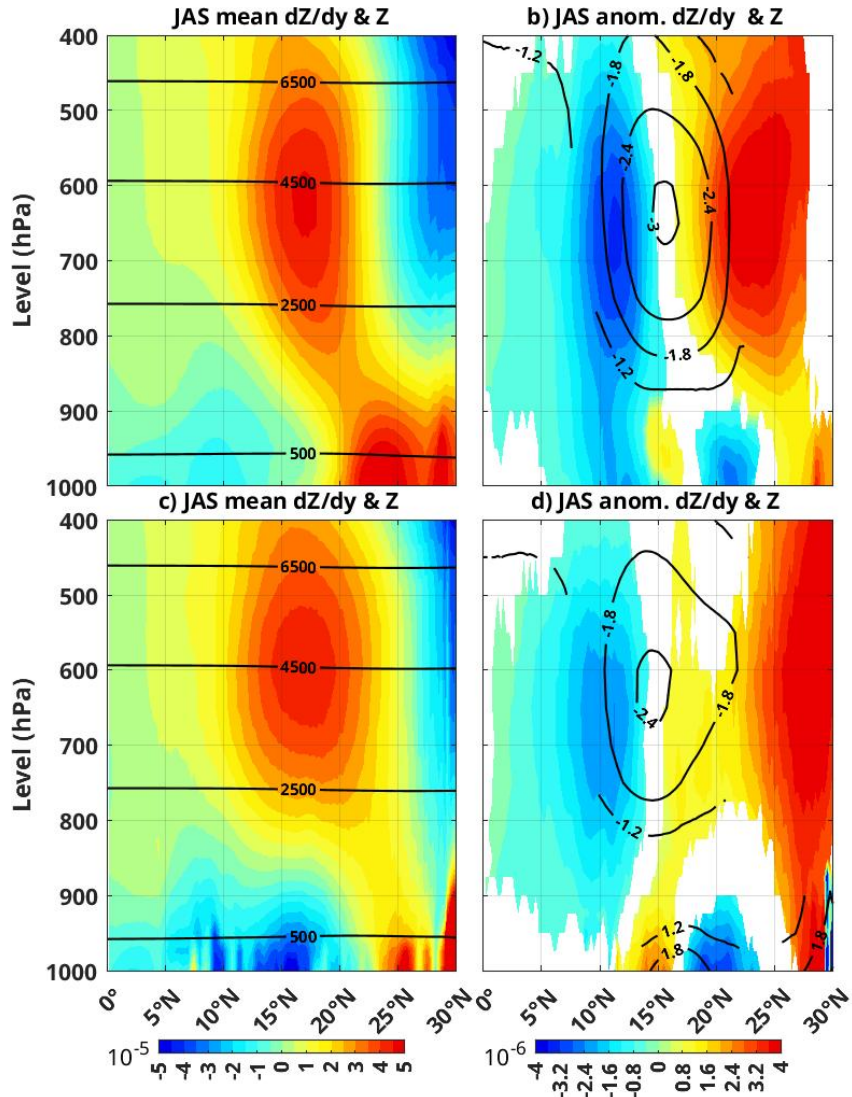
December 3, 2023

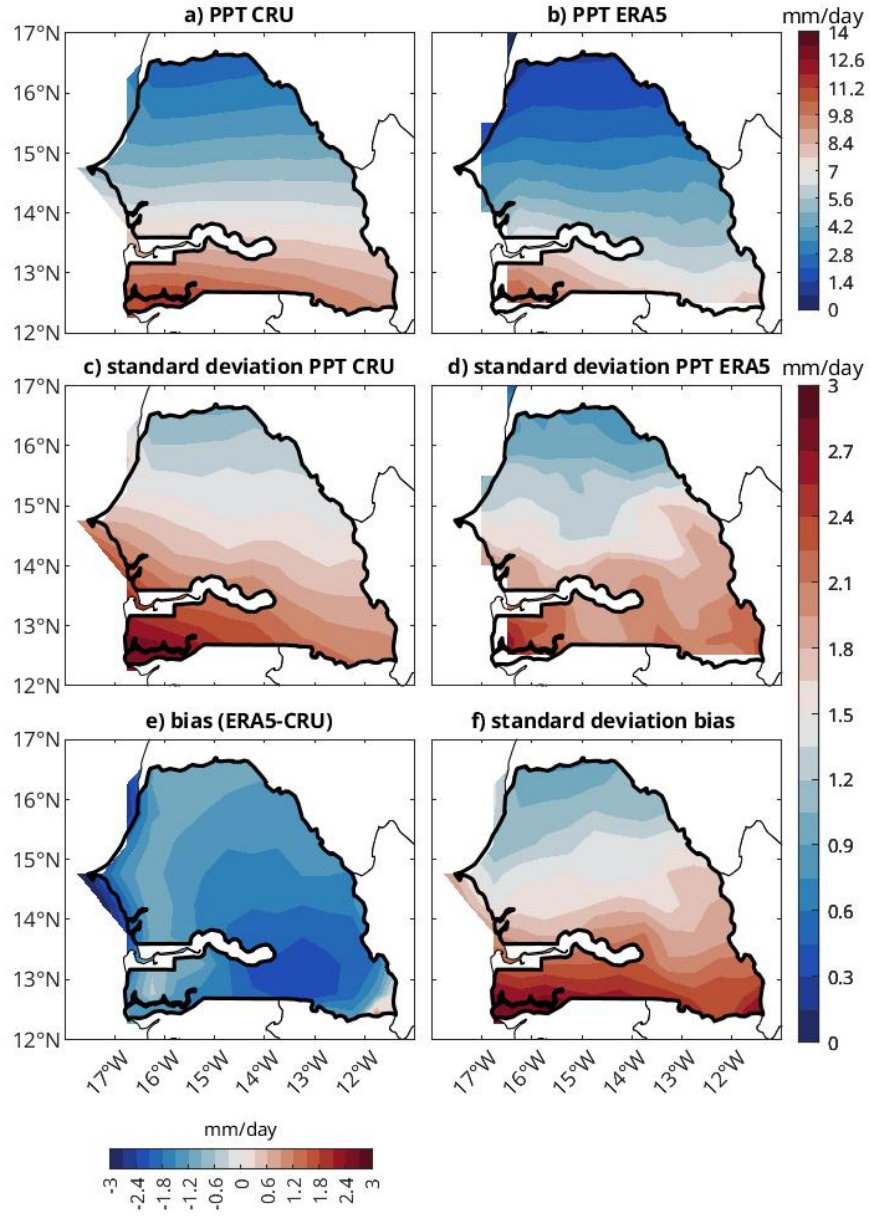
Abstract

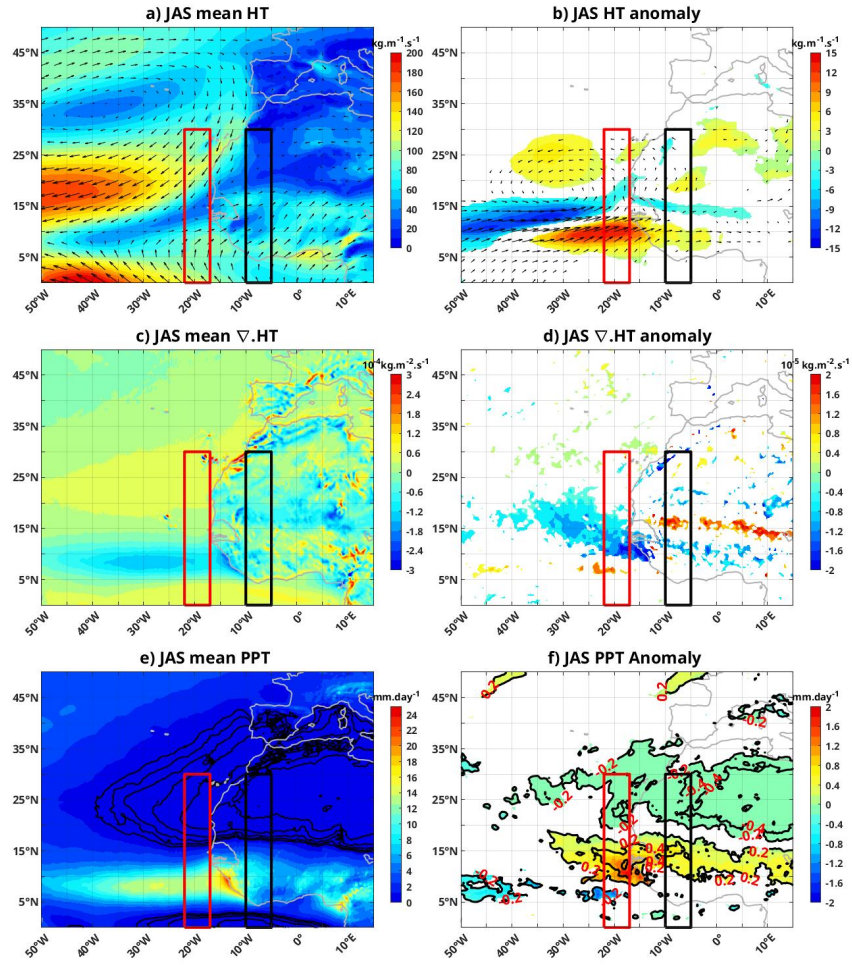
This study examines 40 years of monthly precipitation data in Senegal (1979-2018) using CRU observations and ERA5 re-analyses, aiming to understand the influence of oceanic and atmospheric factors on Senegal's precipitation in July, August and September (JAS). Comparing Senegal's precipitation variability with the broader Sahel region, it emerges that Senegal's precipitation is more closely associated with the Northeastern Tropical Atlantic (NETA) Sea Surface Temperature (SST). The increased Senegal's precipitation is linked to the northward shift of the InterTropical Convergence Zone (ITCZ), consistent with numerous previous studies. Over the continent, this shift corresponds to a northward shift of the African Easterly Jet (AEJ) and, consequently, the Mesoscale Convective Systems responsible for most precipitation. It seems primarily driven by the northward shift of the Heat Low. Over the ocean west of Senegal, there is a comparable shift of the AEJ, accompanied by increased low-level moisture transport convergence within the West African Westerly Jet (WAWJ). This phenomenon is triggered by a negative pressure anomaly in the NETA, located above a positive SST anomaly: we suggest that the latter is the origin of the former, forming a feedback mechanism that potentially significantly influences Senegal's precipitation. The mechanism involves a geostrophic adjustment of the WAWJ to the southern gradients of the SST anomaly. To validate the NETA SST feedback's role in Senegal's precipitation, further investigations using daily data or regional atmospheric models are recommended. The findings hold potential for enhancing seasonal forecasting capabilities.

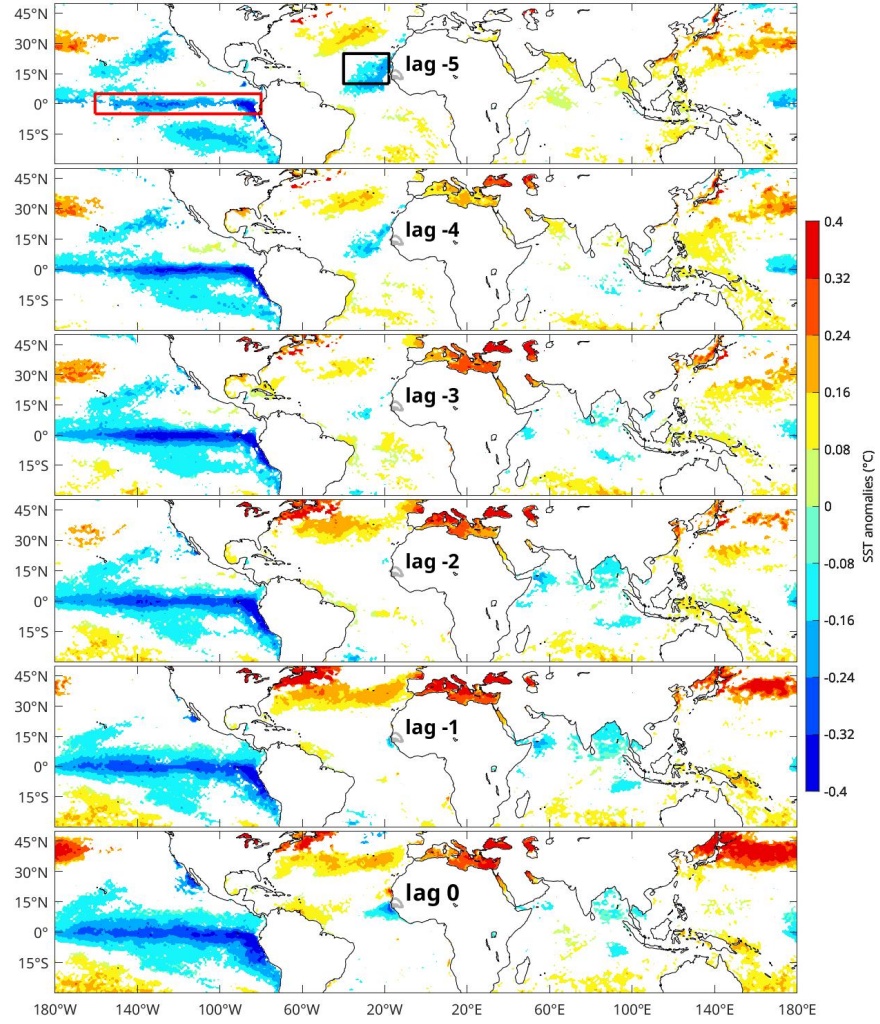


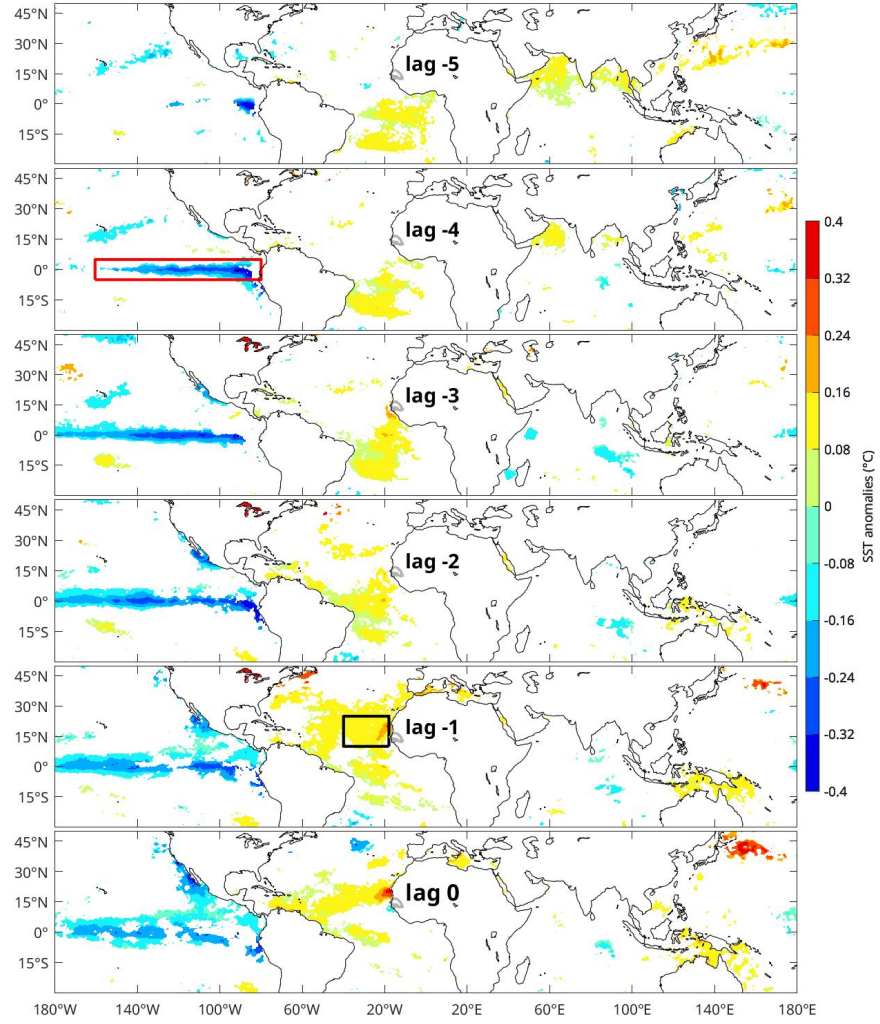


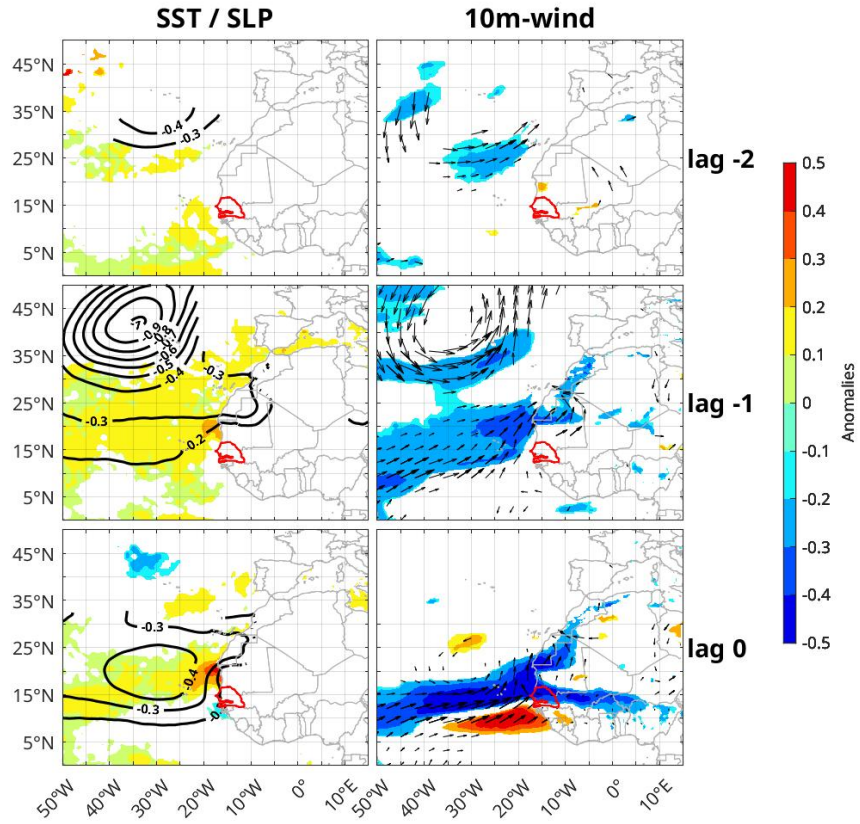


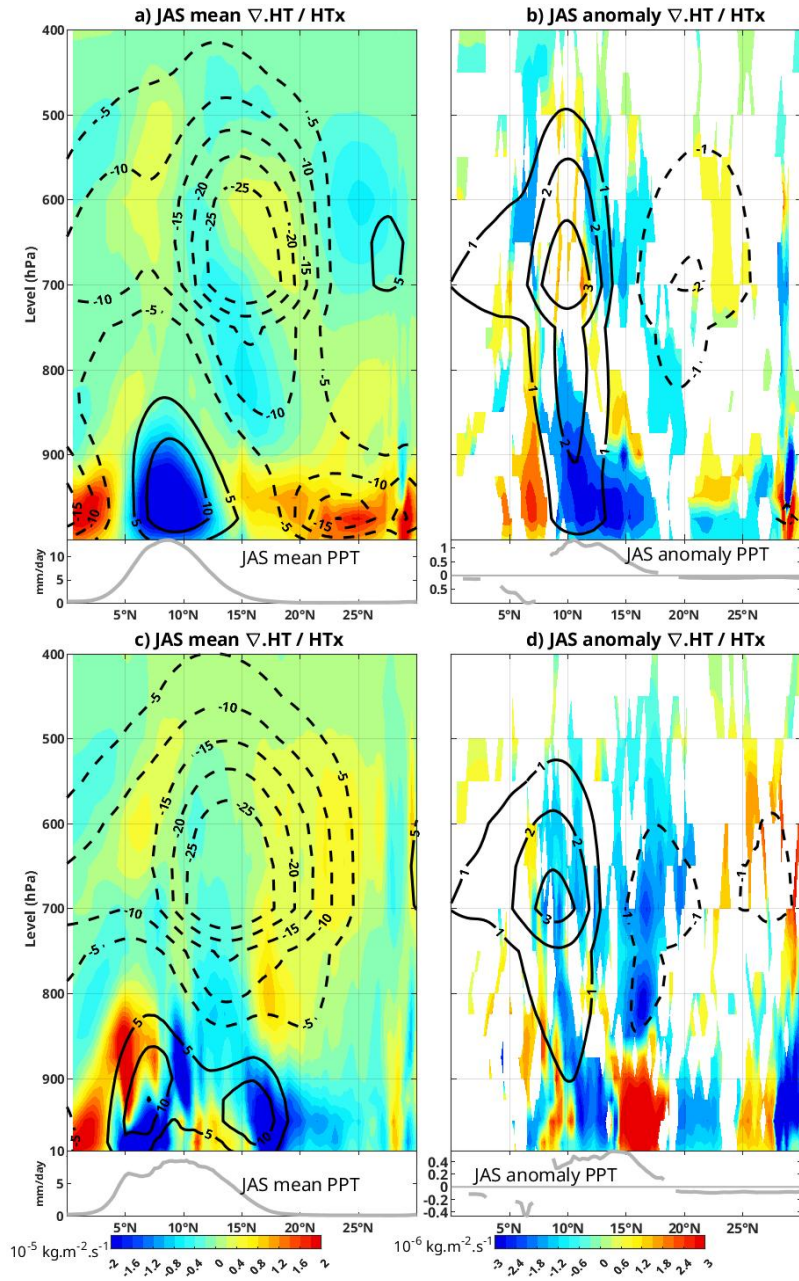












1 **Impact of the sea surface temperature in the**
2 **north-eastern tropical Atlantic on precipitation over**
3 **Senegal**

4 **Mamadou Thiam^{1,2}, Ludivine Oruba², Gaelle de Coetlogon², Malick Wade¹,**
5 **Bouya Diop¹, Abdou Karim Farota¹**

6 ¹Laboratoire des Sciences de l'Atmosphère et des Océans – Matériaux, Énergie et Dispositifs
7 (LSAO-MED), Université Gaston Berger, Saint-Louis, Sénégal

8 ²Laboratoire Atmosphère et Observations Spatiales (LATMOS), Sorbonne Université, Paris, France

9 **Key Points:**

- 10 • Wet summers in Senegal are preceded by La Niña events and warming in the Mediter-
11 ranean but also by warming in the Northeastern Tropical Atlantic
12 • Moisture transport convergence within a stronger West African Westerly Jet (WAWJ)
13 explains this increase in precipitation
14 • Feedback between the North Tropical Atlantic surface temperature and atmospheric
15 pressure is proposed to explain this WAWJ acceleration

Corresponding author: Mamadou Thiam, thiam.mamadou9@ugb.edu.fr

16 **Abstract**

17 This study examines 40 years of monthly precipitation data in Senegal (1979-2018)
 18 using CRU observations and ERA5 reanalyses, aiming to understand the influence of oceanic
 19 and atmospheric factors on Senegal’s precipitation in July, August and September (JAS).
 20 The variability of Senegal’s precipitation is first compared with that of the broader Sa-
 21 hel region: although they share a significant portion of their variance, Senegal appears
 22 more closely related to the Northeastern Tropical Atlantic (NETA) Sea Surface Temper-
 23 ature (SST). A detailed examination of this region reveals that Senegal’s increased pre-
 24 cipitation is linked to the northward shift of the InterTropical Convergence Zone (ITCZ),
 25 consistent with numerous previous studies. Over the continent, this shift corresponds
 26 to a northward shift of the African Easterly Jet (AEJ) and, consequently, the Mesoscale
 27 Convective Systems responsible for most precipitation. It seems primarily driven by the
 28 northward shift of the Heat Low. Over the ocean just west of Senegal, there is a com-
 29 parable shift of the AEJ, accompanied by an increase in low-level moisture transport con-
 30 vergence within the West African Westerly Jet (WAWJ) which explains the majority of
 31 the increase in JAS precipitation in Senegal. This phenomenon is triggered by a nega-
 32 tive pressure anomaly in the NETA, located above a positive Sea Surface Temperature
 33 (SST) anomaly: we suggest that the latter is the origin of the former, forming a feed-
 34 back mechanism that potentially significantly influences Senegal’s precipitation. The mech-
 35 anism involves a geostrophic adjustment of the WAWJ to the southern gradients of the
 36 SST anomaly. Further investigations utilizing daily data or regional atmospheric mod-
 37 els are necessary to validate the role of NETA SST feedback on Senegal’s precipitation,
 38 with potential benefits for enhancing seasonal forecasting capabilities.

39 **Plain Language**

40 This study, spanning 40 years of monthly precipitation data in Senegal, explores
 41 the intricate relationship between oceanic and atmospheric factors shaping precipitation
 42 patterns from July to September. The increased summertime precipitation in the West-
 43 ern Sahel is primarily of continental origin, associated with the northward shift of mesoscale
 44 convective systems linked to lower pressure in the Sahara. However, over the ocean west
 45 of Senegal, there is also an increase in inland moisture transport that explains a signif-
 46 icant part of the intensified precipitation from July to September in Senegal. This trans-
 47 port is reinforced by a low-pressure system over the ocean, potentially caused by warmer
 48 sea surface temperatures between 10°N and 20°N off West Africa. This close connection
 49 between Senegal’s precipitation and ocean surface temperature in the Northeastern Trop-
 50 ical Atlantic could help enhance crucial seasonal forecasts for agricultural planning, the
 51 economy, and food security in West Africa.

52 **1 Introduction**

53 The study of Sahel’s rainfall variability is crucial due to its vulnerability to climate
 54 change. Accurate forecasts are vital for managing water resources, agriculture, and health
 55 (Sultan et al., 2005; Grace & Davenport, 2021). This semi-arid region, experiences most
 56 of its precipitation from July to September (JAS). During this period, a zonal rain belt
 57 spans from approximately 5°N to 15°N across West Africa, shifting southward the rest
 58 of the year (Parker & Diop-Kane, 2017). The summer rains are primarily attributed to
 59 mesoscale convective systems (MCSs), with up to 95% originating above the eastern high-
 60 lands and crossing East to West Africa within one or two days (Nicholson, 2013). These
 61 systems form due to the African Easterly Jet (AEJ)’s presence in the mid-troposphere,
 62 particularly its southern half, with strong horizontal vorticity facilitating barotropic and
 63 baroclinic instabilities (Parker & Diop-Kane, 2017).

64 This zonal band of precipitation experiences strong year-to-year and even decadal
 65 variations between 10°N and 15°N. For instance, an exceptionally severe drought occurred
 66 in the 1980s (Le Barbé & Lebel, 1997). Various mechanisms have been identified to ex-
 67 plain this extensive variability, including the land-atmosphere-ocean system and changes
 68 in atmospheric circulation patterns and weather systems behavior in West Africa dur-
 69 ing the rainy season (Zeng et al., 1999; Nicholson & Palao, 1993; Vizy & Cook, 2001).
 70 Nevertheless, numerous studies highlight the pivotal role of global sea surface temper-
 71 ature (SST) such as the Indian Ocean warming (Hagos & Cook, 2008), which influences
 72 the African monsoon through atmospheric teleconnections through modifications in Walker
 73 cells intensity, or equatorial atmospheric Kelvin and Rossby waves (Wang, 2019). Strong
 74 correlations have indeed been observed between Sahel precipitation and remote SST at
 75 interannual timescales in the Pacific equatorial region (Janicot et al., 2001; Joly & Voldoire,
 76 2009; Diatta & Fink, 2014; Gomara et al., 2017), in the Mediterranean Sea (Rowell, 2003;
 77 Jung et al., 2006; Polo et al., 2008; Fontaine et al., 2009; Diakhate et al., 2019; Worou
 78 et al., 2020), or in the Indian Ocean (Bader & Latif, 2003; Biasutti et al., 2008; Mohino
 79 et al., 2011; Caminade & Terray, 2010).

80 Sahel rainfall variability may also be influenced by coupled regional dynamics in
 81 the Tropical Atlantic (Camberlin et al., 2001; Polo et al., 2008). At interannual timescales,
 82 the SST in the Gulf of Guinea is influenced by an equatorial ocean-atmosphere coupled
 83 mode known as the "zonal mode" or Atlantic Niño (Zebiak, 1993; Cabos et al., 2019),
 84 subsequently affecting precipitation along the Guinea Coast (Meynadier et al., 2016; Polo
 85 et al., 2008; de Coëtlogon et al., 2010, 2014) and, seemingly, in the Sahel (Caniaux et
 86 al., 2011; Steinig et al., 2018; Janicot et al., 1998; Vizy & Cook, 2001; Losada et al., 2010).
 87 Regarding the North Tropical Atlantic, Mo et al. (2001) and Ward (1998) suggested that
 88 NETA SST does not significantly influence West African rainfall. Using a general cir-
 89 culation model, Vizy and Cook (2001) also concluded that precipitation over West Africa
 90 is generally insensitive to NETA SST anomalies. In the other hand, Camberlin and Diop
 91 (1999) found that precipitation in Senegal is more sensitive to climatic anomalies in the
 92 northern Tropical Atlantic than in the rest of the Sahel over the period 1960-1990. More-
 93 over, Fall et al. (2006) found that precipitation over Senegal is well correlated with North
 94 Tropical Atlantic SST from January to May. The role of NETA SST in relation to Sa-
 95 hel precipitation remains therefore unclear, especially for western Sahel. However, Sa-
 96 hel precipitation in summer is strongly linked to the latitude of the intertropical conver-
 97 gence zone (Camberlin et al., 2001; Nicholson, 2013), and the latter could be tied to the
 98 zonal band of maximum SST in the Tropical Atlantic (Diakhaté et al., 2018): when the
 99 SST in the Northeastern Tropical Atlantic (NETA) is warmer than those further south,
 100 the ITCZ migrates northward, leading to positive rainfall anomalies observed in the Sa-
 101 hel (Xie & Carton, 2004; Gu & Adler, 2009; Gu, 2010; Janicot et al., 2001; Biasutti et
 102 al., 2008). It therefore appears important to clarify whether NETA SST has an impact
 103 on Sahel precipitation, carefully distinguishing between Senegal (Western Sahel) and Cen-
 104 tral Sahel.

105 The primary objective of this paper is to build a robust index of Senegal precip-
 106 itation for monitoring its variability based on observations. It then briefly revisits tele-
 107 connections between global SST and precipitation on interannual timescales with a par-
 108 ticular focus on Senegal specifically, in contrast to the broader Sahel region as commonly
 109 done in previous research. Subsequently, we delve deeper into the NETA signatures of
 110 SST, Sea Level Pressure (or SLP), wind fields, and low-level moisture transport anoma-
 111 lies: we discuss their influence on Senegal's precipitation patterns and consider the po-
 112 tentiel role of a regional SST feedback mechanism on precipitation in West Africa. The
 113 paper is divided as follows: Section 2 describes the data and the methods, Section 3 presents
 114 the building of the index, Section 4 discusses the signals found in global SST, Section
 115 5 focuses on the NETA SST and near-surface dynamics, Section 6 discusses the mois-
 116 ture transport and precipitation, Section 7 proposes a mechanism for the SST influence
 117 on the WAWJ, and Section 8 concludes the study.

2 Data and methods

2.1 Data

The present study relies on the Climatic Research Unit (CRU) Time-series (TS). The CRU TS dataset was originally created and subsequently updated by the UK Natural Environment Research Council (NERC) and the US Department of Energy. In this paper, we utilized Version 4.03 of the CRU TS dataset, which spans the period from 1901 to 2018 at a high resolution of $0.5^\circ \times 0.5^\circ$. Monthly averaged precipitation data for the mainland, covering the period from 1979 to 2018, were acquired from various weather services and other sources.

CMWF Reanalysis v5 (ERA5) data are employed in this study to monitor the atmospheric dynamics associated with Senegal precipitation fluctuations. ERA5 is produced by the Copernicus Climate Change Service (C3S) and incorporates data assimilation, combining model data with observations from worldwide sources. It provides estimates for numerous atmospheric, terrestrial, and oceanic climate variables from 1979 to the present day, with a horizontal grid resolution of $0.25^\circ \times 0.25^\circ$ and 37 vertical levels ranging from 1000 to 1 hPa and we also use monthly average data. Global SST data from ERA5 are used to identify global teleconnections with precipitation. These SST data are based on the Hadley Centre Sea Ice and Sea Surface Temperature dataset version 2 (HadISST2) from 1979 to August 2007 and the Office Operational Sea Surface Temperature and Sea Ice Analysis (OSTIA) daily product from September 2007 to the present. These SST datasets closely align with the Reynolds observation product (Yang et al., 2021).

The atmospheric parameters used in this study are SLP, zonal (u) and meridional wind (v) at 10 meters above the surface, and at the available pressure levels in ERA5. Additionally, geopotential height (Z) and specific humidity (q) are also used. Wind speed ($\sqrt{u^2 + v^2}$) is treated as an additional parameter: we calculate its monthly seasonal anomalies separately from the zonal and meridional components. Linear regressions of wind speed anomalies hence indicate whether the wind anomalies correspond to a weaker (negative anomalies) or stronger (positive) wind speed in comparison to the average.

2.2 Linear statistical tools

The calculation of monthly seasonal anomalies is conducted over the 40-year period from 1979 to 2018 for all parameters. Anomalies are determined by subtracting the seasonal cycle, computed by averaging the values for each month over the 1979-2018 period. Additionally, to remove long-term periodicities (decadal and beyond), a quadratic trend computed over the 480 monthly anomalies is removed from these anomalies in all parameters.

Empirical Orthogonal Function (EOF) decomposition are performed in both the CRU and ERA5 precipitation anomalies in JAS over Senegal in section 3. The Principal Components (PCs) represent the eigenvectors of the estimated covariance matrix. Following the approach outlined in Von Storch and Zwiers (1999), the spatial patterns, also known as EOFs, correspond to the linear regression of the JAS anomalies on the PCs as described just below.

Given an independent, identically distributed sample of random parameters X_i and Y_i for $i = 1$ to $n = 120$ (i.e. 40 years times 3 months), the correlation is computed

with the following maximum likelihood estimator:

$$\hat{R} = \frac{\sum_{i=1}^n (X_i - \bar{X})(Y_i - \bar{Y})}{\sqrt{\left(\sum_{i=1}^n (X_i - \bar{X})^2\right) \left(\sum_{i=1}^n (Y_i - \bar{Y})^2\right)}} \quad (1)$$

Here, $\bar{X} = \frac{1}{n} \sum_{i=1}^n X_i$ and $\bar{Y} = \frac{1}{n} \sum_{i=1}^n Y_i$ are estimators of the variables means. Subsequently, we apply the least squares estimate of the slope of the simple linear regression, as described in Von Storch and Zwiers (1999):

$$\hat{a} = \frac{\sum_{i=1}^n (X_i - \bar{X})(Y_i - \bar{Y})}{\sqrt{\sum_{i=1}^n (X_i - \bar{X})^2}} \quad (2)$$

159 The resulting \hat{a} field represents the variation of Y associated with a fluctuation of
 160 one standard deviation of X . For example, if (X_i) represents the normalized PC1CRU
 161 index, and (Y_i) represents the SST, \hat{a} indicates the change in SST anomalies (in °C) as-
 162 sociated with a one-standard deviation increase in the precipitation index. This result-
 163 ing field is typically referred to as the SST anomaly obtained from the regression of SST
 164 on the precipitation index. Note that all descriptions in this study pertain to positive
 165 values of this index, reflecting anomalies associated with higher-than-average JAS pre-
 166 cipitation in Senegal. However, we could have chosen to describe opposite anomalies (i.e.,
 167 related to a dry summer) without altering the interpretation of our results.

168 Moreover, we employ the unbiased estimator $\sigma(X) = \sqrt{\frac{1}{n-1} \sum_{i=1}^n X_i^2}$ to calculate
 169 the standard deviation of a random variable X based on a sample of n values. By con-
 170 sidering X_i as the July anomalies, Y_i as the August anomalies and Z_i as the Septem-
 171 ber anomalies, we proceed to estimate the typical interannual anomaly (i.e., averaged
 172 over the entire JAS season) as follows:

$$\sigma_{interannual} = \sqrt{\frac{1}{N-1} \sum_{i=1}^N XYZ_i^2}$$

173 where $N = 40$ years and $XYZ_i = \frac{X_i+Y_i+Z_i}{3}$ is the yearly anomaly in JAS, whereas
 174 the intraseasonal signal, representing the typical monthly anomaly within each JAS sea-
 175 son (independently of the variations between the different JAS averages), is estimated
 176 as follows:

$$\sigma_{intraseasonal} = \sqrt{\frac{1}{3N-1} \sum_{i=1}^N (X_i - XYZ_i)^2 + (Y_i - XYZ_i)^2 + (Z_i - XYZ_i)^2}$$

177 Finally, to distinguish meaningful correlations from chance occurrences, a p-value
 178 of 0.05 (95% confidence level) is chosen, indicating a one-in-twenty probability that a cor-
 179 relation exceeds the threshold by pure coincidence. The determination of this thresh-
 180 old depends on the number of independent data points in the time series. In this study,
 181 we allocate one degree of freedom per month, having verified that the three monthly data
 182 points per year are uncorrelated in the reference time series (PC1CRU, defined in sec-
 183 tion 3). The correlation between July and August anomalies is indeed 0.16, and 0.21 be-
 184 tween August and September, both well below the significant correlation threshold of

185 0.31 with 40 degrees of freedom, ensuring the independence of the 120 monthly values.
 186 With a degree of freedom of 120, the 95% confidence level for correlation yields the thresh-
 187 old of 0.18: only linear regression values with correlations exceeding this value are de-
 188 picted in the following figures or discussed in the text as either "positive anomalies" or
 189 "negative anomalies."

190 2.3 Moisture transport and divergence

We calculate moisture transport using specific humidity (q) and horizontal winds $\mathbf{U} = (u, v)$. At each pressure level, moisture transport is computed as $q \cdot \mathbf{U}$. To integrate this calculation from p_b to p_t , we apply a weight factor to each pressure level, dP/g . This factor corresponds to the mass per unit area of the respective pressure interval (i.e., ρdz , where ρ represents the air density) using the hydrostatic approximation ($dp = -\rho g dz$):

$$\mathbf{HT} = \frac{1}{g} \int_{p_b}^{p_t} q \cdot \mathbf{U} \cdot dp \quad (3)$$

191 The result gives the integrated moisture transport between p_b and p_t in $kg \cdot m^{-1} \cdot s^{-1}$

192 The horizontal divergence of the moisture transport is calculated at each pressure
 193 level by using a centered scheme on the zonal and meridional components HT_x and HT_y
 194 as follows:

$$\nabla \cdot \mathbf{HT}(i, j) = \frac{HT_x(i+1, j) - HT_x(i-1, j)}{2 \delta x} + \frac{HT_y(i, j+1) - HT_y(i, j-1)}{2 \delta y} \quad (4)$$

195 where i and j are the indices of the gridpoints, and δx and δy are the zonal and merid-
 196 ional lengths of the gridpoints.

197 3 JAS precipitation index for Senegal

198 The highest rainfall in Senegal is observed during July, August and September (JAS),
 199 with the peak occurring in August. In the other quarters (not shown), it decreases to
 200 approximately 10-30% of this peak, consistent with prior research (Rowell et al., 1995;
 201 Sultan & Janicot, 2000; Grist & Nicholson, 2001; Lebel et al., 2003; Fall et al., 2006).
 202 JAS averages are presented for both the CRU observation-based data product (Figure
 203 1a) and ERA5 reanalyses (Figure 1b). Both datasets exhibit a clear zonal symmetry, with
 204 values increasing from north to south (Figure 1a, b), consistent with previous studies (Camberlin
 205 et al., 2001; Moron et al., 2006; Rust et al., 2013). The maximum precipitation occurs
 206 in the southern region, ranging from 8 to 12 mm/day in the southwest, while it remains
 207 below 3 mm/day in the northern part. A bias of about 1-2 mm/day is noted in ERA5
 208 reanalyses, with a maximum of 2-3 mm/day along the western coast and in the south-
 209 east (Figure 1e).

210 We first examine the interannual variability: monthly JAS anomalies were aver-
 211 aged for each year, resulting in 40 annual anomalies from 1979 to 2018, and their stan-
 212 dard deviation $\sigma_{interannual}$ (see section 2.2) plotted in Figures 1c and d. Like the aver-
 213 age, they exhibit a zonal pattern with values decreasing from south to north: regions with
 214 higher average precipitation also display larger interannual variability. The standard devi-
 215 ation appears slightly smaller in ERA5 than in observations (by about 0.5 mm/day);
 216 however, the standard deviation of this bias (obtained by computing the standard devi-
 217 ation of the time series differences between observations and ERA5) is comparable to
 218 or smaller than the JAS precipitation standard deviation (Figure 1f), accounting for ap-
 219 proximately only 10-25% of the mean value. Consequently, ERA5 data reasonably cap-
 220 ture the interannual variability of Senegal precipitation in JAS. Nevertheless, averaging
 221 values in JAS to a single value per year results in the loss of the intraseasonal signal con-
 222 tained within these three summer months. Since we aim to identify related signals in SST,

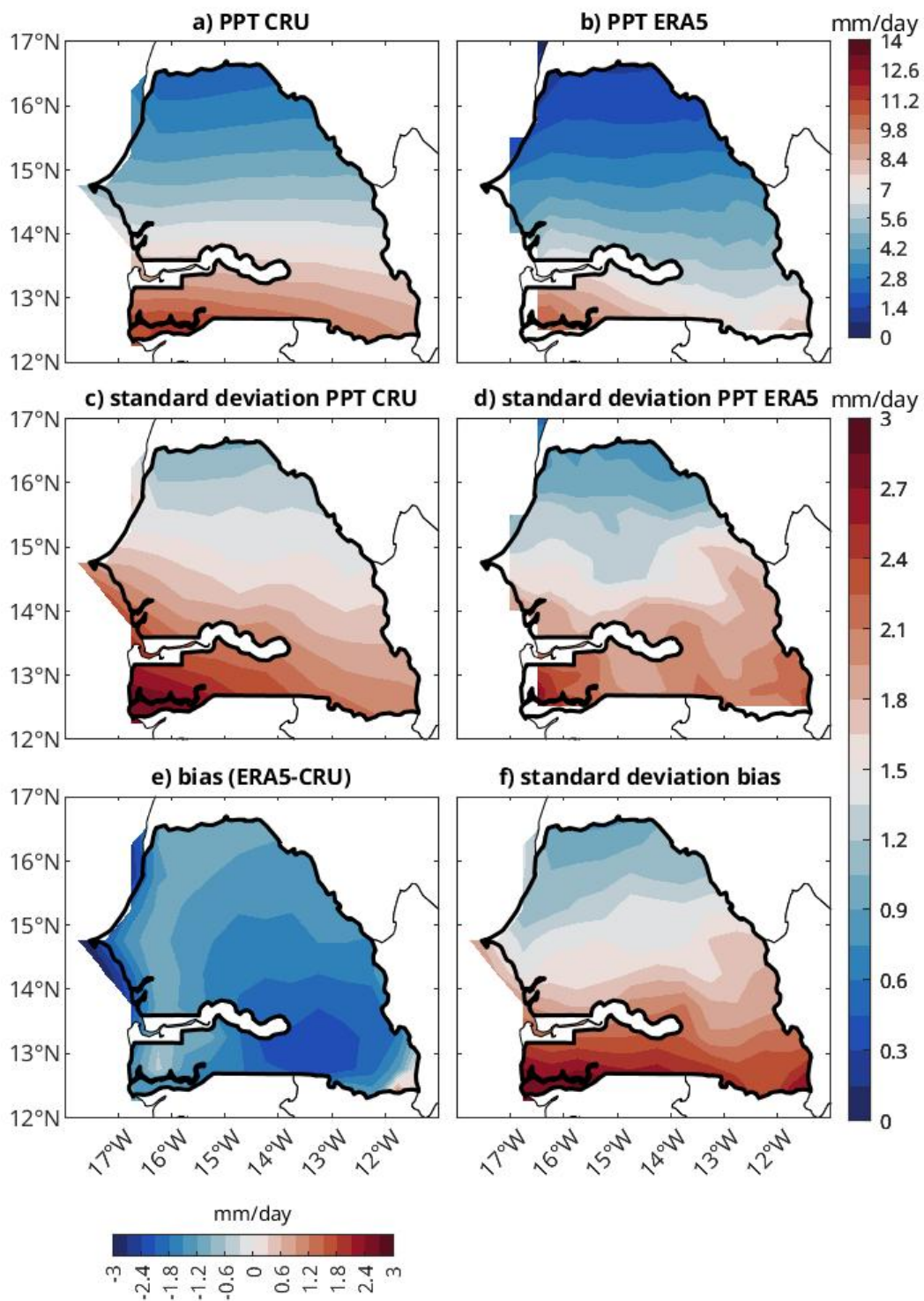


Figure 1. JAS 1979-2018 precipitation (PPT) in Senegal (mm/day): a. CRU observations, b. ERA5 reanalyses, c. standard deviation of CRU anomalies, d. standard deviation of ERA5 anomalies, e. mean bias between CRU observations and ERA5 reanalyses, f. standard deviation of the bias.

223 which has proven challenging due to the contrasting findings in previous studies, it is crucial to preserve the maximum signals. Therefore, we retain each individual July, August, and September anomaly throughout the remainder of the paper, including in the EOF decomposition.

227 The resulting first EOF of the CRU data (EOF1) accounts for 66.1% of the total variance (Figure 2a). Interestingly, the associated principal component (or PC1) time series yields a $\sigma_{intra\text{seasonal}}$ of 0.75, larger than the $\sigma_{inter\text{annual}}$ of 0.66. This indicates that retaining three summer monthly values per year significantly enhances the representation of the intraseasonal (or intermonthly) variability in our analysis. The ERA5 EOF1 accounts for 48.5% of the total variance (Figure 2b). EOF1 are very similar in ERA5 and CRU: they both exhibit a monopolar structure (i.e. with values of the same sign all over Senegal) of the precipitation anomalies. With zonal symmetry, an increase in the anomaly amplitude is observed from north to south, logically reflecting the standard deviation (Figure 1c,d): it is maximum in the southwest of Senegal (in Casamance), with more than 0.1 mm/day in CRU mode, and about half of that in ERA5 mode. The time series associated with EOF1 (or PC1) for CRU and ERA5 (Figure 2c) both exhibit strong interannual and intraseasonal monthly variability in precipitation. Their correlation (0.71) is highly significant, and they also demonstrate substantial covariability within the three-month summer periods, with common extreme months (e.g., August 1984, September 1986, July 1997, July 2002, September 2010, etc.).

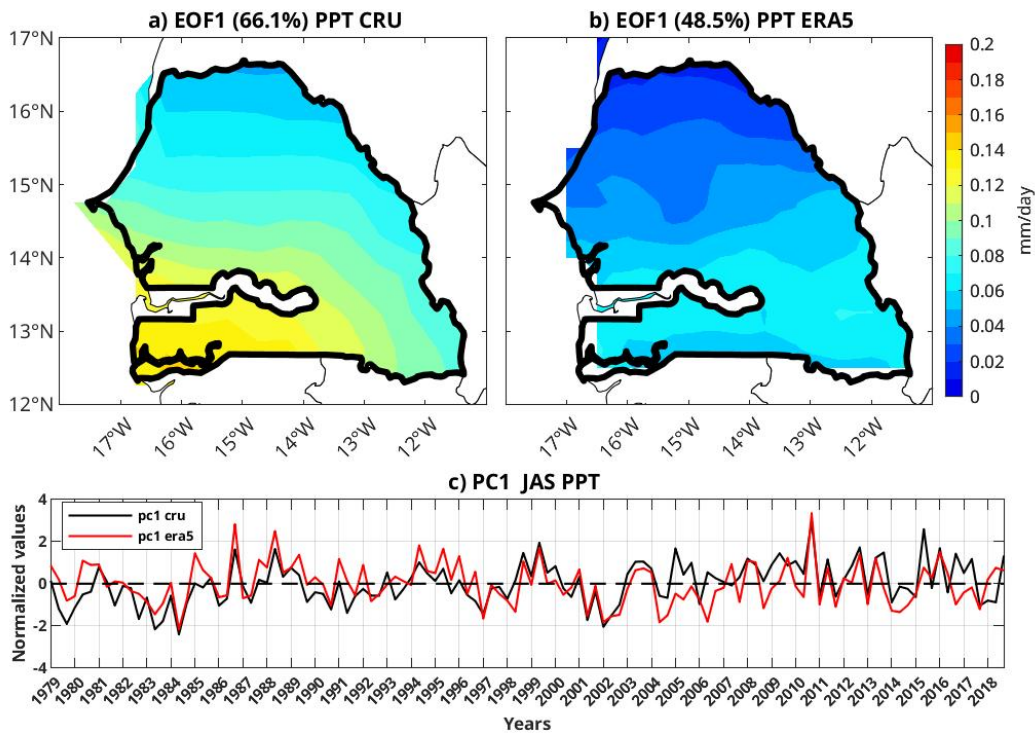


Figure 2. JAS 1979-2018, principal mode of variability (EOF1) for precipitation (PPT) anomalies (mm/day): a. CRU observations, b. ERA5 reanalyses and c. corresponding time series (black contours for CRU, red contours for ERA5).

243 The JAS mean and EOF1 precipitation for the entire Sahel region in both CRU
 244 and ERA5 datasets are not reproduced here but only in the annex (additional Figures
 245 A2 and A3), as they align with the findings of numerous previous studies, such as Quagraine
 246 et al. (2020). They exhibit similar zonal patterns, particularly covering the Senegal re-

gion, with maximum anomalies located in the west in both datasets. Although the Sahel’s first mode explains approximately 33% of the variance in ERA5 and slightly over 40% in CRU observations (see Table A1), both Senegal’s and Sahel’s modes show a high degree of correlation in both datasets, indicating shared interannual / summer monthly intraseasonal variance of more than 50% in CRU and ERA5 (see Figure A3c).

In summary, we observe that ERA5 reanalyses effectively capture months of extreme precipitation in JAS, both at regional and local scales. These findings align with the conclusions of Quagraine et al. (2020). They are also in agreement with the work of Fall et al. (2006) and Wade et al. (2015), who identified a moderate but significant correlation between seasonal rainfall in Senegal and the rest of West Africa. While precipitation patterns are generally consistent across much of the Sahel, they exhibit slight variations in the western region near the Atlantic (primarily Senegal) compared to the continental sector (Nicholson & Palao, 1993). However, when performing an EOF decomposition over the entire West Africa region - not just the Sahel - Fall et al. (2006) found that Senegal’s precipitation is more correlated with the second mode of variability of precipitation across West Africa than with the first mode, but this could only highlight the strong dependence of interannual variability modes on the selected region for analysis. Focusing on Senegal’s modes, the second mode in the CRU data accounts for approximately 10% of the total variance (see additional Figure A1 and Table A1), whereas the first mode explains two-thirds of the variance: consequently, in the subsequent analysis, we use CRU’s PC1 for JAS as a summer monthly interannual / intraseasonal index of JAS precipitation in Senegal. This index is hereafter referred to as PC1CRU. Lastly, while ERA5 precipitation does not perfectly match CRU observations, they do share a significant portion of their variance, indicating that the atmospheric dynamics in ERA5 are relevant for identifying the mechanisms leading to increased precipitation in Senegal.

4 Global SST anomalies

This section explores linear regressions of global SST anomalies on a reference index. First, we use the index characterizing precipitation variability across the entire Sahel in observations (plotted in additional Figure A3c, black). Following that, we compare these findings with the results obtained using the precipitation index specific to Senegal (PC1CRU). We present SST anomalies during the three summer months (JAS) and also the preceding months: the term ‘lag -1’ refers to the correlation between PC1CRU in JAS and SST anomalies with a 1-month lag (i.e., in JJA); ‘lag -2’ indicates a 2-month lag (MJJ), and so forth.

A wetter-than-average summer in Sahel is clearly associated with a La Niña-like signal in the eastern equatorial Pacific (red box, 170-80°W, 5°S-5°N), characterized by negative SST anomalies, reaching more than -0.4°C at lag -5 (Figure 3). This signal reflects an anticorrelation between SST anomalies in the eastern equatorial Pacific and PC1CRU Sahel. It begins to show significance in spring (lag -5, or FMA), but the maximum anticorrelation is observed at lag -3 (in AMJ): SST in this region between April and June would have a significant impact on Sahel’s summer rainfall, as discussed in numerous previous studies (Folland et al., 1986; Janicot et al., 2001; Giannini et al., 2003; Joly & Voldoire, 2009; Rodríguez-Fonseca et al., 2011; Diatta & Fink, 2014; Gomara et al., 2017; Diakhaté et al., 2020): during an El Niño event (warm waters in the equatorial Pacific), warm Pacific waters trigger a Kelvin atmospheric wave associated with increased subsidence and reduced precipitation in West Africa (Semazzi et al., 1988; Moron & Ward, 1998; Rowell, 2001; Mohino et al., 2011). Joly and Voldoire (2009) suggested that the inverse mechanism is involved during a La Niña event, leading to increased monsoon rainfall in West Africa.

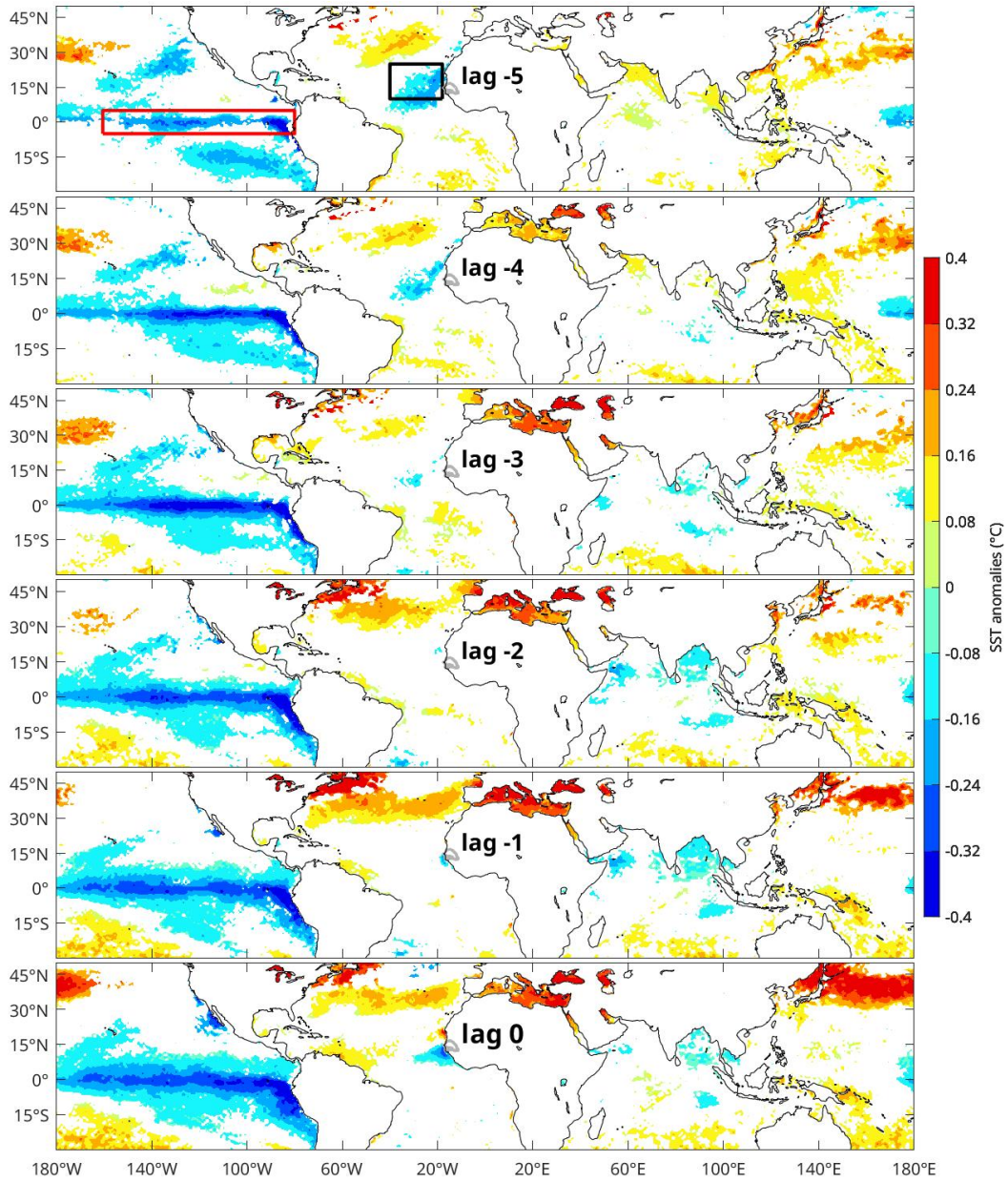


Figure 3. Linear regression of SST anomalies on PC1CRU Sahel ($^{\circ}\text{C}$) from lags -5 to 0 (indicating that SST precedes PC1CRU Sahel by 5 to 0 months). Only values significant at the 95% confidence level are plotted. The red box outlines the eastern equatorial Pacific (180°W - 80°W , 5°S - 5°N). The black box frames the Northeastern Tropical Atlantic (40°W - 17°W , 10°N - 25°N).

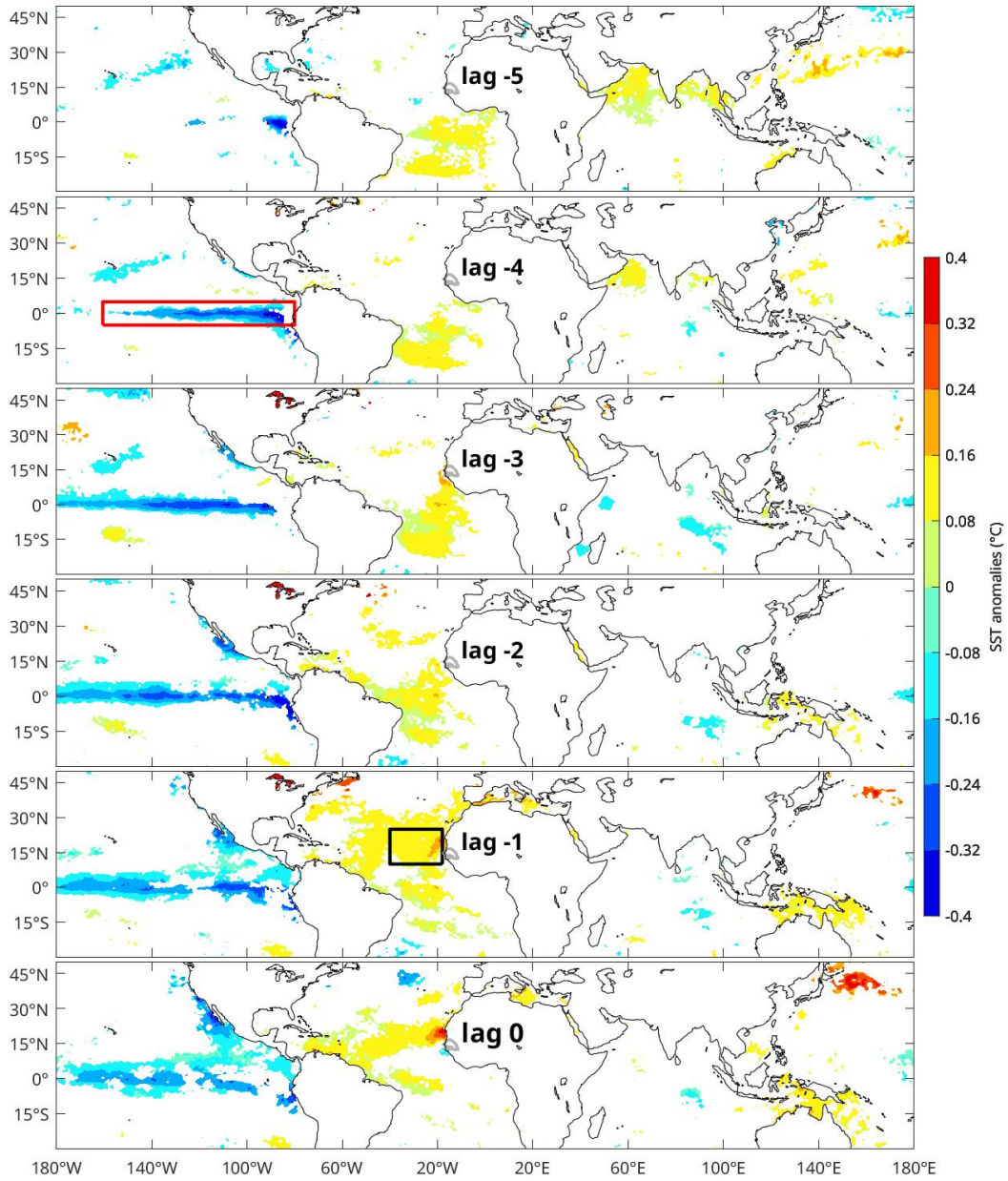


Figure 4. Identical to Figure 3 but for PC1CRU Senegal.

297 Strong significant positive SST anomalies in the Mediterranean precede a wetter-
 298 than-average summer in Sahel in the preceding months (Figure 3). This finding aligns
 299 with previous studies suggesting that increased SST leads to more rainfall through the
 300 supply of moisture over the Sahel, impacting Sahel precipitation (Rowell, 2003; Polo et
 301 al., 2008; Fontaine et al., 2009; Diakhate et al., 2019; Worou et al., 2020; Polo et al., 2008;
 302 Gaetani et al., 2010; Mohino et al., 2011; Gomara et al., 2017; Diakhate et al., 2019; Worou
 303 et al., 2020). Notably, Jung et al. (2006) identified a significant increase in Sahel rain-
 304 fall following the 2003 Mediterranean heat episode. Very strong correlations are also found
 305 in the northern Atlantic, with anomalies exceeding 0.4° in the Gulf Stream region north
 306 of 30°N (Wang et al., 2012; Y. Liu et al., 2014; Monerie et al., 2020) or in the northwest-
 307 ern Pacific: Northern Hemisphere extratropical warming indeed induces a significant in-
 308 crease in Sahel rainfall through the modification of the large-scale meridional heat dis-
 309 tribution, according to Park et al. (2015) or Suárez-Moreno et al. (2018).

310 Other significant signals are found in the Indian Ocean between lags -3 and -1, also
 311 highlighted in previous studies for the post-1970 period (Mohino et al., 2011; Fontaine
 312 et al., 2011). Although these signals appear relatively weak, they could nonetheless im-
 313 pact precipitation in the Sahel, as suggested in several studies (Bader & Latif, 2003; Bi-
 314 asutti et al., 2008; Mohino et al., 2011; Caminade & Terray, 2010). Hardly significant
 315 but large warm anomalies are found in the western tropical Pacific in the preceding months,
 316 likely as a continuation of the La Niña signal (Figure 3). However, no particular signal
 317 is found in the equatorial and subtropical South Atlantic. A signal corresponding to the
 318 'Atlantic Niño' in the eastern equatorial Atlantic is observed, as in Dommenget and Latif
 319 (2000), but approximately one year before the start of the rainy season, at lags -10 and
 320 -9 (not shown).

321 In the linear regression on PC1CRU Senegal, the vast majority of the signals iden-
 322 tified with PC1CRU Sahel are once again present but with weaker correlations and much
 323 less significant amplitudes (Figure 4). For example, the 'La Niña' signal in the eastern
 324 equatorial Pacific reaches up hardly -0.3°C at lag -3. The warm signal in the Mediter-
 325 ranean Sea is also significantly weaker and not observed until lag -1. On the other hand,
 326 a warm signal is found at lag -5 (FMA) in the equatorial Atlantic, disappearing by lag
 327 -1 (in JJA), and a warm anomaly appears around $15\text{-}20^\circ\text{S}$ from lag -5 with a peak at lag
 328 -4: Camberlin and Diop (1999) and Fall et al. (2006) have also found this predictive power
 329 of the South Subtropical Atlantic on Senegal precipitation with approximately a 5-month
 330 lead time. Moreover, significant differences are observed in the NETA (black box, 40°-
 331 20°W , $5^\circ\text{-}25^\circ\text{N}$), off the coast of Senegal and Mauritania: a positive anomaly of 0.2 to
 332 0.3°C is observed in phase with and one month before heavy rainfall in Senegal (lags 0
 333 and -1), where a negative anomaly was found instead in the regression on the Sahel in-
 334 dex (Figure 3).

335 These results indicate that despite the high correlation observed between the two
 336 principal modes of precipitation, one obtained over the entire Sahel and the other specifi-
 337 cally over Senegal, the latter appears to be less affected by remote SST anomalies com-
 338 monly discussed in the literature. Instead, it is more influenced by regional SST in the
 339 NETA region as well as the South Tropical Atlantic. The latter aspect is beyond the scope
 340 of the present study. However, in the following sections, we examine in more detail the
 341 oceanic and atmospheric signals linked to Senegal's precipitation in the NETA region.

342 5 Anomalies of SST and near-surface atmospheric circulation in the 343 Northeastern Tropical Atlantic

344 The JAS averages of SLP, SST, and surface winds from ERA5 reanalyses for the
 345 period 1979-2018 are shown in Figure 5. Over the continent, the primary characteris-
 346 tic of SLP is the "Heat Low" (Lavaysse et al., 2009), with values below 1010 hPa between
 347 15°N and 30°N (Figure 5a, black contours). Further west and slightly northward over the

348 ocean, there is a maximum SLP in the Azores region, around 35°N. The significant pres-
 349 sure gradient between these two regions results in very strong northeasterlies over the
 350 ocean along the coast, and northerlies over the Western Sahara and southern Morocco
 351 (Figure 5b). In response, the signature of a coastal upwelling can be observed north of
 352 20°N off Cap Blanc (the border between Mauritania and Western Sahara), with SST val-
 353 ues decreasing to as low as 20-22°C (Figure 5a). Furthermore, north of 15°N, SST is warmer
 354 in the west than in the east: this is likely explained by the fact that, on a seasonal scale,
 355 SST is primarily balanced between solar heating on one hand and cooling through la-
 356 tent heat fluxes on the other hand (Foltz & McPhaden, 2006), with surface winds be-
 357 ing stronger in the east compared to the west.

358 South / southeast trade winds are found south of 5°N (Figure 5b). East of 10-15°W,
 359 they turn north/northeastward while bringing moisture to West Africa ("monsoon flow").
 360 Further west, over the ocean, they converge with the northeast trade winds between 5°N
 361 and 15°N, defining the Intertropical Convergence Zone (ITCZ) where SST is maximum.
 362 The convergence of surface winds and maximum SST are indeed closely linked in the trop-
 363 ics (Fontaine & Janicot, 1996; Xie & Carton, 2004). For instance, Diakhaté et al. (2018)
 364 suggested that SST gradients significantly influence pressure gradients along the edges
 365 of the ITCZ in the Atlantic Ocean. Following the mechanism of Lindzen and Nigam (1987),
 366 a SST gradient tends to induce an opposite gradient in SLP just above through turbu-
 367 lent heat fluxes and hydrostatic adjustment. Consequently, surface winds tend to con-
 368 verge toward the center of a warm tropical SST region, favoring weak surface winds and
 369 deep atmospheric convection in the core of the ITCZ. However, east of 30°W, these winds
 370 turn eastward under the influence of the Heat Low and its extension over the ocean, form-
 371 ing the WAWJ (highlighted in red frame), which blows from the Atlantic towards the
 372 continent around 10°N (Grotsky, 2003; Pu & Cook, 2010). This low-level jet, observed
 373 below 800 hPa (Bonner, 1968; Stensrud, 1996), is known to be a significant source of mois-
 374 ture for the West African Monsoon in boreal summer (Cadet & Nnoli, 1987; Grams et
 375 al., 2010; Thorncroft et al., 2011; Pu & Cook, 2012; Lélé et al., 2015; W. Liu et al., 2020).
 376 The moisture transport into West Africa, and consequently precipitation, is thus poten-
 377 tially influenced by NETA SST through its impact on the WAWJ.

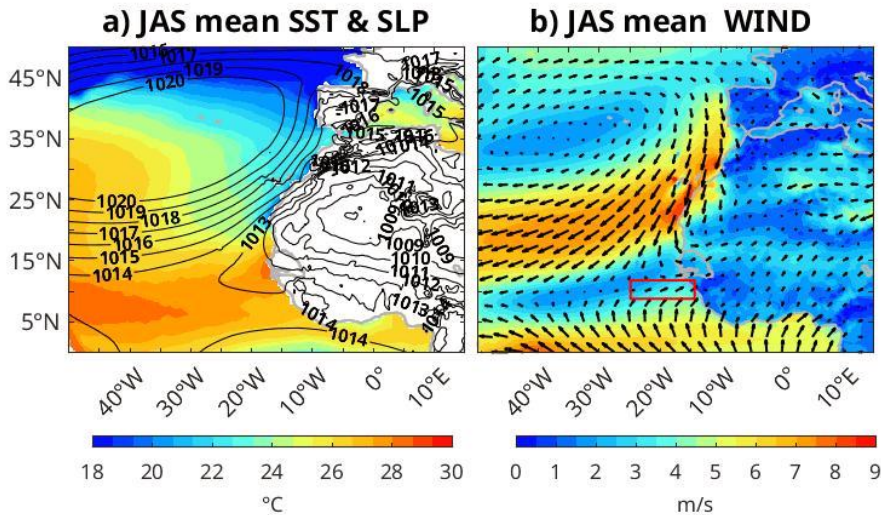


Figure 5. JAS 1979-2018 ERA5 reanalyses: a. SST (colors) and SLP (black contours). b. 10m-wind speed (colors) and direction (arrows). The red frame indicates the location of the WAWJ (25°W-14°W, 9°N-12°N).

378 Figure 6 presents the linear regression of SST, SLP and 10-meter wind on PC1CRU,
 379 with lags ranging from -2 (meaning the parameters precede PC1CRU by two months)
 380 to 0. Two months prior to a wet summer in Senegal, a significant negative SLP anomaly
 381 (exceeding -0.4 hPa) begins to emerge in the North Atlantic, reflecting a weakening of
 382 the Azores high (Figure 6, left, lag -2). This results in a weakening of the trade winds
 383 by approximately -0.3 m/s off Mauritania and Western Sahara (Figure 6, right), reduc-
 384 ing the intensity of coastal upwelling and latent heat fluxes, thereby creating a warm SST
 385 anomaly off Senegal and Cap Blanc (Figure 6, left, lags -1). At lag -1, the subtropical
 386 SLP anomaly strengthens and extends over the continent to the eastern border of Mau-
 387 ritania (around 5°W) between 20°N and 30°N, with a significant weakening of the north-
 388 easterlies to -0.3 to -0.4 m/s off Senegal and Cap Blanc (between 10°N and 25°N). In re-
 389 sponse, the warm SST anomaly off Cap Blanc reaches +0.4°C at lag 0 and extends hor-
 390 izontally southwestward between 10°N and 15°N at 50°W. This small yet significant warm-
 391 ing, owing to its extended coverage, could contribute to the formation of a negative pres-
 392 sure anomaly (exceeding -0.4 hPa) between 15°N and 25°N at lag 0 over the ocean (Fig-
 393 ure 6, left, lag 0). This negative SLP anomaly indicates the northward shift of low-pressure
 394 systems within the marine ITCZ. The most significant anomalies it generates are pri-
 395 marily located in the southern half of the anomaly, between 10°N and 20°N. In this re-
 396 gion, it decelerates surface winds in the north and intensifies them in the south (com-
 397 pare Figure 6, right, lag 0, and Figure 5b). Westerly anomalies are subsequently observed
 398 between 7°N and 12°N off the coast, signifying a strengthening of the WAWJ. Finally,
 399 over the continent, a positive pressure signal is observed around 20°N to 30°N, associ-
 400 ated with a less intense Heat Low than average. Although this signal is visible only at
 401 the 1000 hPa pressure level over the continent (not shown), its extension over the ocean
 402 is evident in the SLP anomaly near the coast around 25°N (Western Sahara).

403 A similar linear regression was conducted using the PC1CRU index calculated for
 404 the entire Sahel (not shown): no significant differences in surface wind or SLP were iden-
 405 tified, which is expected given the strong correlation between the two indices. However,
 406 disparities in NETA SST anomalies, as discussed in the previous section, still exist: Sen-
 407 egal JAS precipitation, although sharing the majority of its interannual / summer monthly
 408 intraseasonal variance with the entire Sahel, appears to be influenced by a different SST
 409 anomaly: it supports the hypothesis that a regional feedback involving NETA SST, SLP
 410 and surface winds could be at work.

411 6 Moisture transport

412 The JAS average of the low-level moisture transport (integrated between 1000 hPa
 413 and 850 hPa) is plotted in Figure 7a. Over the ocean, it closely resembles the surface
 414 wind pattern (Figure 5b): moisture transport carried along by the trade winds, controlled
 415 by the Azores and Saint Helena anticyclones, converge between 8°N and 15°N. East of
 416 30°W, at approximately 10°N, there is a notable inland-directed moisture transport, likely
 417 carried by the WAWJ, in agreement with Pu and Cook (2010, 2011), and Lélé et al. (2015).

418 The divergence of the moisture transport exhibits a zonal band of significant con-
 419 vergence along the ITCZ between 5°N and 13°N, slightly south of the wind maximum
 420 convergence (Figure 7c). This convergence aligns perfectly with the zonal band of av-
 421 erage JAS precipitation (Figure 7e). The most significant precipitation is located along
 422 the coast (Figure 7c), induced by the strong coastal convergence of moisture transport
 423 driven by the WAWJ around 10°N and further south by the southern monsoon flux (Fig-
 424 ure 7a). Indeed, given that the lower atmospheric layer is consistently close to moisture
 425 saturation in oceanic areas, near-surface convergence and precipitation are co-located
 426 most of the time (Weller et al., 2017).

427 Over the continent, there is a noticeable contrast in moisture transport patterns.
 428 To the south of 18°N, the moisture transport is south / southwestern and relatively in-

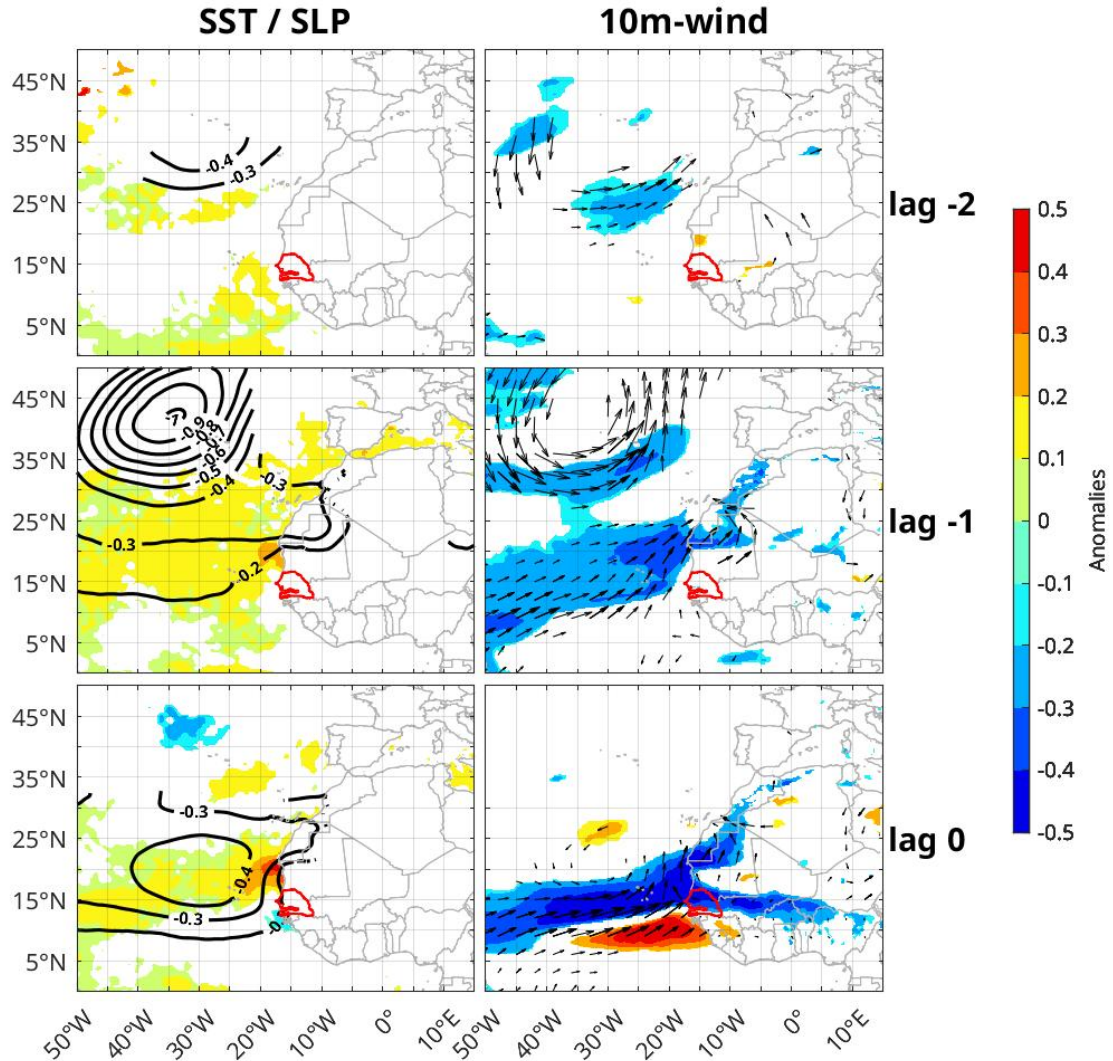


Figure 6. Linear regression of ERA5 reanalyses on PC1CRU, from lags -2 (ERA5 leads PC1CRU by 2 months) to lag 0. Left: SST (colors, °C) and SLP (black contours, hPa). Right: 10m-wind speed (colors, m/s) and direction (arrow). Only values significant at the 95% level are plotted.

429 tense. It strongly weakens north of 18°N and reaches a minimum in the core of the Heat
 430 Low (Figure 7a). This naturally leads to a notable convergence of moisture transport
 431 around 18°N, roughly corresponding to the "Intertropical Front", or "Intertropical Dis-
 432 continuity" (ITD). However, unlike over the ocean, this pronounced near-surface con-
 433 vergence does not coincide with a precipitation peak: the latter is observed further south
 434 between 5°N and 15°N (Figure 7e). Indeed, precipitation is primarily associated with the
 435 formation of MCSs south of the AEJ, as mentioned in the introduction, and is more in-
 436 fluenced by moisture transport convergence in the mid-to-high troposphere rather than
 437 in the lower troposphere.

438 A last notable feature of the mean moisture transport over the continent is a distinct
 439 weakening of the westerly flow around 10°N-10°W, where the largest mountain in
 440 Sierra Leone, the Loma Mansa, rises to almost 2000m in height (Figure 7a). More gen-
 441 erally, the high relief near the coast contributes to the amplification of precipitation on
 442 the windward side of these mountains (Figure 7e), in agreement with Kante et al. (2020).

443 The linear regressions of low-level moisture transport, its divergence, and precip-
 444 itation in JAS are presented in Figure 7 (right). Over the ocean, a wetter than usual sum-
 445 mer in Senegal is associated with a cyclonic moisture transport anomaly that clearly cor-
 446 responds to the negative SLP anomaly found previously between 10°N and 30°N (Fig-
 447 ure 7b). The induced strengthening of the WAWJ in the southern edge of this anomaly
 448 results in an increase in eastward moisture transport between approximately 6°N and
 449 12°N, while a decrease in westward transport is observed between 12°N and 16°N (Fig-
 450 ure 7b). This leads to a significant increase in the coastal convergence of moisture trans-
 451 port between 6°N and 12°N (Figure 7d), and consequently, higher oceanic and coastal
 452 precipitation, with a maximum anomaly reaching up to 2 mm/day over the ocean be-
 453 tween 8°N and 15°N (Figure 7f).

454 On the continent, there is a narrow zonal band of reduced moisture transport be-
 455 tween 12°N and 15°N (Figure 7b), bordered by opposite positive anomalies further south
 456 and in the region of the Heat Low further north. Consequently, there is a zonal band of
 457 negative divergence anomaly to the south (around 10°N) and positive to the north (around
 458 15°N) of this zonal band. The Heat Low anomaly probably explains most of the weak
 459 but highly correlated negative precipitation anomalies detected between 18°N and 25°N,
 460 as well as part of the positive precipitation anomalies between 10°N and 18°N (Figure
 461 7f, black contours). The increase in Sahel precipitation is indeed mostly controlled by
 462 the weakening of the Heat Low in its southern half, which shifts moisture transport fur-
 463 ther north (Cook, 1999). However, the convergence anomalies (Figure 7d) may also con-
 464 tribute to the increase in precipitation between 10°N and 18°N, following the inland ex-
 465 tension of the WAWJ acceleration and eastward moisture transport around 10°N.

466 These results highlight the complex nature of the atmospheric dynamics control-
 467 ling precipitation in West Africa. They lend support to investigations of the ITCZ, mois-
 468 ture transport, and precipitation, spanning the entire troposphere. Two vertical merid-
 469 ional cross-sections are conducted on either side of the coast, one over the ocean, span-
 470 ning from 22°W to 17°W, and the other to the east of Senegal, spanning from 10°W to
 471 5°W. Note that the results presented below remain consistent when the width of the sec-
 472 tions is slightly adjusted or increased by 5°. Horizontal divergence of moisture transport
 473 is calculated as in equation (4) (Figure 8, colors). Given that zonal transport (black con-
 474 tours) typically surpasses meridional transport above 850 hPa, only the former is plot-
 475 ted in the figures.

476 In the mean profile over the ocean, in the lower layer (below 850 hPa), we observe
 477 similar signals to those in Figure 7: framed by divergent moisture transports south of
 478 5°N or north of 15°N, a robust convergence coincides with the peak of eastward mois-
 479 ture transport within the WAWJ between 5°N and 13°N (Figure 8a). It also coincides
 480 with the heaviest rainfall (Figure 8a, bottom panel, gray profile). This convergence re-
 481 sults from the south and north trade winds meeting within the ITCZ, and an increase
 482 in eastward moisture transport toward the coast via the WAWJ around 10°N (Figure 8a,
 483 solid black contours). Above 850 hPa, there is an intense westward moisture transport
 484 between 750 and 550 hPa, at 12-18°N (Figure 8a, dashed black contours), indicating the
 485 presence of the AEJ. No signal is detected above 400 hPa, suggesting that moisture trans-
 486 port by the Tropical Easterly Jet, located at approximately 5°N between 100 and 200
 487 hPa, is negligible.

488 In the mean profile over the continent, above 850 hPa, a similar maximum of zonal
 489 moisture transport is found at the location of the AEJ (Figure 8c, black contours). Be-

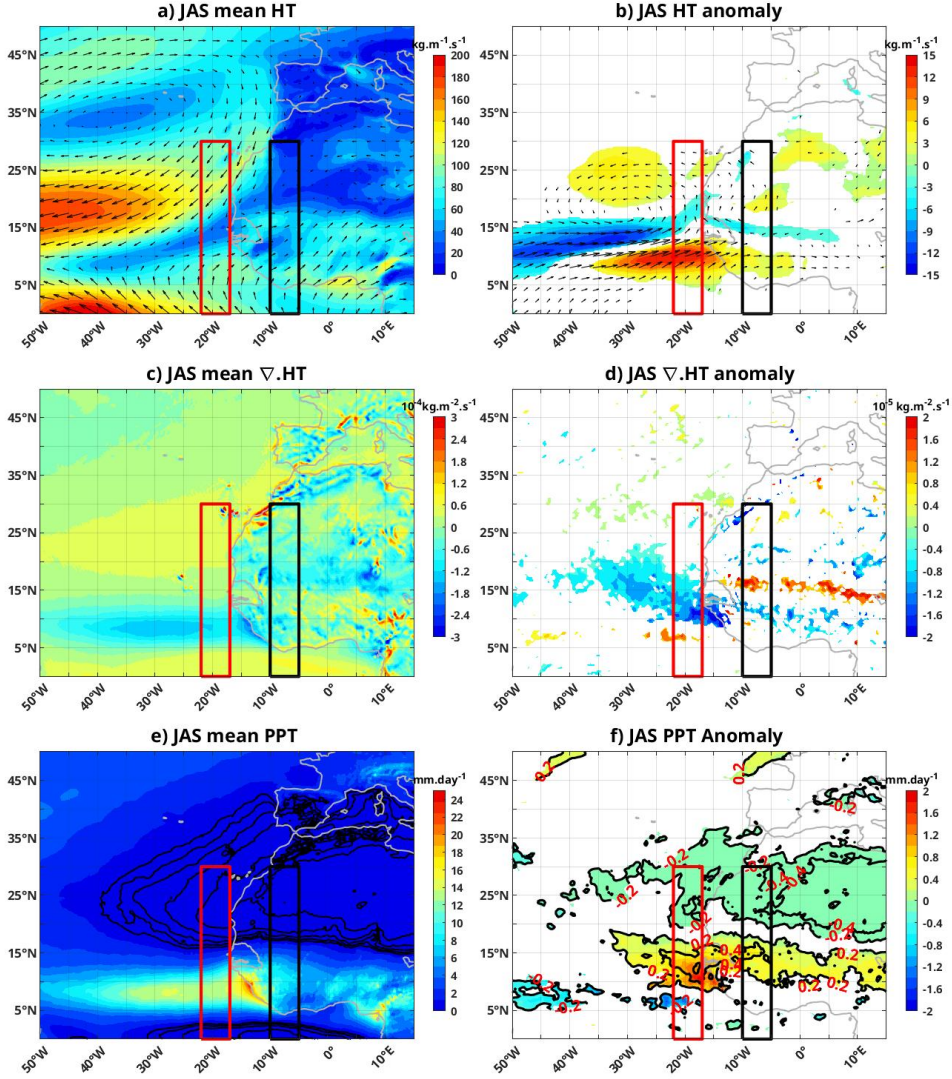


Figure 7. JAS 1978-2018 ERA5 reanalyses, average (left) and linear regression on PC1CRU index (right): a., b. magnitude (colors) and direction (arrow) of moisture transport (HT). c., d. divergence of moisture transport ($\nabla \cdot \text{HT}$). e., f. precipitation (PPT). In e., values less than 1 mm/day are outlined in black (intervals of 0.1 mm/d). In b., d. and f., only values significant at the 95% confidence level are plotted. In f., correlations are depicted using black contours with intervals of 0.2. Red and black frames indicate the location of the meridional-vertical sections plotted in Figures 8 and 9.

490 low 850 hPa, the western moisture transport extends as far north as 18°N (15°N over the
 491 ocean). A minimum in moisture transport convergence is found at 9-12°N, dividing the
 492 flow into two segments on either side of the Loma Mansa mountains as observed in Fig-
 493 ure 7a. Strong convergence takes place at the bottom of the southern branch, explain-
 494 ing the heavy precipitation south of 10°N (Figure 8c, bottom panel). A second conver-
 495 gence maximum is observed in the northern branch, in the ITD region around 18°N, but
 496 it does not correspond to strong precipitation. The latter is governed by MCSs gener-
 497 ated along the AEJ north of 17°N, as mentioned earlier, which probably explains why
 498 the precipitation peak is located around 10°N, at the latitude of the AEJ southern edge.

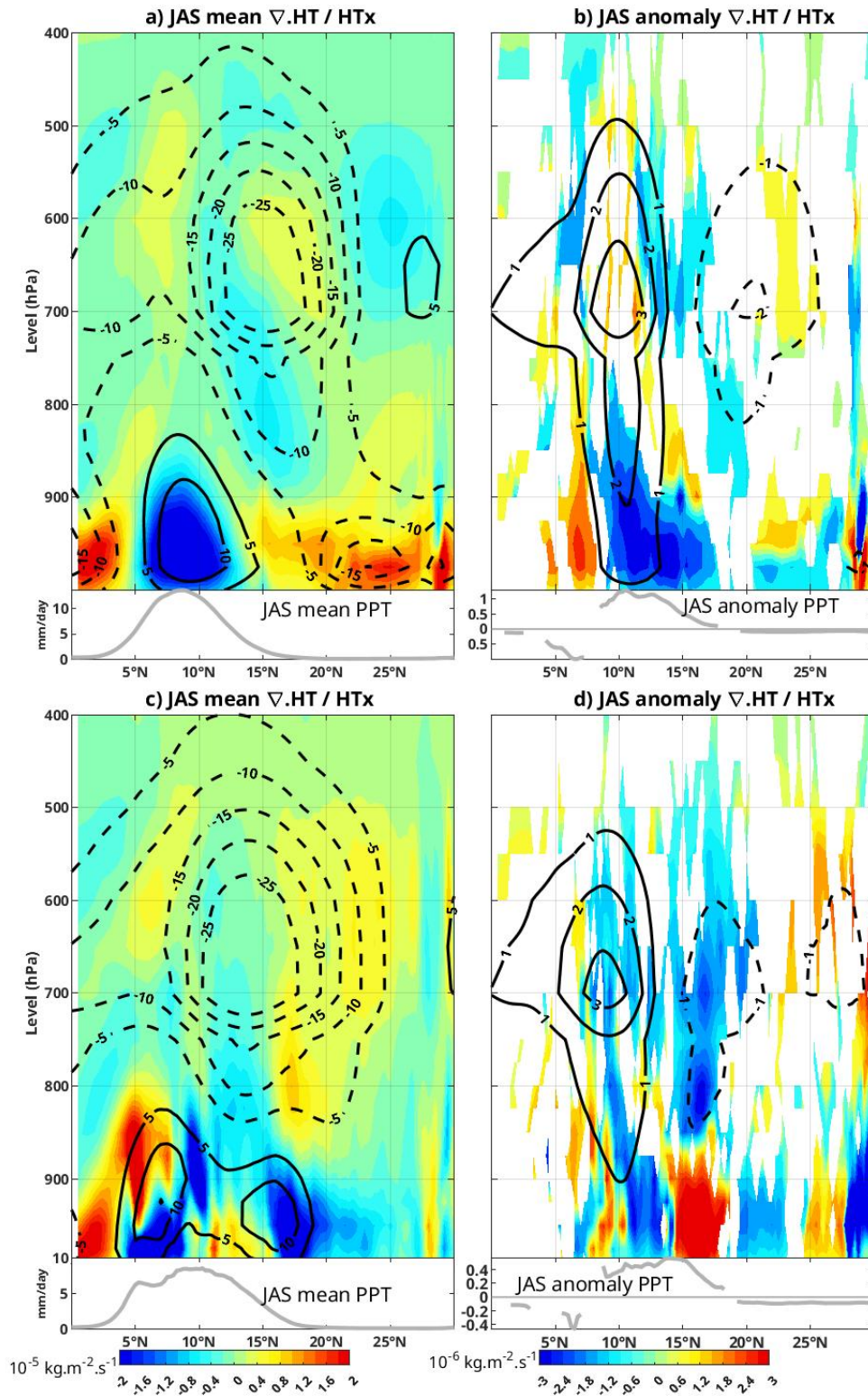


Figure 8. JAS 1978-2018 ERA5 reanalyses, average (left) and linear regressions on the PC1CRU index (right) in vertical meridional sections over the ocean (22°W-17°W, a., b.) and over the continent (10°-5°W, c., d.): Divergence of moisture transport (colors) and zonal moisture transport (black contours, solid for positive, dashed for negative), superimposed on precipitation (gray line in panels at the bottom). Only values significant at the 95% confidence level are plotted.

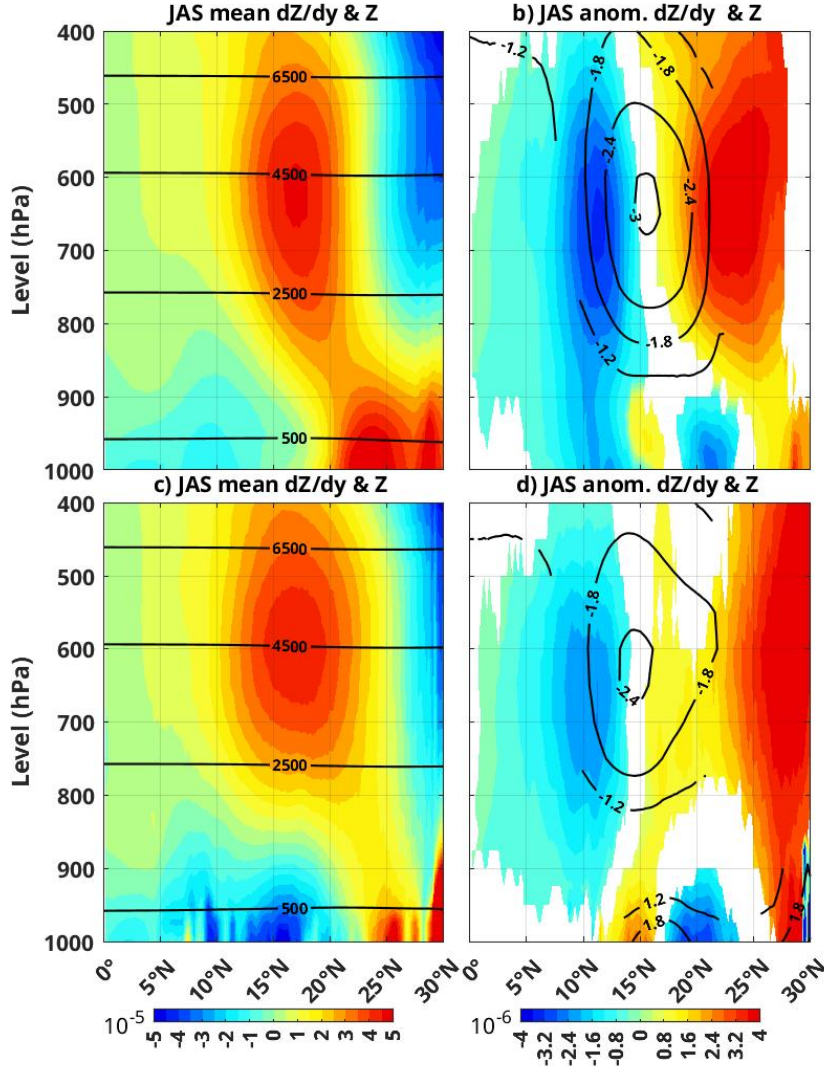


Figure 9. Same as Figure 8, but for geopotential height (black contours) and its meridional gradient (colors).

499 Over the ocean, the linear regression on PC1CRU shows an increase in low-level
 500 convergence of moisture transport between 9°N and 18°N (Figure 8b, colors), aligning
 501 with positive precipitation anomalies a few degrees north of their mean position (Fig-
 502 ure 8b, bottom panel, grey profile). The increased convergence is caused by the accel-
 503 eration of the WAWJ along its northern edge, as indicated by the positive anomaly in
 504 zonal transport between 9°N and 13°N (black contours). This anomaly extends in alti-
 505 tude up to about 500 hPa, peaking between 600 and 700 hPa: at this altitude, it indi-
 506 cates a deceleration of the AEJ on the southern edge of its mean position. At the same
 507 altitude, a negative anomaly in zonal transport is observed further north, around 20°N,
 508 indicating an acceleration of the AEJ on its northern edge: the AEJ has slightly shifted
 509 north.

510 In the linear regression over the continent, above 850 hPa, anomalies of zonal mois-
 511 ture transport resemble those over the ocean. However, the negative anomaly north of
 512 15°N is less pronounced and extends further north (Figure 8d, black contours). More-

513 over, the positive anomaly between 9°N and 12°N remains above 850 hPa without reach-
 514 ing the surface, in contrast to the situation above the ocean. Below 850 hPa, alternat-
 515 ing positive and negative divergence anomalies emerge approximately every 5°: north of
 516 15°N, they probably result from the weakening of the Heat Low in its southern half, as
 517 mentioned earlier. However, between 10°N and 15°N, the convergence anomaly rather
 518 corresponds to a continental extension of the large WAWJ acceleration found over the
 519 ocean at the same latitude: it probably contributes significantly to the heavy precipi-
 520 tation observed between 10°N and 15°N.

521 In summary, the increase in summer precipitation in Senegal is partly of continen-
 522 tal origin and controlled by the Heat Low and the AEJ. However, there are also clear
 523 signs of an influence coming from the Atlantic ocean through the WAWJ: a northward
 524 shift of the ITCZ comes with an intensification of the latter, which increases the west-
 525 ern moisture transport between 10°N and 15°N and its convergence. It results in an in-
 526 crease in precipitation at the same latitudes. The SST could play a role in this inten-
 527 sification by altering low-level meridional pressure gradients through hydrostatic adjust-
 528 ment along its southern edge, along 10-15°N: the WAWJ would then respond to the pres-
 529 sure gradient signal via geostrophic adjustment. We test the plausibility of this hypoth-
 530 esis in the next section.

531 7 Geostrophic adjustment to the NETA SST anomaly

532 In this section, the geopotential height (or Z) at different pressure levels is used to
 533 calculate a meridional gradient (dZ/dy , colors): anomalies in dZ/dy can then be assim-
 534 ilated as anomalies in meridional pressure gradient of the same sign and provide infor-
 535 mation about the geostrophic zonal wind north of 5°N (geostrophic approximation is no
 536 longer valid near the equator), through the formula: $u_g = -\frac{g}{f} \frac{\partial Z}{\partial y}$.

537 A large peak of positive dZ/dy is found at 10-20°N around 500-700 hPa over the
 538 ocean (Figure 9a), emphasizing the clear geostrophic origin of the AEJ (Cook, 1999). Neg-
 539 ative values of dZ/dy are found further north, indicating a high in the mid and upper
 540 tropospheric pressure around 20-25°N. Below 850 hPa, dZ/dy displays a negative value
 541 within the WAWJ (driving eastward geostrophic wind) south of 18°N and a positive value
 542 to the north (westward wind). The value of dZ/dy at 10°N is approximately -1 to -2×10^{-5}
 543 units, which corresponds to a geostrophic zonal wind speed of 3.8 to 7.8 m/s when mul-
 544 tiplied by $-g/f$ (with $g = 9.81 \text{ m/s}^2$, $f = 2\Omega \sin(10^\circ)$ and $\Omega = 2\pi \text{ rad / day}$), i.e.
 545 representative of the speeds typically found within the WAWJ. This is in line with Pu
 546 and Cook (2010) who show that while the jet is largely ageostrophic during its seasonal
 547 transitions, it is dominated by geostrophy on average.

548 The local negative minimum of dZ/dy around 10°N is located over an ocean region
 549 where the meridional SST gradient is positive and may reach a local maximum, as can
 550 be observed in Figure 5 (left). A positive maximum of dZ/dy is located further north
 551 around 23-25°N, over a strongly negative SST gradient in the southern front of the coastal
 552 upwelling off Cap Blanc. These alignments of dZ/dy and $dSST/dy$ extrema are in agree-
 553 ment with the theory of Lindzen and Nigam (1987) suggesting that the near-surface pres-
 554 sure gradients adjust to the SST gradients. This is also in agreement with Diakhaté et
 555 al. (2018), who suggested that the equatorial low, thus the marine ITCZ, is partially con-
 556 trolled on its edges by meridional SST gradients.

557 A similar signature of the AEJ is found in the mid-troposphere above the conti-
 558 nent, but the subtropical high is shifted north by 2 or 3 degrees (Figure 9c). Below 850
 559 hPa, negative values of dZ/dy are found to the south and positive values to the north
 560 of the Heat Low, whose center is located around 20-25°N. Large values of dZ/dy at 25°N
 561 and at 16-17°N reflect the very steep "walls" of the Heat Low, with the southernmost
 562 corresponding to the ITD.

563 Above the continent, the linear regression of Z and dZ/dy on PC1CRU shows a sig-
 564 nificant drop in pressure within the AEJ, indicating its northward shift (weakening of
 565 easterlies in the southern half of its mean position, strengthening in the north, Figure
 566 9d). The dominant signal in dZ/dy is a positive anomaly north of 15°N : as it is partic-
 567 ularly intense north of 25°N , it likely reflects the influence of the large-scale subtropi-
 568 cal atmospheric circulation and / or the Mediterranean. Extending down to the surface,
 569 this anomaly covers a positive pressure anomaly confined under 900 hPa between 15°N
 570 and 20°N , which reflects the weakening of the Heat Low in its southern half, inducing
 571 a northward shift of the pressure minimum. This is primarily what controls the north-
 572 ward shift of the MCSs path, thus partly explaining the increase in precipitation between
 573 10°N and 18°N in Senegal. However, the signal corresponding to the weakening of the
 574 AEJ on its southern edge (negative anomalies in dZ/dy around 10°N at 600-700 hPa)
 575 appears to be somewhat weaker, and does not reach the surface, suggesting it is an east-
 576 ward extension of a similar anomaly found above the ocean.

577 Above the ocean, the overall anomalies in dZ/dy are similar to those over the con-
 578 tinent, with a slight northward shift of one or two degrees (Figure 9b). Below 850 hPa,
 579 the signals north of 15°N are likely an extension over the ocean of the anomalies observed
 580 above the continent, thus controlled by the variability of the Heat Low. However, south
 581 of 15°N , the negative anomaly of dZ/dy is significant between 8°N and 14°N , whereas
 582 it is not over the continent (Figure 9d). This suggests that it is forced by the SST anomaly.
 583 With a value of approximately -2×10^{-6} units, such a dZ/dy anomaly drives a geostrophic
 584 zonal wind anomaly of about 0.7 m/s, which is of the same magnitude than the surface
 585 wind anomaly observed at the same latitudes (Figure 6, right, lag 0).

586 This highlights that the strengthening of westerlies around 10°N - 15°N , which cor-
 587 responds to an acceleration of the WAWJ on its northern side and leads to increased pre-
 588 cipitation in Senegal, is clearly a geostrophic response to near-surface pressure fluctu-
 589 ations. Since the latter is likely controlled by the SST warm anomaly between 10°N and
 590 20°N , via the mechanism theorized in Lindzen and Nigam (1987), this suggests the ex-
 591 istence of a regional feedback mechanism between SST and surface winds in the NETA.

592 8 Discussion and conclusions

593 This work documents the oceanic and atmospheric signals related to monthly pre-
 594 cipitation from July to September in Senegal, using CRU observations and ERA5 reanal-
 595 yses covering the period from 1979 to 2018 (40 years). It compares the signals related
 596 to precipitation variability in Senegal versus the entire Sahel region. Noting a significant
 597 difference in Northeast Tropical Atlantic (NETA) SST, it takes a closer look at surface
 598 signals (pressure, wind, and moisture transport) and along two vertical sections in the
 599 mid and lower troposphere. Finally, it proposes a mechanism linking NETA SST to pre-
 600 cipitation in Senegal.

601 First, monthly precipitation values in Senegal for 40 years are used. Anomalies for
 602 the months of July to September are extracted, and an EOF decomposition is performed:
 603 this yields an index, PC1CRU. This index characterizes interannual variability, but since
 604 three successive monthly values per year are retained, it also captures some intraseasonal
 605 variability in JAS. This mode is highly significant, as it explains two-thirds of the to-
 606 tal precipitation variance in Senegal, with a pattern of anomalies of the same sign across
 607 the country and a strong gradient in their amplitude, from very weak in the north to very
 608 strong in the southwest of Senegal.

609 A comparison with a similar index calculated using ERA5 reanalysis precipitation
 610 data shows good correspondence, which suggests using the SST and atmospheric param-
 611 eters from these reanalyses to explore the dynamic environment of the dominant mode,
 612 PC1CRU, in Senegal's precipitation variability. All subsequent analyses are therefore based

613 on linear regressions performed on this index. It should be noted that the results are pre-
 614 sented for a positive anomaly of PC1CRU, indicating increased precipitation, but sim-
 615 ilar discussions would apply to a negative anomaly, as the regression is linear.

616 Increased JAS precipitation in Senegal is generally preceded by cold SST anoma-
 617 lies in the eastern equatorial Pacific (La Niña event) and warm SST anomalies in the Mediter-
 618 ranean Sea. These results are in line with many previous studies, including those by Rowell
 619 (2001), Giannini et al. (2003), Mohino et al. (2011), Rodríguez-Fonseca et al. (2011), and
 620 Diakhate et al. (2019). However, we obtained much weaker correlations than in these stud-
 621 ies, especially in the East Equatorial Pacific and the Mediterranean, because we used a
 622 Senegal precipitation index instead of a Sahel one. Moreover, completely different anoma-
 623 lies are found in the NETA: this suggests that the western part of the Sahel, as Sene-
 624 gal, is more influenced by the Atlantic Ocean and less by large-scale atmospheric forc-
 625 ing and teleconnections than the entire Sahel. Therefore, the atmospheric dynamic anoma-
 626 lies in the NETA related to increased JAS precipitation in Senegal are examined.

627 The main result obtained indicates that increased JAS precipitation in Senegal is
 628 attributed to the increased convergence of low-level moisture transport, driven by an in-
 629 crease in the West African Westerly Jet (WAWJ). It also appears to be linked to the north-
 630 ward shift of the African Easterly Jet (AEJ) between 750 hPa and 550 hPa.

631 Above the continent, just east of Senegal, this northward shift of the AEJ is likely
 632 due to a northward migration of the Heat Low, in agreement with previous studies such
 633 as Diallo et al. (2013) and Sylla et al. (2013) that used regional climate models, or Grist
 634 and Nicholson (2001) and Dezfuli and Nicholson (2011) who used reanalysis data. At-
 635 mospheric teleconnections, both regional and larger scale with ENSO or Mediterranean
 636 SSTs, are also likely to play an important role. This probably leads to a northward mi-
 637 gration of the trajectories of the Mesoscale Convective Systems (MCSs) responsible for
 638 most of the summer precipitation, explaining their increase between 10°N and 15°N.

639 However, over the ocean, just west of Senegal, the same northward shift of the AEJ
 640 as over the continent is observed, but the increase in precipitation is largely explained
 641 by an increase in low-level moisture transport convergence, created by an acceleration
 642 of the WAWJ. This is controlled by a significant negative pressure anomaly located in
 643 the NETA (10°N-30°N), reflecting the northward movement of the low-pressure areas char-
 644 acterizing the marine ITCZ. This negative pressure anomaly is situated above a posi-
 645 tive SST anomaly, and the near-surface winds anomalies are compatible with a geostrophic
 646 response of the WAWJ to a reinforcement of the negative meridional pressure gradient
 647 between 10°N and 15°N. The latter could itself result from an increase in the positive SST
 648 gradient on the southern edge of the warm anomaly, following the mechanism proposed
 649 by Lindzen and Nigam (1987). The SST - surface wind feedback mechanism would then
 650 be as follows: first, the northeastern Trade Winds weaken, forcing a warming of the SST
 651 between 10°N and 25°N. Second, the SLP adjusts to the warmer SST and becomes weaker
 652 between 10°N and 25°N; its increased negative meridional gradient to the south forces
 653 a strengthening of the near-surface winds in the WAWJ region. This eventually results
 654 in an increased convergence of moisture transport and precipitation between 10°N and
 655 15°N.

656 Between these two zones (ocean and continent), Senegal likely receives the influ-
 657 ence of atmospheric teleconnections and the Mediterranean through the mode of vari-
 658 ability it shares with the Sahel, but it could also be strongly influenced by NETA SST
 659 through the previously suggested feedback mechanism. As the initial Trade Winds anomaly
 660 seems driven by an anomaly of the Azores High, hence linked to the North Atlantic Os-
 661 cillation (NAO), these results could possibly explain the link between Sahel precipita-
 662 tion and the North Atlantic, as shown for example in Paeth and Friederichs (2004). How-
 663 ever, the ocean-atmosphere feedback mechanism suggested in this study needs further
 664 exploration at shorter time scales than the monthly data presented here, as the atmo-

665 spheric response to SST fluctuations is very rapid (within hours/days). Therefore, fur-
666 ther studies using daily data or a regional atmospheric model are needed to confirm or
667 refute this potential role of NETA SST feedback on the WAWJ. This could lead to a bet-
668 ter understanding of the mechanisms driving precipitation variability in Senegal and, ul-
669 timately, to improved seasonal forecasts.

670 **9 Open Research**

671 Version 4.03 of CRU TS precipitation observation data covering the period from
672 January 1901 to December 2018 (Harris et al., 2020) is available on [https://data.ceda](https://data.ceda.ac.uk/badc/cru/data/cru_ts/cru_ts.4.03/data7)
673 [.ac.uk/badc/cru/data/cru_ts/cru_ts.4.03/data7](https://data.ceda.ac.uk/badc/cru/data/cru_ts/cru_ts.4.03/data7)

674 Monthly average ERA5 data on simple levels and pressure levels from 1940 to present
675 are also available respectively at [https://cds.climate.copernicus.eu/doi/10.24381/](https://cds.climate.copernicus.eu/doi/10.24381/cds.f17050d7)
676 [cds.f17050d7](https://cds.climate.copernicus.eu/doi/10.24381/cds.f17050d7) and at <https://cds.climate.copernicus.eu/doi/10.24381/cds.6860a573>.

677 **Acknowledgments**

678 This work was supported by the IRD (institut de Recherche pour le Développement through
679 PDI-MSc program (Programme Doctoral International- Modélisation des Systèmes Com-
680 plexes). This work was also supported by the Laboratoire Mixte International ECLAIRS2.

681 **Appendix A**

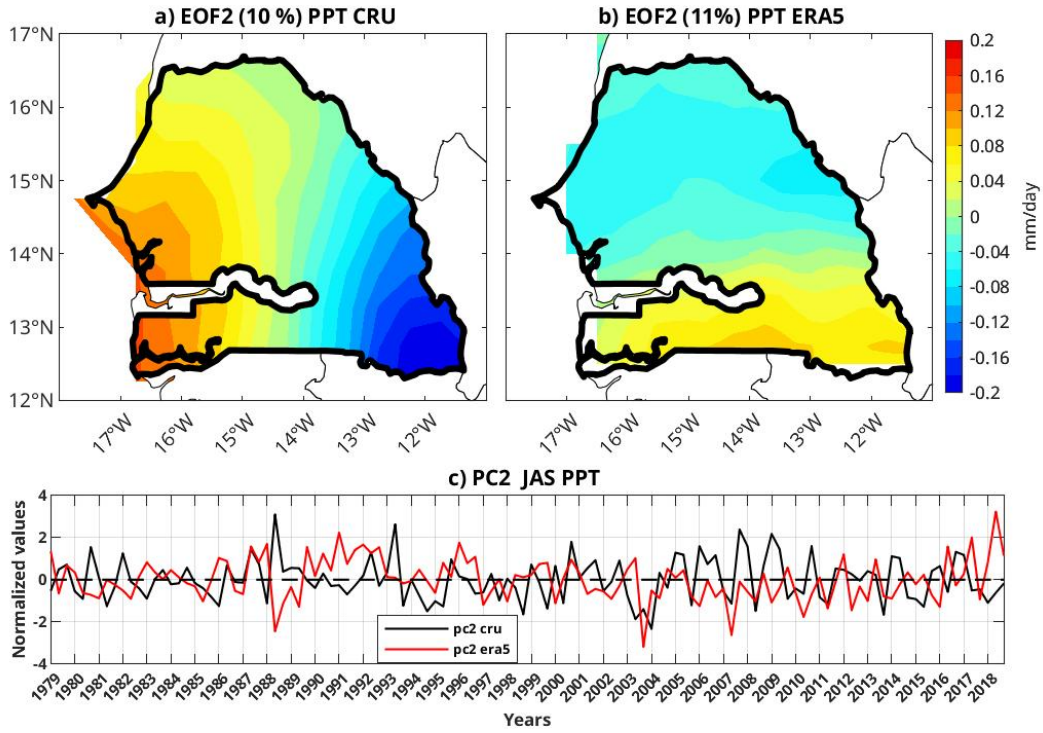


Figure A1. JAS 1979-2018 EOF2 of precipitation (mm/day): a. CRU observations, b. ERA5 reanalyses, and c. corresponding time series (black for CRU and red for ERA5).

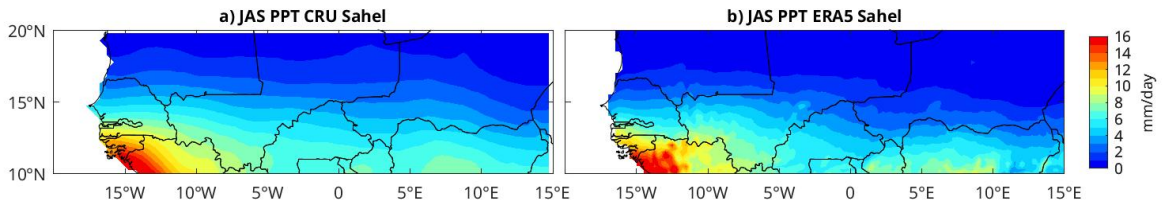


Figure A2. JAS 1978-2018 CRU (left) and ERA5 (right) precipitation.

	EOF1-Sn	EOF1-Sah	EOF2-Sn	EOF2-Sah
CRU	66.1%	41.6%	10%	9.3%
ERA5	48.5%	33%	11%	8.2%

Table A1. Percentage of total variance explained by EOF1 and EOF2 in Senegal and Sahel, using CRU or ERA5 precipitation.

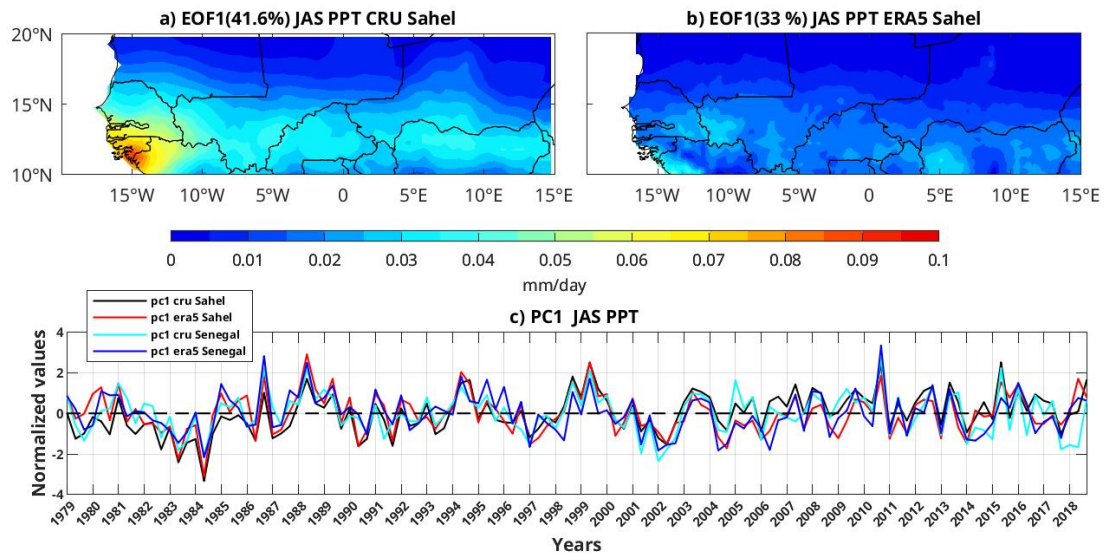


Figure A3. JAS 1979-2018 precipitation, EOF1 over the Sahel (mm/day): a. in CRU observations, b. in ERA5 reanalyses and c. their corresponding time series (CRU in black and ERA5 in red). CRU Senegal (cyan) and ERA5 Senegal (blue) time series are also plotted.

682

683

References

684

Bader, J., & Latif, M. (2003). The impact of decadal-scale indian ocean sea surface temperature anomalies on sahelian rainfall and the north atlantic oscillation. *Geophysical Research Letters*, *30*(22).

685

686

Biasutti, M., Held, I. M., Sobel, A. H., & Giannini, A. (2008). Sst forcings and sahel rainfall variability in simulations of the twentieth and twenty-first centuries.

687

688

Journal of Climate, *21*(14), 3471–3486. doi: 10.1175/2007JCLI1896.1

689

Bonner, W. D. (1968). Climatology of the low level jet. *Monthly Weather Review*, *96*(12), 833–850. doi: 10.1175/1520-0493(1968)096<0833:COTLLJ>2.0.CO;2

690

691

Cabos, W., de la Vara, A., & Koseki, S. (2019). Tropical atlantic variability: Observations and modeling. *Atmosphere*, *10*(9). Retrieved from <https://www.mdpi.com/2073-4433/10/9/502>

692

693

Cadet, D. L., & Nnoli, N. O. (1987). Water vapour transport over africa and the atlantic ocean during summer 1979. *Quarterly Journal of the Royal Meteorological Society*, *113*(476), 581–602. doi: 10.1002/qj.49711347609

694

695

Camberlin, P., & Diop, M. (1999). Inter-relationships between groundnut yield in senegal, interannual rainfall variability and sea-surface temperatures. *Theoretical and Applied Climatology*, *63*(3), 163–181. doi: 10.1007/s007040050101

696

697

Camberlin, P., Janicot, S., & Poccarr, I. (2001). Seasonality and atmospheric dynamics of the teleconnection between african rainfall and tropical sea-surface temperature: Atlantic vs. enso. *International Journal of Climatology*, *21*(8), 973–1005. doi: 10.1002/joc.673

698

699

Caminade, C., & Terray, L. (2010). Twentieth century sahel rainfall variability as simulated by the arpege agcm, and future changes. *Climate Dynamics*, *35*(1432-0894).

700

701

Caniaux, G., Giordani, H., Redelsperger, J.-L., Guichard, F., Key, E., & Wade, M. (2011). Coupling between the atlantic cold tongue and the west african monsoon in boreal spring and summer. *Journal of Geophysical Research: Oceans*, *116*(C4).

702

703

Cook, K. H. (1999). Generation of the african easterly jet and its role in determining west african precipitation. *Journal of Climate*, *12*(5), 1165 - 1184.

704

705

de Coëtlogon, G., Janicot, S., & Lazar, A. (2010). Intraseasonal variability of the ocean—atmosphere coupling in the gulf of guinea during boreal spring and summer. *Quarterly Journal of the Royal Meteorological Society*, *136*, 426–441. doi: 10.1002/qj.554

706

707

de Coëtlogon, G., Leduc-Leballeur, M., Meynadier, R., Bastin, S., Diakhaté, M., Eymard, L., . . . Lazar, A. (2014). Atmospheric response to sea-surface temperature in the eastern equatorial atlantic at quasi-biweekly time-scales. *Quarterly Journal of the Royal Meteorological Society*, *140*(682). doi: 10.1002/qj.2250

708

709

Dezfuli, A. K., & Nicholson, S. E. (2011). A note on long-term variations of the african easterly jet. *International Journal of Climatology*, *31*(13), 2049–2054. doi: 10.1002/joc.2209

710

711

Diakhate, M., Rodriguez-Fonseca, B., Gomara, I., Mohino, E., Dieng, A. L., & Gaye, A. T. (2019). Oceanic forcing on interannual variability of sahel heavy and moderate daily rainfall. *Journal of Hydrometeorology*, *20*(3). doi: 10.1175/JHM-D-18-0035.1

712

713

Diakhaté, M., Lazar, A., de Coëtlogon, G., & Gaye, A. T. (2018). Do sst gradients drive the monthly climatological surface wind convergence over the tropical atlantic? *International Journal of Climatology*, *38*, e955–e965. doi: 10.1002/joc.5422

714

715

Diakhaté, M., Suárez-Moreno, R., Gómara, I., & Mohino, E. (2020). Statistical-observational analysis of skillful oceanic predictors of heavy daily precipitation events in the sahel. *Atmosphere*, *11*(6), 584. doi: 10.3390/atmos11060584

716

717

Diallo, I., Sylla, M. B., Camara, M., & Gaye, A. T. (2013). Interannual variability of rainfall over the sahel based on multiple regional climate models simulations.

718

719

- 738 *Theoretical and Applied Climatology*, 113(1). doi: 10.1007/s00704-012-0791-y
- 739 Diatta, S., & Fink, A. H. (2014). Statistical relationship between remote climate indices and west african monsoon variability. *International Journal of Climatology*, 34(12), 3348–3367. doi: 10.1002/joc.3912
- 740 indices and west african monsoon variability. *International Journal of Climatology*, 34(12), 3348–3367. doi: 10.1002/joc.3912
- 741
- 742 Dommenges, D., & Latif, M. (2000). Interannual to decadal variability in the tropical atlantic. *Journal of Climate*, 13(4), 777–792. doi: 10.1175/1520-0442(2000)013<0777:ITDVT>2.0.CO;2
- 743
- 744
- 745 Fall, S., Semazzi, F. H. M., Dutta, D., Niyogi, S., Anyah, R. O., & Bowden, J. (2006). The spatiotemporal climate variability over senegal and its relationship to global climate. *International Journal of Climatology*, 26(14), 2057–2076. doi: 10.1002/joc.1355
- 746
- 747
- 748
- 749 Folland, C., Palmer, T., & Parker, D. (1986). Sahel rainfall and worldwide sea temperatures, 1901–85. *Nature*, 320(6063), 602–607. doi: 10.1038/320602a0
- 750
- 751 Foltz, G. R., & McPhaden, M. J. (2006). The role of oceanic heat advection in the evolution of tropical north and south atlantic sst anomalies. *Journal of Climate*, 19(19), 6122–6138. doi: 10.1175/JCLI3961.1
- 752
- 753
- 754 Fontaine, B., Gaetani, M., Ullmann, A., & Roucou, P. (2011). Time evolution of observed july-september sea surface temperature-sahel climate teleconnection with removed quasi-global effect (1900–2008). *Journal of Geophysical Research-Atmospheres*, 116, D04105. doi: 10.1029/2010JD014843
- 755
- 756
- 757
- 758 Fontaine, B., Garcia-Serrano, J., Roucou, P., Rodriguez-Fonseca, B., Losada, T., Chauvin, F., ... Janicot, S. (2009). Impacts of warm and cold situations in the mediterranean basins on the west african monsoon: observed connection patterns (1979–2006) and climate simulations. *Climate Dynamics*, 35(1), 95–114. doi: 10.1007/s00382-009-0599-3
- 759
- 760
- 761
- 762
- 763 Fontaine, B., & Janicot, S. (1996). Sea surface temperature fields associated with west african rainfall anomaly types. *Journal of Climate*, 9(11), 2935–2940. doi: 10.1175/1520-0442(1996)009<2935:SSTFAW>2.0.CO;2
- 764
- 765
- 766 Gaetani, M., Fontaine, B., Roucou, P., & Baldi, M. (2010). Influence of the mediterranean sea on the west african monsoon: Intraseasonal variability in numerical simulations. *Journal of Geophysical Research: Atmospheres*, 115. doi: 10.1029/2010JD014436
- 767
- 768
- 769
- 770 Giannini, A., Saravanan, R., & Chang, P. (2003). Oceanic forcing of sahel rainfall on interannual to interdecadal time scales. *Science*, 302(5647), 1027–1030. doi: 10.1126/science.1089357
- 771
- 772
- 773 Gomara, I., Mohino, E., Losada, T., Dominguez, M., Suarez-Moreno, R., & Rodriguez-Fonseca, B. (2017). Impact of dynamical regionalization on precipitation biases and teleconnections over west africa. *Climate Dynamics*, 50(11), 4481–4506. doi: 10.1007/s00382-017-3886-4
- 774
- 775
- 776
- 777 Grace, K., & Davenport, F. (2021). Correction to: Climate variability and health in extremely vulnerable communities: investigating variations in surface water conditions and food security in the west african sahel. *Population and Environment*, 42(4), 578–578. doi: 10.1007/s11111-021-00381-x
- 778
- 779
- 780
- 781 Grams, C. M., Jones, S. C., Marsham, J. H., Parker, D. J., Haywood, J. M., & Heuveline, V. (2010). The atlantic inflow to the saharan heat low: observations and modelling. *Quarterly Journal of the Royal Meteorological Society*, 136, 125–140. doi: 10.1002/qj.429
- 782
- 783
- 784
- 785 Grist, J. P., & Nicholson, S. E. (2001). A study of the dynamic factors influencing the rainfall variability in the west african sahel. *Journal of Climate*, 14(7), 1337–1359. doi: 10.1175/1520-0442(2001)014<1337:ASOTDF>2.0.CO;2
- 786
- 787
- 788 Grodsky, S. A. (2003). Near surface westerly wind jet in the atlantic itcz. *Geophysical Research Letters*, 30(19), 2009. doi: 10.1029/2003GL017867
- 789
- 790 Gu, G. (2010). *Summer-time rainfall variability in the tropical atlantic* (S. W. Simard & M. E. Austin, Eds.). Intech Europe.
- 791
- 792 Gu, G., & Adler, R. F. (2009). Interannual variability of boreal summer rainfall in

- 793 the equatorial atlantic. *International Journal of Climatology*, 29(2), 175–184.
794 doi: 10.1002/joc.1724
- 795 Hagos, S. M., & Cook, K. H. (2008). Ocean warming and late-twentieth-century
796 sahel drought and recovery. *Journal of Climate*, 21(15), 3797–3814. doi: 10
797 .1175/2008JCLI2055.1
- 798 Harris, I., Osborn, T. J., Jones, P., & Lister, D. (2020). Version 4 of the cru ts
799 monthly high-resolution gridded multivariate climate dataset. *Scientific Data*,
800 7(1), 109. doi: 10.1038/s41597-020-0453-3
- 801 Janicot, S., Harzallah, A., Fontaine, B., & Moron, V. (1998). West african monsoon
802 dynamics and eastern equatorial atlantic and pacific sst anomalies (1970–88).
803 *Journal of Climate*, 11(8), 1874–1882. doi: 10.1175/1520-0442-11.8.1874
- 804 Janicot, S., Trzaska, S., & Pocard, I. (2001). Summer sahel-enso teleconnection and
805 decadal time scale sst variations. *Climate Dynamics*, 18(3), 303–320. doi: 10
806 .1007/s003820100172
- 807 Joly, M., & Voldoire, A. (2009). Influence of enso on the west african monsoon:
808 Temporal aspects and atmospheric processes. *Journal of Climate*, 22(12),
809 3193–3210. doi: 10.1175/2008JCLI2450.1
- 810 Jung, T., Ferranti, L., & Tompkins, A. M. (2006). Response to the summer of
811 2003 mediterranean sst anomalies over europe and africa. *Journal of Climate*,
812 19(20), 5439–5454. doi: 10.1175/JCLI3916.1
- 813 Kante, I. K., Sall, S. M., Badiane, D., Diouf, I., Dieng, A. L., Diaby, I., & Guichard,
814 F. (2020). Analysis of rainfall dynamics in conakry, republic of guinea. *Atmo-
815 spheric and Climate Sciences*, 10(1), 1. doi: 10.4236/acs.2020.101001
- 816 Lavaysse, C., Flamant, C., Janicot, S., Parker, D. J., Lafore, J.-P., Sultan, B.,
817 & Pelon, J. (2009). Seasonal evolution of the west african heat low:
818 a climatological perspective. *Climate Dynamics*, 33(2), 313–330. doi:
819 10.1007/s00382-009-0553-4
- 820 Le Barbé, L., & Lebel, T. (1997). Rainfall climatology of the hapex-sahel region dur-
821 ing the years 1950–1990. *Journal of hydrology*, 188, 43–73.
- 822 Lebel, T., Diedhiou, A., & Laurent, H. (2003). Seasonal cycle and interannual vari-
823 ability of the sahelian rainfall at hydrological scales. *Journal of Geophysical
824 Research: Atmospheres*, 108. doi: 10.1029/2001JD001580
- 825 Lindzen, R. S., & Nigam, S. (1987). On the role of sea surface temperature gradients
826 in forcing low-level winds and convergence in the tropics. *Journal of the Atmo-
827 spheric Sciences*, 44(17), 2418–2436. doi: 10.1175/1520-0469(1987)044<2418:
828 OTROSS>2.0.CO;2
- 829 Liu, W., Cook, K. H., & Vizzy, E. K. (2020). Role of the west african westerly jet in
830 the seasonal and diurnal cycles of precipitation over west africa. *Climate Dy-
831 namics*, 54(1), 843–861. doi: 10.1007/s00382-019-05035-1
- 832 Liu, Y., Chiang, J. C. H., Chou, C., & Patricola, C. M. (2014). Atmospheric tele-
833 connection mechanisms of extratropical north atlantic sst influence on sahel
834 rainfall. *Climate Dynamics*, 43, 2797 - 2811.
- 835 Losada, T., Rodríguez-Fonseca, B., Polo, I., Janicot, S., Gervois, S., Chauvin,
836 F., & Ruti, P. (2010). Tropical response to the atlantic equatorial mode:
837 Agcm multimodel approach. *Climate Dynamics*, 35(1), 45–52. doi:
838 10.1007/s00382-009-0624-6
- 839 Lélé, M. I., Leslie, L. M., & Lamb, P. J. (2015). Analysis of low-level atmospheric
840 moisture transport associated with the west african monsoon. *Journal of Cli-
841 mate*, 28(11), 4414–4430. doi: 10.1175/JCLI-D-14-00746.1
- 842 Meynadier, R., de Coëtlogon, G., Leduc-Leballeur, M., Eymard, L., & Janicot, S.
843 (2016). Seasonal influence of the sea surface temperature on the low atmo-
844 spheric circulation and precipitation in the eastern equatorial atlantic. *Climate
845 Dynamics*, 47(1432-0894).
- 846 Mo, K., Bell, G. D., & Thiaw, W. M. (2001). Impact of sea surface temper-
847 ature anomalies on the atlantic tropical storm activity and west african

- 848 rainfall. *Journal of the Atmospheric Sciences*, 58(22), 3477–3496. doi:
849 10.1175/1520-0469(2001)058<3477:IOSSTA>2.0.CO;2
- 850 Mohino, E., Rodríguez-Fonseca, B., Mechoso, C. R., Gervois, S., Ruti, P., & Chau-
851 vin, F. (2011). Impacts of the tropical pacific/indian oceans on the seasonal
852 cycle of the west african monsoon. *Journal of Climate*, 24(15), 3878–3891. doi:
853 10.1175/2011JCLI3988.1
- 854 Monerie, P.-A., Sanchez-Gomez, E., Gaetani, M., Mohino, E., & Dong, B. (2020).
855 Future evolution of the sahel precipitation zonal contrast in cesm1. *Climate*
856 *Dynamics*, 55, 2801–2821.
- 857 Moron, V., Robertson, A. W., & Ward, M. N. (2006). Seasonal predictability and
858 spatial coherence of rainfall characteristics in the tropical setting of senegal.
859 *Monthly Weather Review*, 134(11), 3248–3262. doi: 10.1175/MWR3252.1
- 860 Moron, V., & Ward, M. N. (1998). Enso teleconnections with climate variability
861 in the european and african sectors. *Weather*, 53(9), 287–295. doi: 10.1002/j
862 .1477-8696.1998.tb06403.x
- 863 Nicholson, S. E. (2013). The west african sahel: A review of recent studies on the
864 rainfall regime and its interannual variability. *International Scholarly Research*
865 *Notices*, 2013.
- 866 Nicholson, S. E., & Palao, I. (1993). A reevaluation of rainfall variability in the sahel
867 .1. characteristics of rainfall fluctuations. *International Journal of Climatology*,
868 13(4), 371–389. doi: 10.1002/joc.3370130403
- 869 Paeth, H., & Friederichs, P. (2004). Seasonality and time scales in the relationship
870 between global sst and african rainfall. *Climate Dynamics*, 23(7), 815–837.
871 doi: 10.1007/s00382-004-0466-1
- 872 Park, J.-Y., Bader, J., & Matei, D. (2015). Northern-hemispheric differential
873 warming is the key to understanding the discrepancies in the projected sahel
874 rainfall. *Nature Communications*, 6. doi: 10.1038/ncomms6985
- 875 Parker, D., & Diop-Kane, M. (2017). *Meteorology of tropical west africa: The fore-*
876 *casters' handbook*. John Wiley & Sons, Ltd.
- 877 Polo, I., Rodriguez-Fonseca, B., Losada, T., & Garcia-Serrano, J. (2008). Trop-
878 ical atlantic variability modes (1979–2002). part i: Time-evolving sst modes
879 related to west african rainfall. *Journal of Climate*, 21(24), 6457–6475. doi:
880 10.1175/2008JCLI2607.1
- 881 Pu, B., & Cook, K. H. (2010). Dynamics of the west african westerly jet. *Journal of*
882 *Climate*, 23(23), 6263–6276. doi: 10.1175/2010JCLI3648.1
- 883 Pu, B., & Cook, K. H. (2011). Role of the west african westerly jet in sahel rain-
884 fall variations. *Journal of Climate*, 25(8), 2880–2896. doi: 10.1175/JCLI-D-11
885 -00394.1
- 886 Pu, B., & Cook, K. H. (2012). Role of the west african westerly jet in sahel rain-
887 fall variations. *Journal of Climate*, 25(8), 2880–2896. doi: 10.1175/JCLI-D-11
888 -00394.1
- 889 Quagraine, K. A., Nkrumah, F., Klein, C., Klutse, N. A. B., & Quagraine, K. T.
890 (2020). West african summer monsoon precipitation variability as represented
891 by reanalysis datasets. *Climate*, 8(10), 111. doi: 10.3390/cli8100111
- 892 Rodríguez-Fonseca, B., Janicot, S., Mohino, E., Losada, T., Bader, J., Caminade,
893 C., . . . Voltaire, A. (2011). Interannual and decadal sst-forced responses of
894 the west african monsoon. *Atmospheric Science Letters*, 12(1), 67–74. doi:
895 10.1002/asl.308
- 896 Rowell, D. P. (2001). Teleconnections between the tropical pacific and the sahel.
897 *Quarterly Journal of the Royal Meteorological Society*, 127(575), 1683–1706.
898 doi: 10.1002/qj.49712757512
- 899 Rowell, D. P. (2003). The impact of mediterranean ssts on the sahelian rainfall
900 season. *Journal of Climate*, 16(5), 849–862. doi: 10.1175/1520-0442(2003)
901 016<0849:TIOMSO>2.0.CO;2
- 902 Rowell, D. P., Folland, C., Maskell, K., & Ward, M. (1995). Variability of summer

- 903 rainfall over tropical north-africa (1906-92) - observations and modeling. *Quar-*
 904 *terly Journal of the Royal Meteorological Society*, 121(523), 669–704. doi: 10
 905 .1002/qj.49712152311
- 906 Rust, H. W., Vrac, M., Sultan, B., & Lengaigne, M. (2013). Mapping weather-
 907 type influence on senegal precipitation based on a spatial-temporal sta-
 908 tistical model. *Journal of Climate*, 26(20), 8189–8209. doi: 10.1175/
 909 JCLI-D-12-00302.1
- 910 Semazzi, F., Mehta, V., & Sud, Y. (1988). An investigation of the relationship be-
 911 tween sub-saharan rainfall and global sea surface temperatures. *Atmosphere-*
 912 *Ocean*, 26(1), 118–138. doi: 10.1080/07055900.1988.9649293
- 913 Steinig, S., Harlass, J., Park, W., & Latif, M. (2018). Sahel rainfall strength and
 914 onset improvements due to more realistic atlantic cold tongue development in
 915 a climate model. *Scientific Reports*, 8(2569).
- 916 Stensrud, D. J. (1996). Importance of low-level jets to climate: A review. *Journal*
 917 *of Climate*, 9(8), 1698–1711. doi: 10.1175/1520-0442(1996)009<1698:IOLLJT>2
 918 .0.CO;2
- 919 Sultan, B., & Janicot, S. (2000). Abrupt shift of the itcz over west africa and intra-
 920 seasonal variability. *Geophysical Research Letters*, 27(20), 3353–3356. doi: 10
 921 .1029/1999GL011285
- 922 Sultan, B., Labadi, K., Guégan, J.-F., & Janicot, S. (2005). Climate drives the
 923 meningitis epidemics onset in west africa. *PLOS Medicine*, 2(1), e6. doi: 10
 924 .1371/journal.pmed.0020006
- 925 Suárez-Moreno, R., Rodríguez-Fonseca, B., Barroso, J. , & Fink, A. (2018). Inter-
 926 decadal changes in the leading ocean forcing of sahelian rainfall interannual
 927 variability: Atmospheric dynamics and role of multidecadal sst background.
 928 *Journal of Climate*. doi: 10.1175/JCLI-D-17-0367.1
- 929 Sylla, M. B., Giorgi, F., Coppola, E., & Mariotti, L. (2013). Uncertainties in daily
 930 rainfall over africa: assessment of gridded observation products and evaluation
 931 of a regional climate model simulation. *International Journal of Climatology*,
 932 33(7), 1805–1817. doi: 10.1002/joc.3551
- 933 Thorncroft, C. D., Nguyen, H., Zhang, C., & Peyrillé, P. (2011). Annual cycle of
 934 the west african monsoon: regional circulations and associated water vapour
 935 transport: Annual cycle of west african monsoon. *Quarterly Journal of the*
 936 *Royal Meteorological Society*, 137(654), 129–147. doi: 10.1002/qj.728
- 937 Vizy, E. K., & Cook, K. H. (2001). Mechanisms by which gulf of guinea and eastern
 938 north atlantic sea surface temperature anomalies can influence african rainfall.
 939 *Journal of Climate*, 14(5), 795–821. doi: 10.1175/1520-0442(2001)014<0795:
 940 MBWGOG>2.0.CO;2
- 941 Von Storch, H., & Zwiers, F. W. (1999). *Statistical analysis in climate research*.
 942 Cambridge University Press. doi: 10.1017/CBO9780511612336
- 943 Wade, M., Mignot, J., Lazar, A., Gaye, A. T., & Carre, M. (2015). On the spatial
 944 coherence of rainfall over the saloum delta (senegal) from seasonal to decadal
 945 time scales. *Frontiers in Earth Science*, 3. doi: 10.3389/feart.2015.00030
- 946 Wang, C. (2019). Three-ocean interactions and climate variability: a review and per-
 947 spective. *Climate Dynamics*, 53, 5119-5136.
- 948 Wang, C., Dong, S., Evan, A. T., Foltz, G. R., & Lee, S.-K. (2012). Multidecadal
 949 covariability of north atlantic sea surface temperature, african dust, sahel
 950 rainfall, and atlantic hurricanes. *Journal of Climate*, 25(15), 5404 - 5415.
- 951 Ward, M. N. (1998). Diagnosis and short-lead time prediction of summer rainfall
 952 in tropical north africa at interannual and multidecadal timescales. *Journal of*
 953 *Climate*, 11(12), 3167–3191. doi: 10.1175/1520-0442(1998)011<3167:DASLTP>2
 954 .0.CO;2
- 955 Weller, E., Shelton, K., Reeder, M. J., & Jakob, C. (2017). Precipitation associated
 956 with convergence lines. *Journal of Climate*, 30(9), 3169 - 3183.
- 957 Worou, K., Goosse, H., Fichet, T., Guichard, F., & Diakhate, M. (2020). In-

- 958 terannual variability of rainfall in the guinean coast region and its links with
959 sea surface temperature changes over the twentieth century for the different
960 seasons. *Climate Dynamics*, 55(3), 449–470. doi: 10.1007/s00382-020-05276-5
961 Xie, S.-P., & Carton, J. (2004). Tropical atlantic variability: Patterns, mechanisms,
962 and impacts. *Earth Clim*, 147. doi: 10.1029/147GM07
963 Yang, C., Leonelli, F. E., Marullo, S., Artale, V., Beggs, H., Nardelli, B. B., ...
964 Pisano, A. (2021). Sea surface temperature intercomparison in the framework
965 of the copernicus climate change service (c3s). *Journal of Climate*, 34(13),
966 5257–5283. doi: 10.1175/JCLI-D-20-0793.1
967 Zebiak, S. (1993, 08). Air–sea interaction in the equatorial atlantic region. *Jour-*
968 *nal of Climate*, 6, 1567-1586. doi: 10.1175/1520-0442(1993)006<1567:AIITEA>2
969 .O.CO;2
970 Zeng, N., Neelin, J. D., Lau, K.-M., & Tucker, C. J. (1999). Enhancement of in-
971 terdecadal climate variability in the sahel by vegetation interaction. *Science*,
972 286(5444), 1537-1540. Retrieved from [https://www.science.org/doi/abs/10](https://www.science.org/doi/abs/10.1126/science.286.5444.1537)
973 .[1126/science.286.5444.1537](https://www.science.org/doi/abs/10.1126/science.286.5444.1537) doi: 10.1126/science.286.5444.1537

Figure 1.

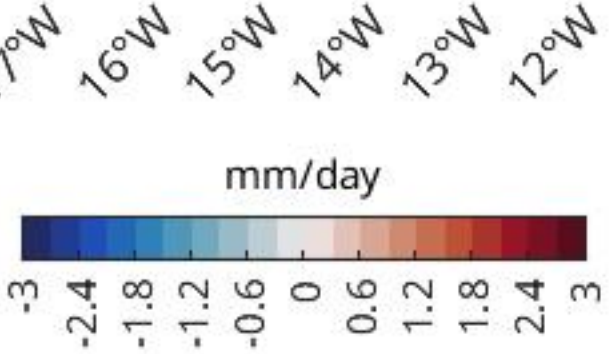
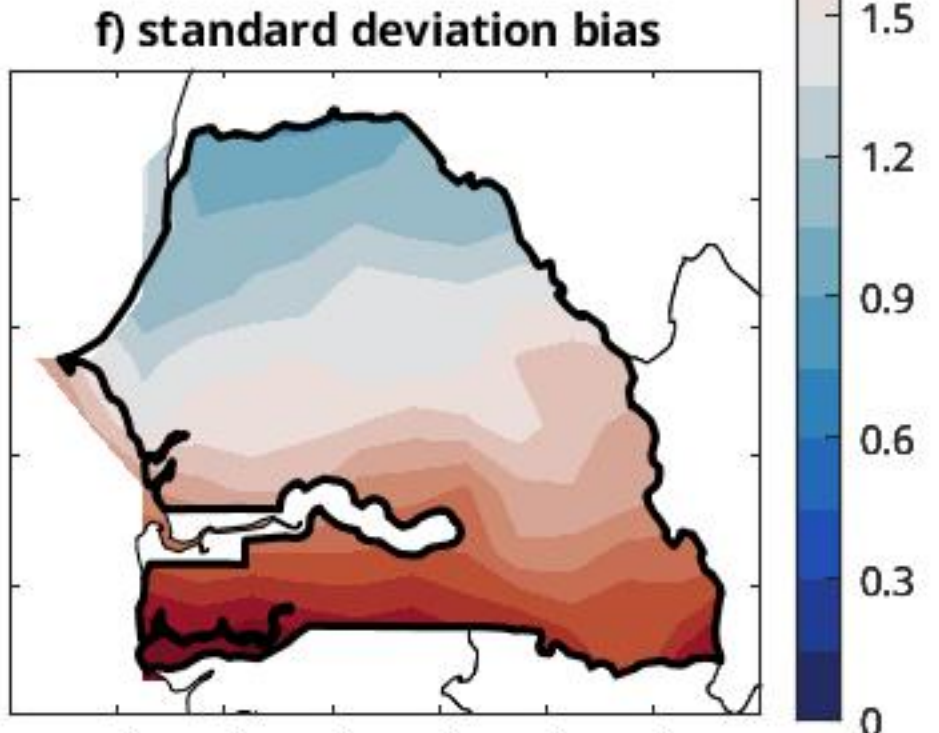
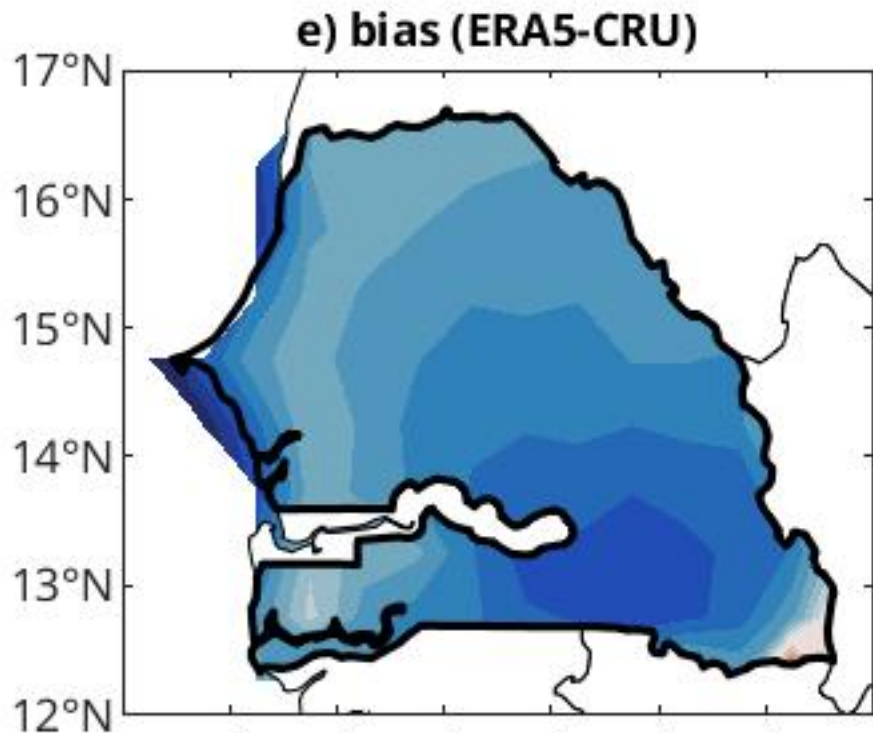
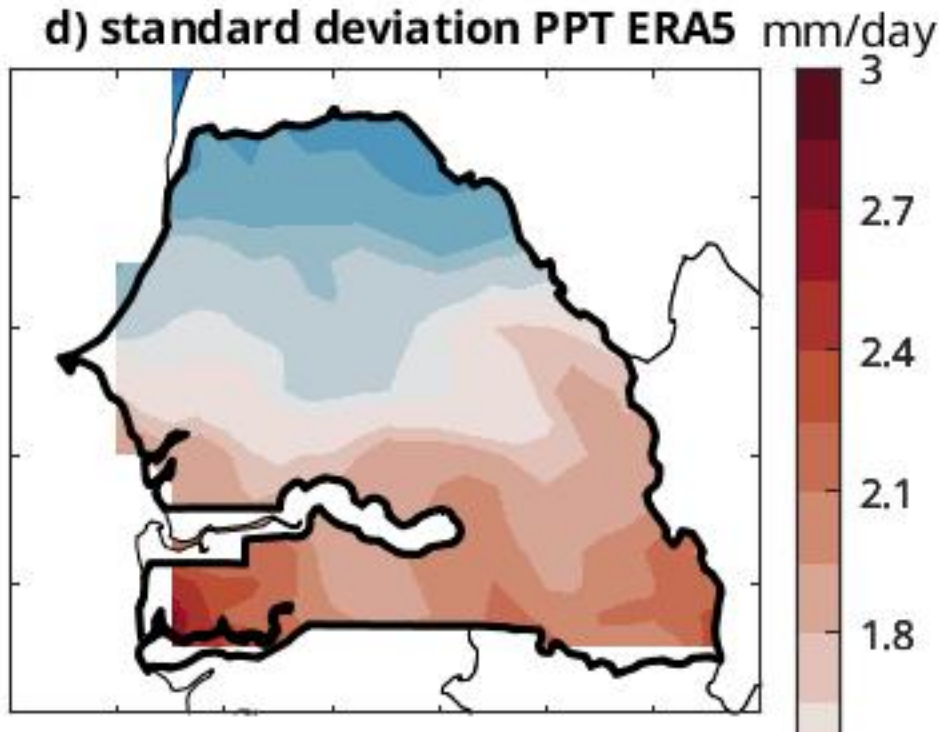
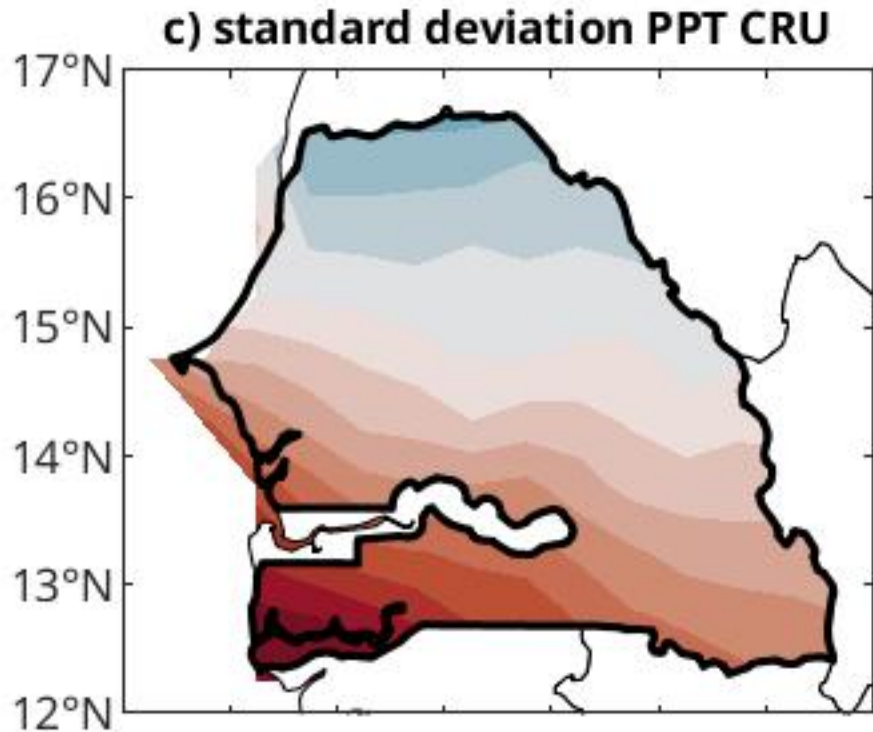
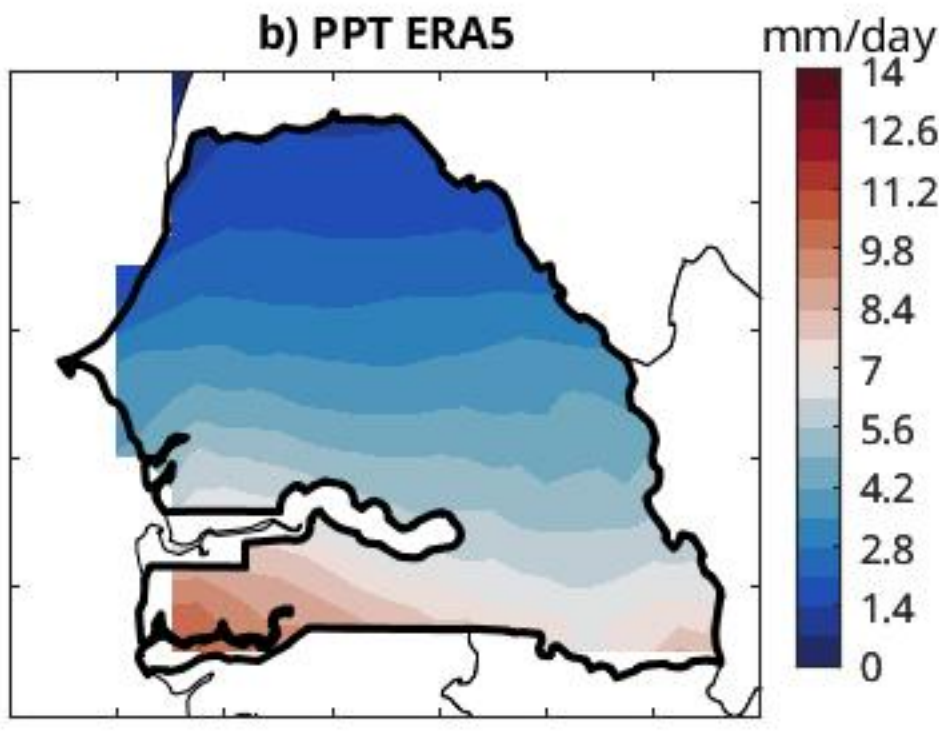
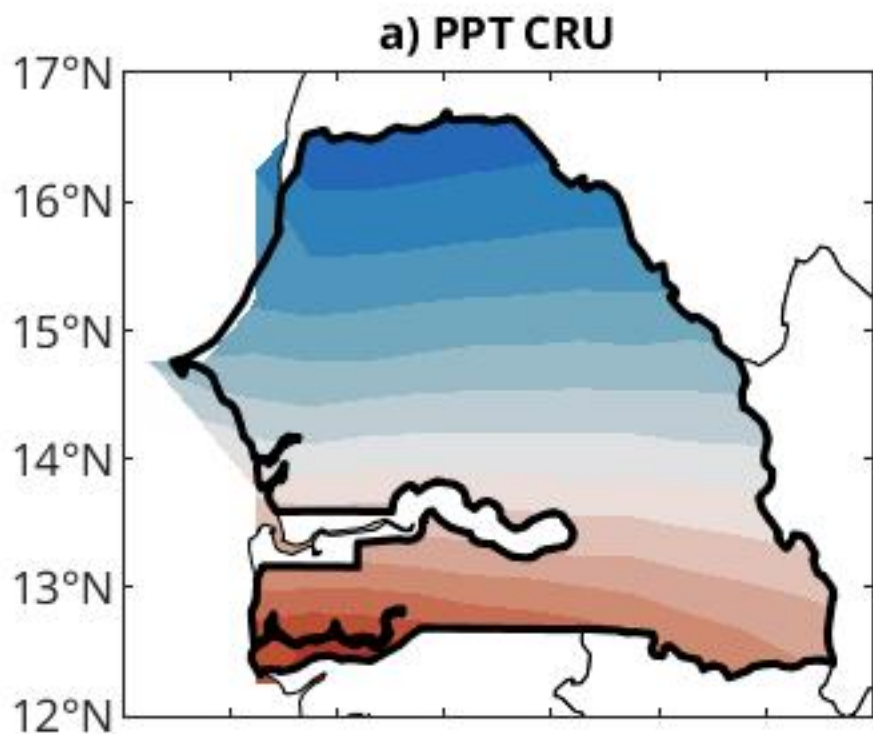


Figure 2.

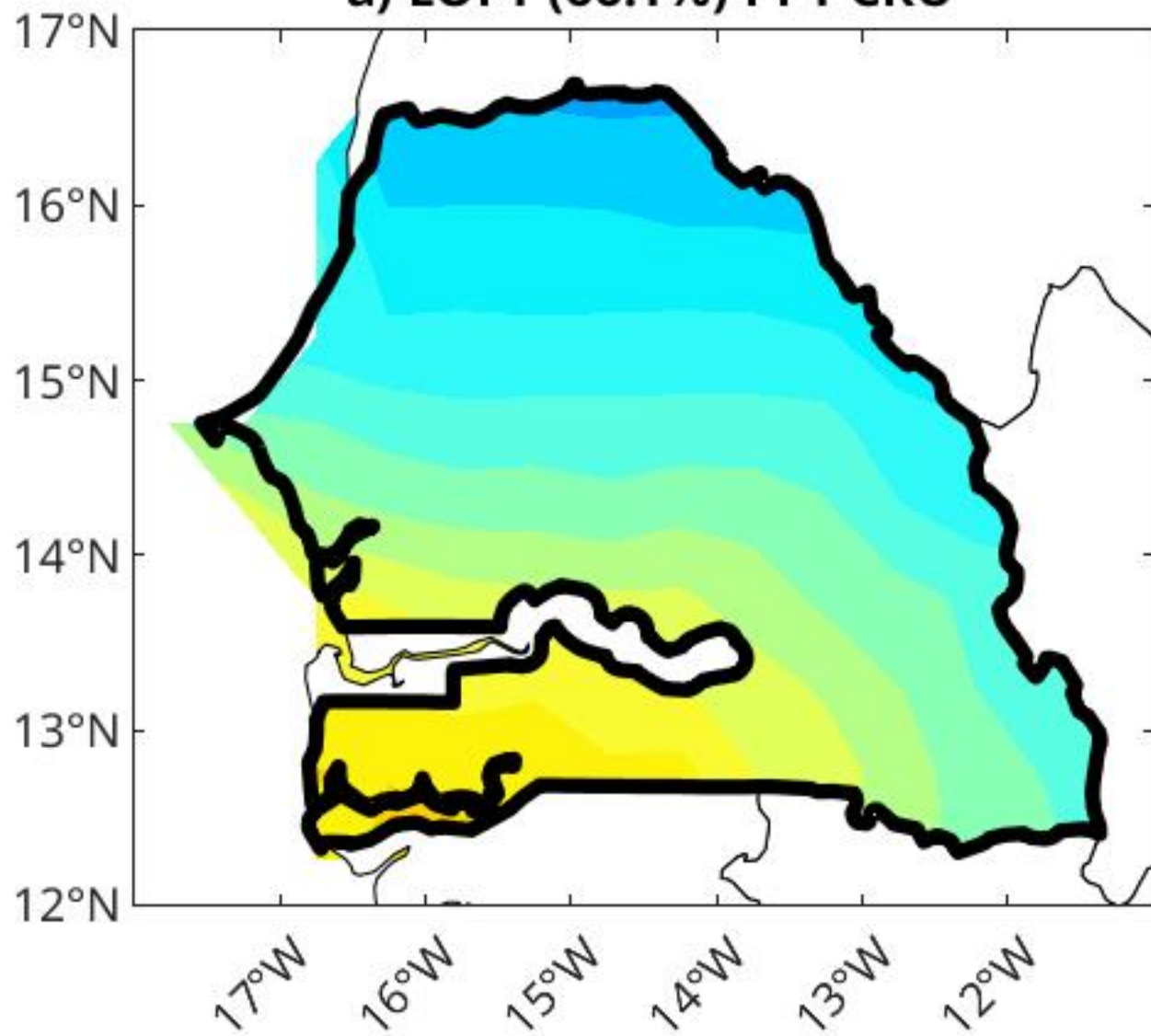
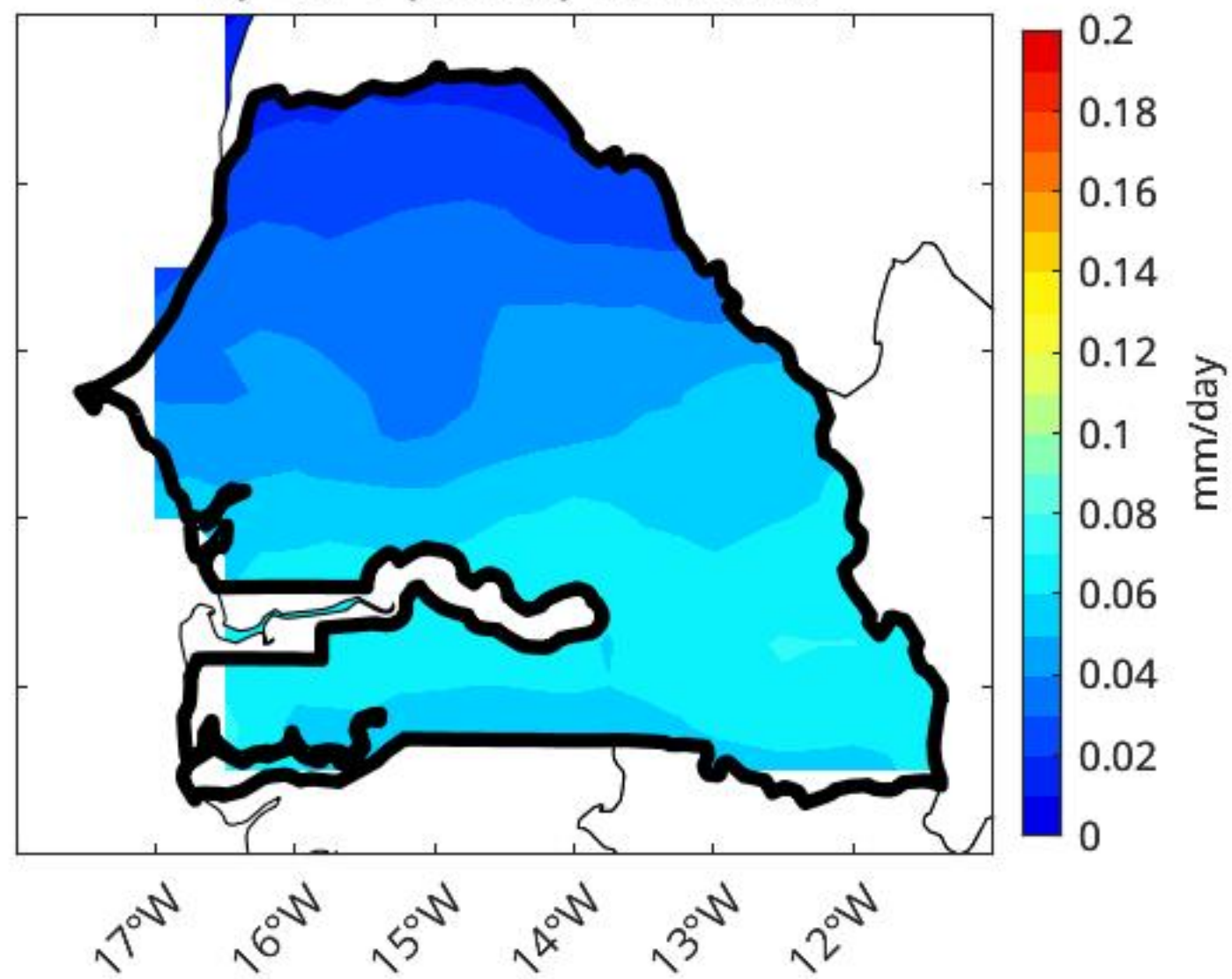
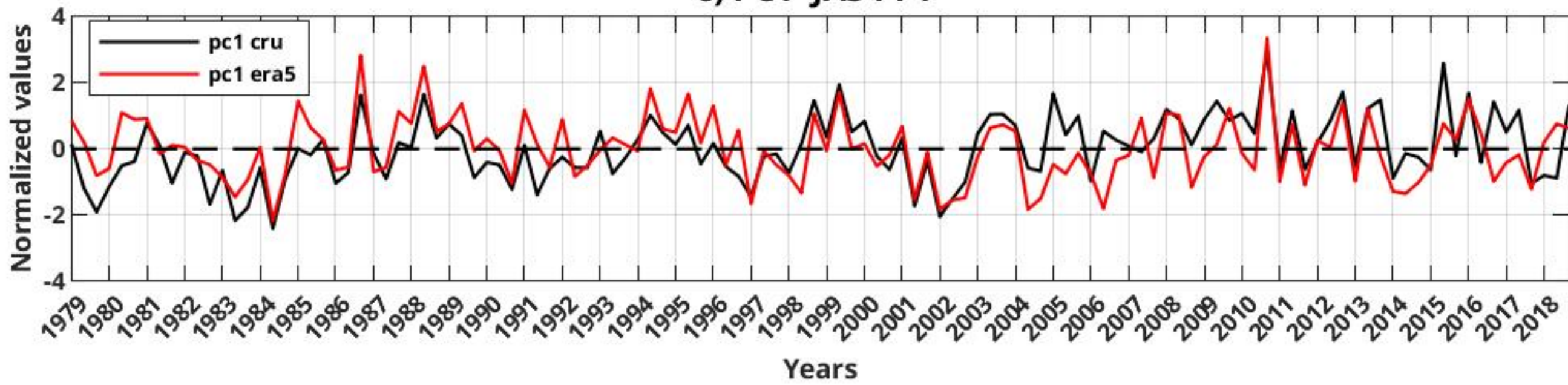
a) EOF1 (66.1%) PPT CRU**b) EOF1 (48.5%) PPT ERA5****c) PC1 JAS PPT**

Figure 3.

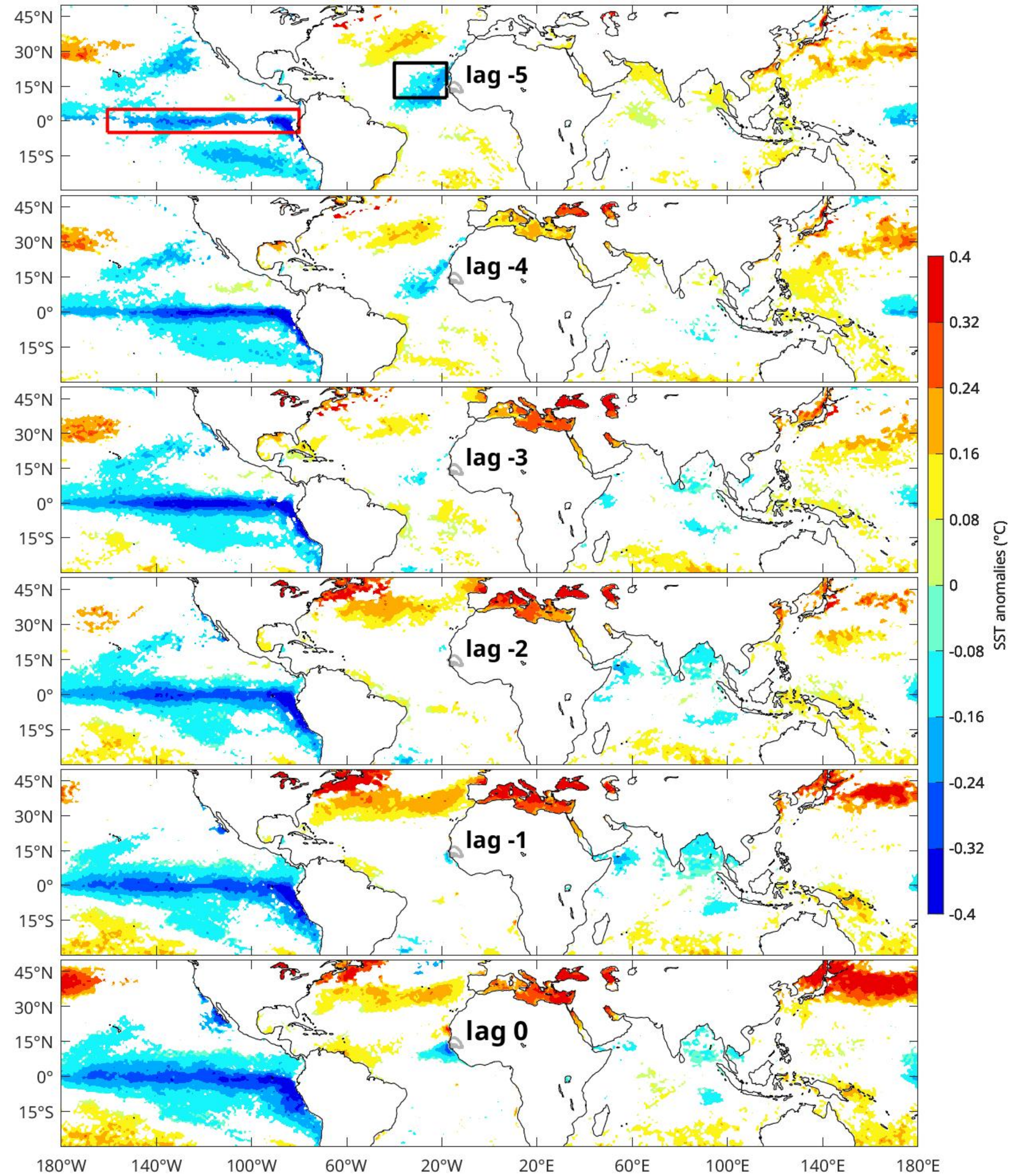


Figure 4.

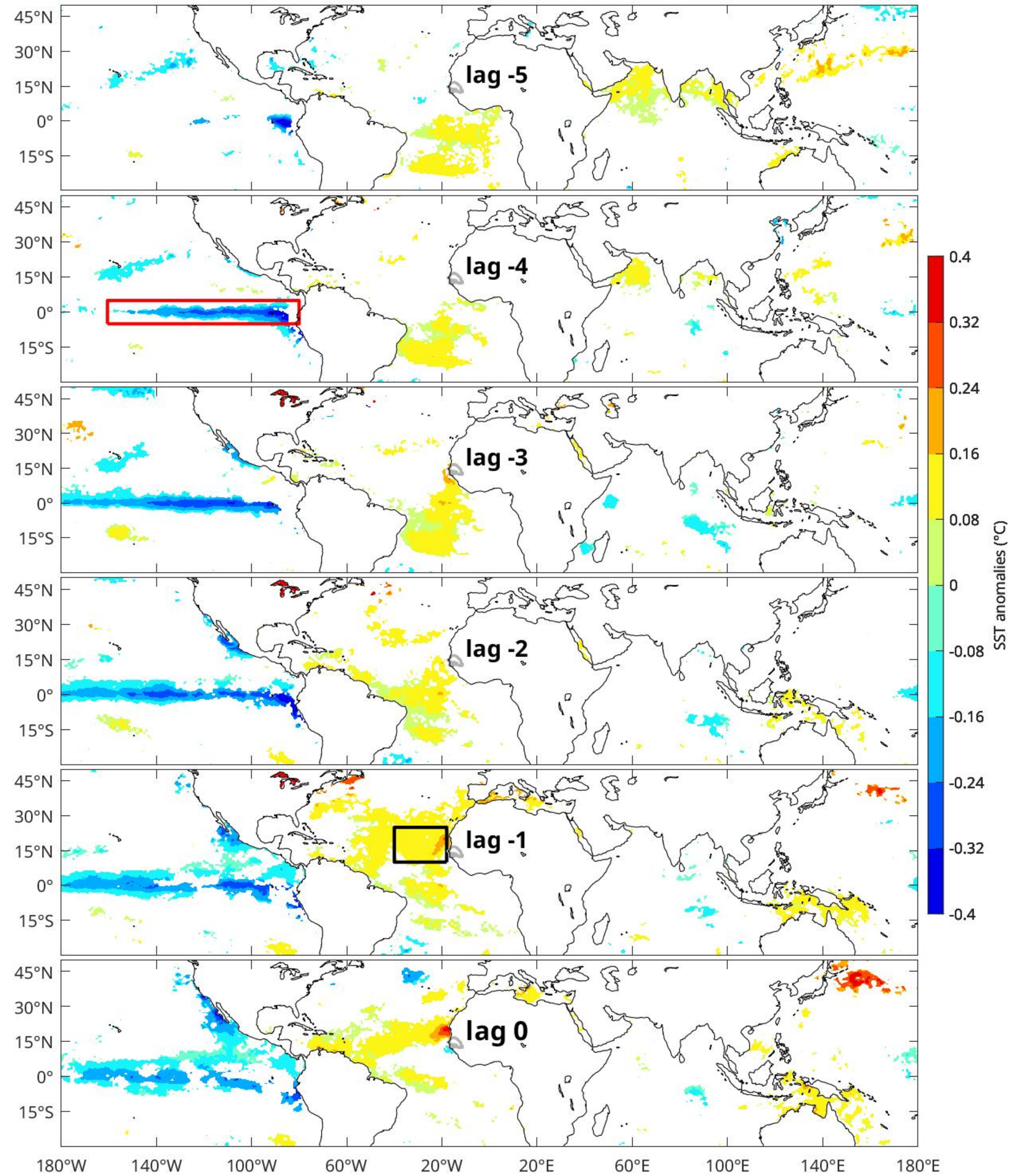
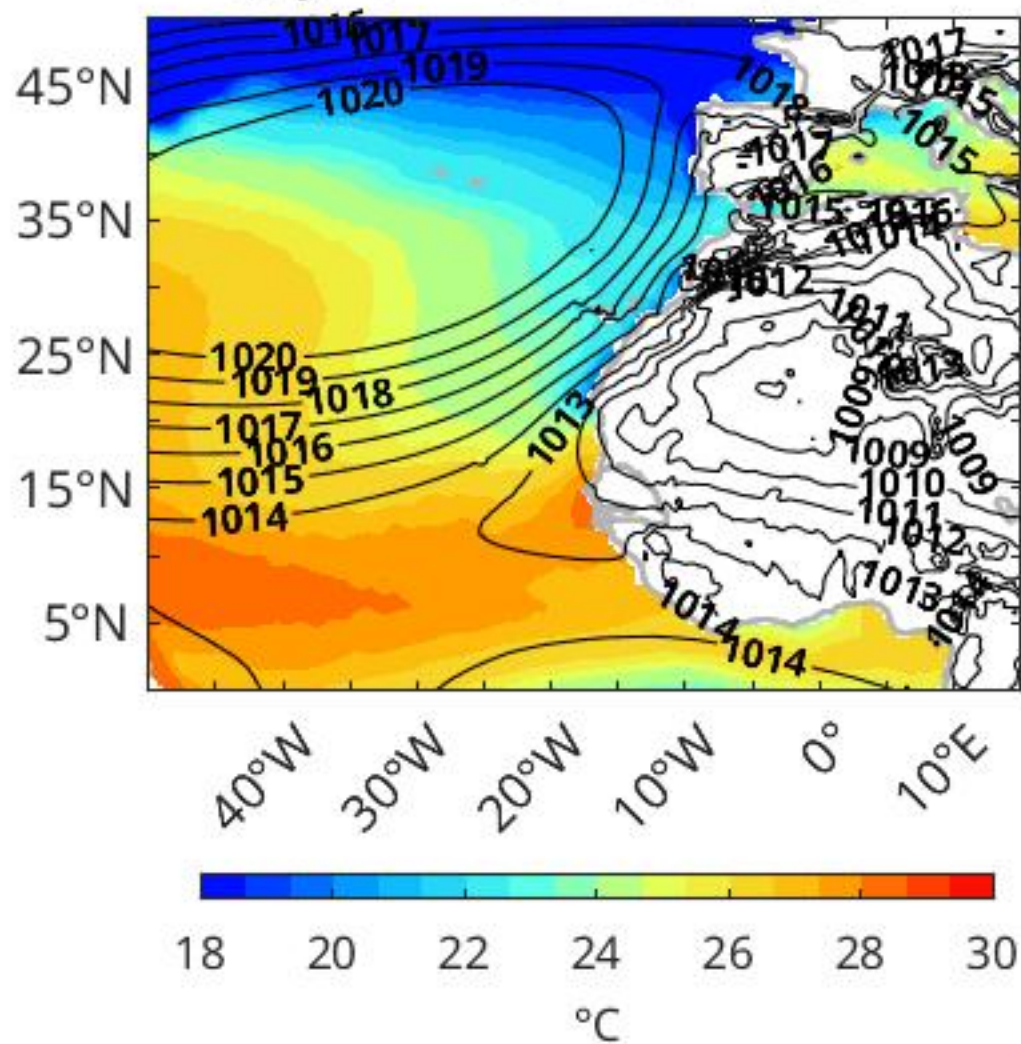


Figure 5.

a) JAS mean SST & SLP



b) JAS mean WIND

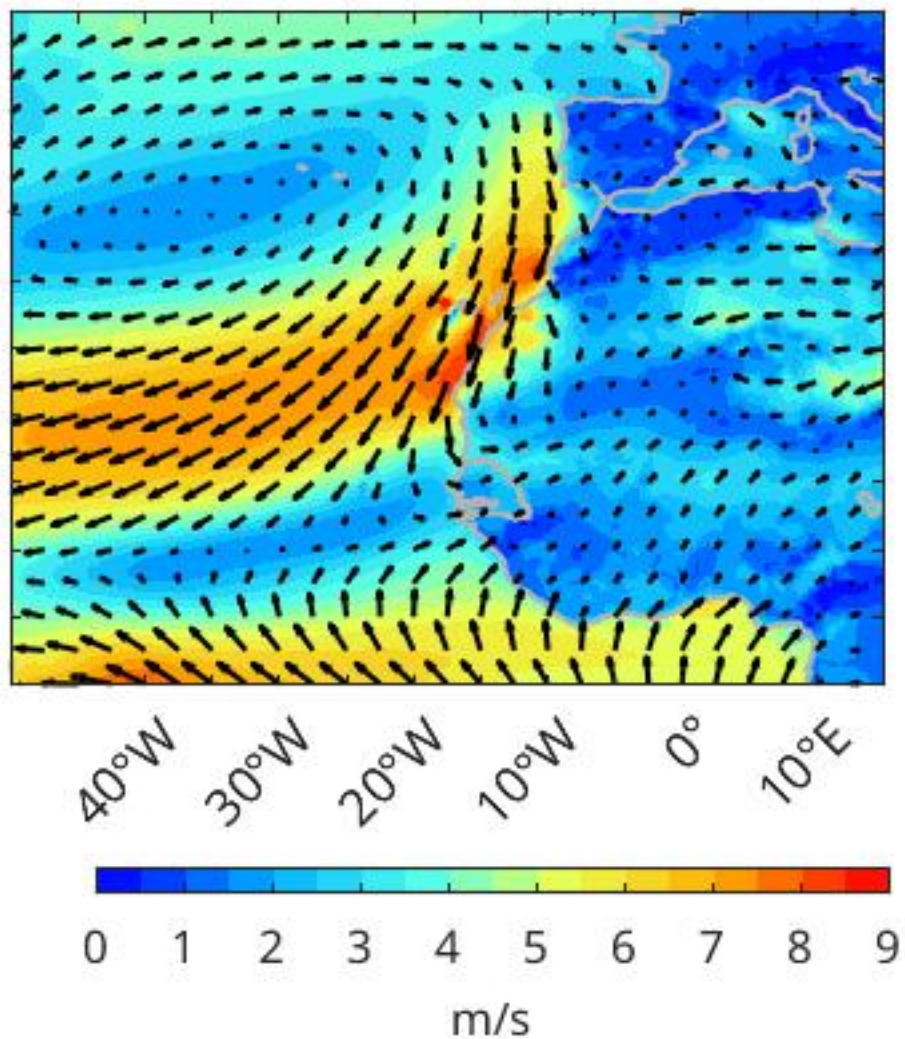


Figure 6.

SST / SLP

10m-wind

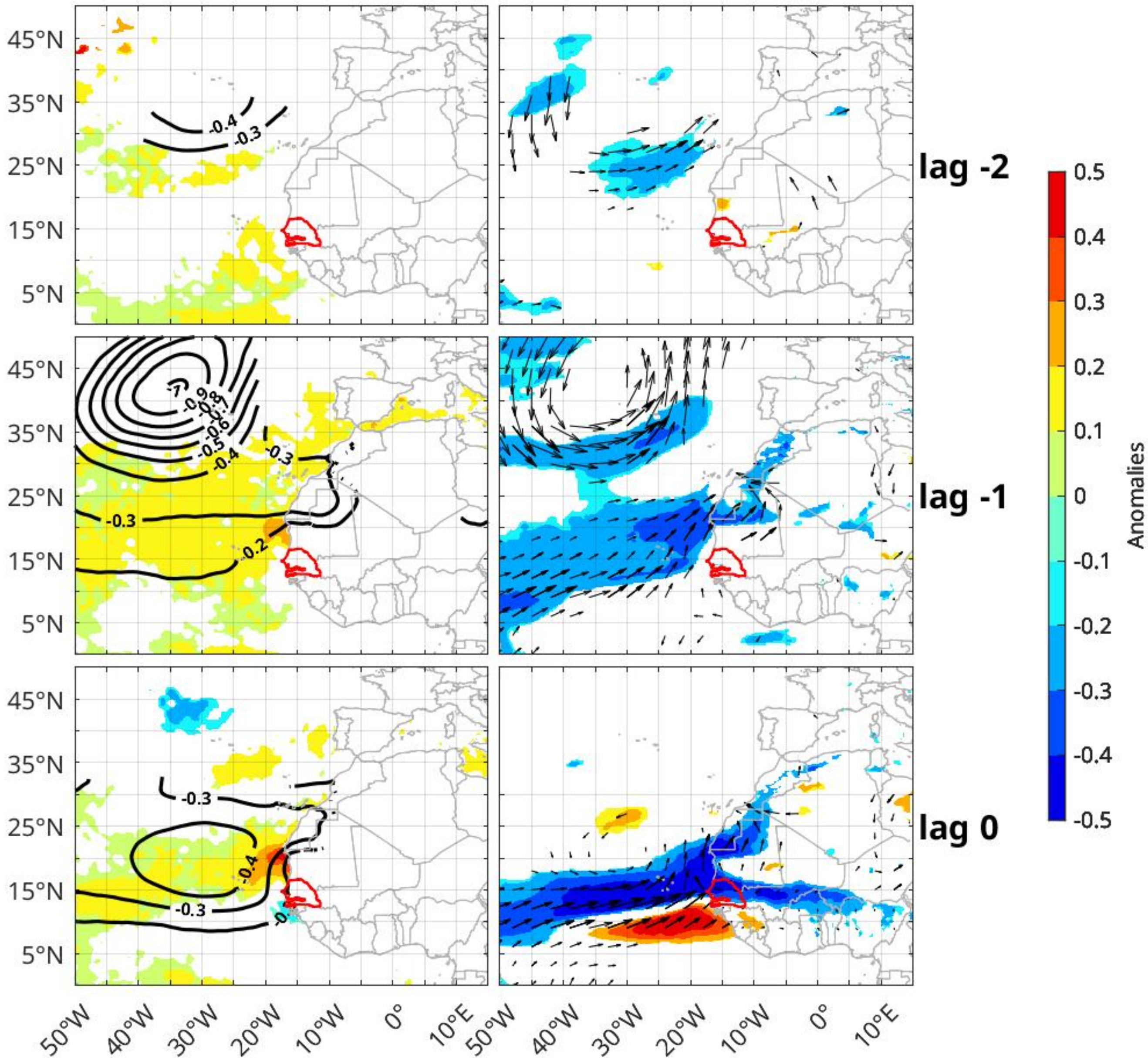
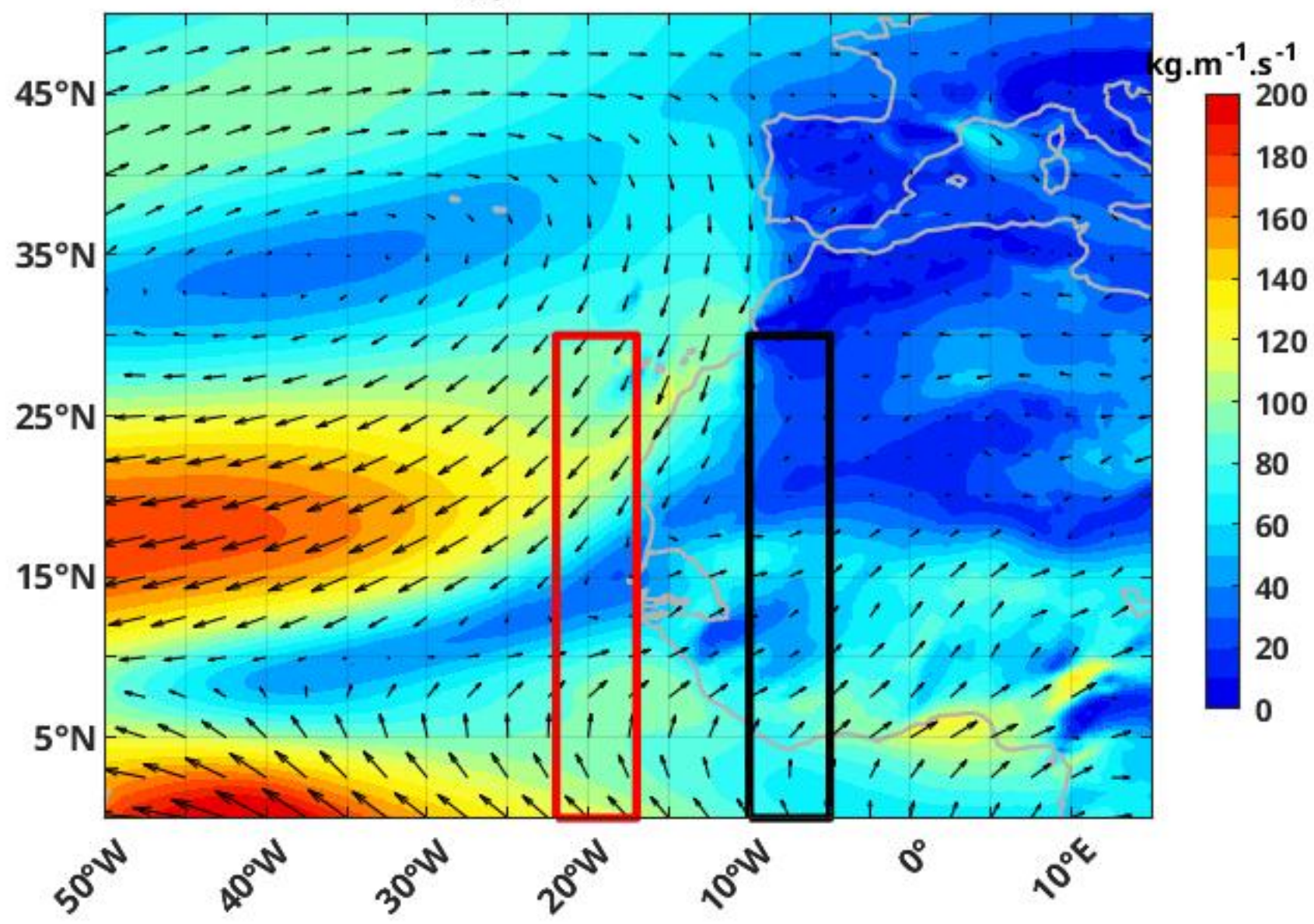
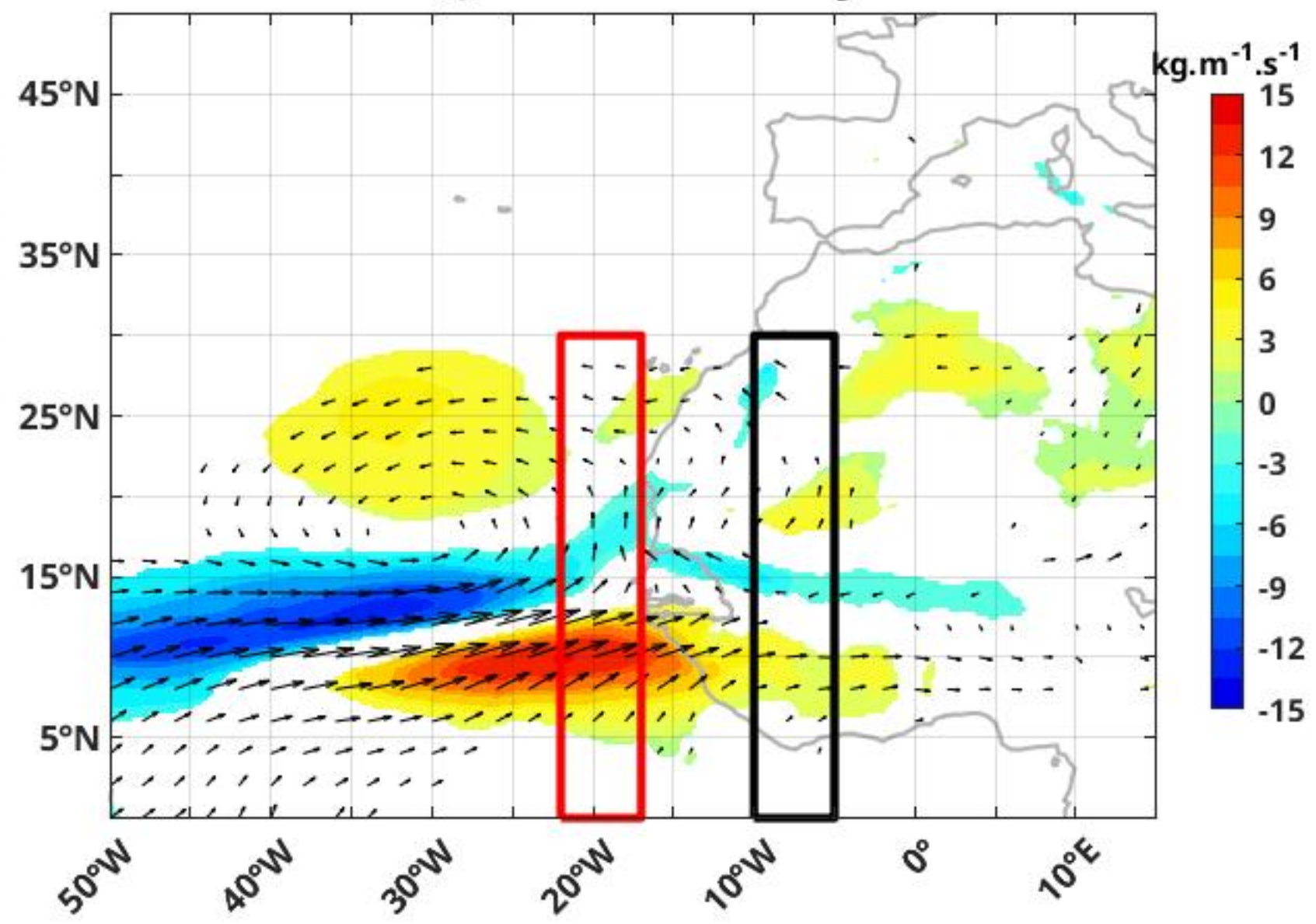
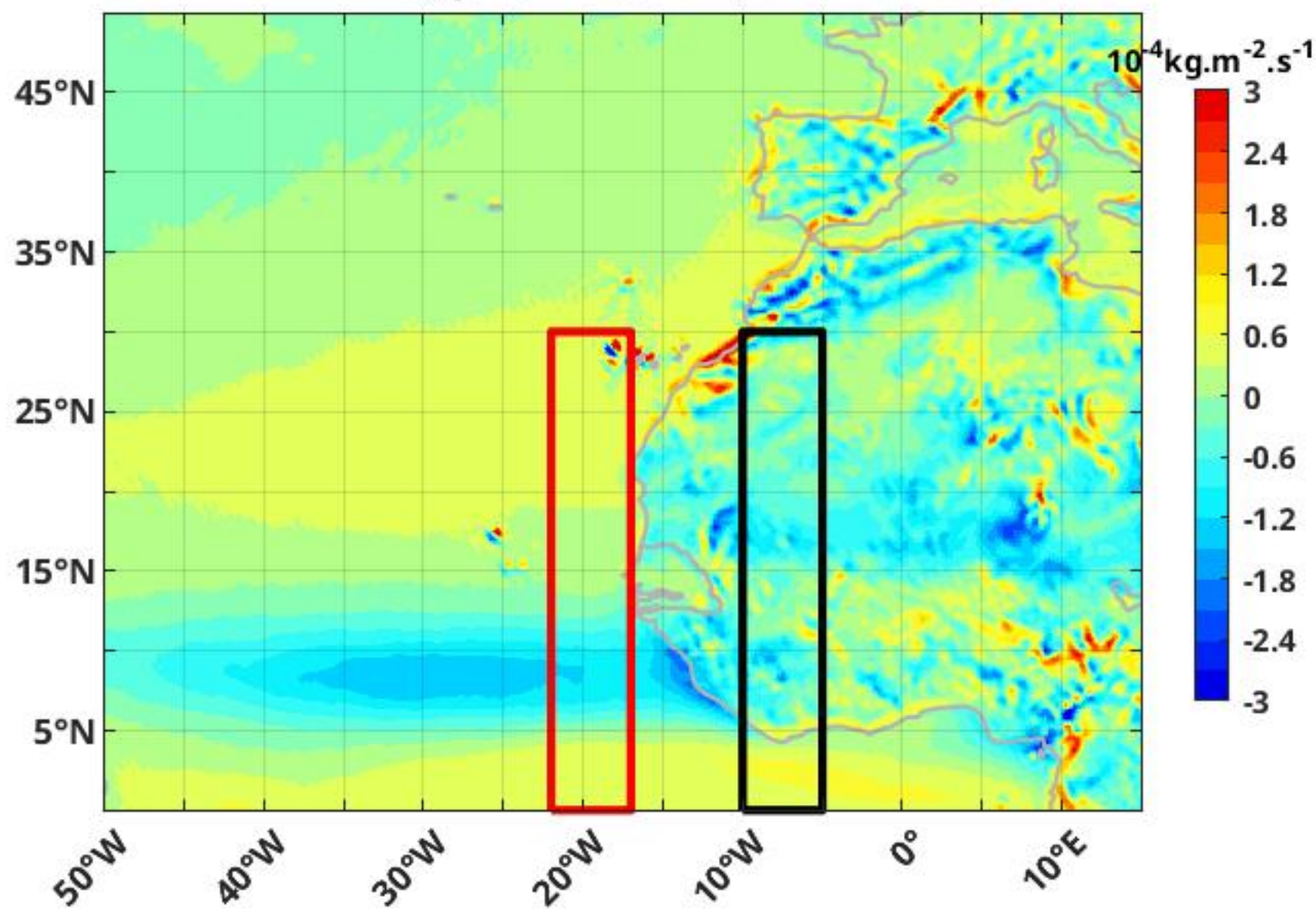
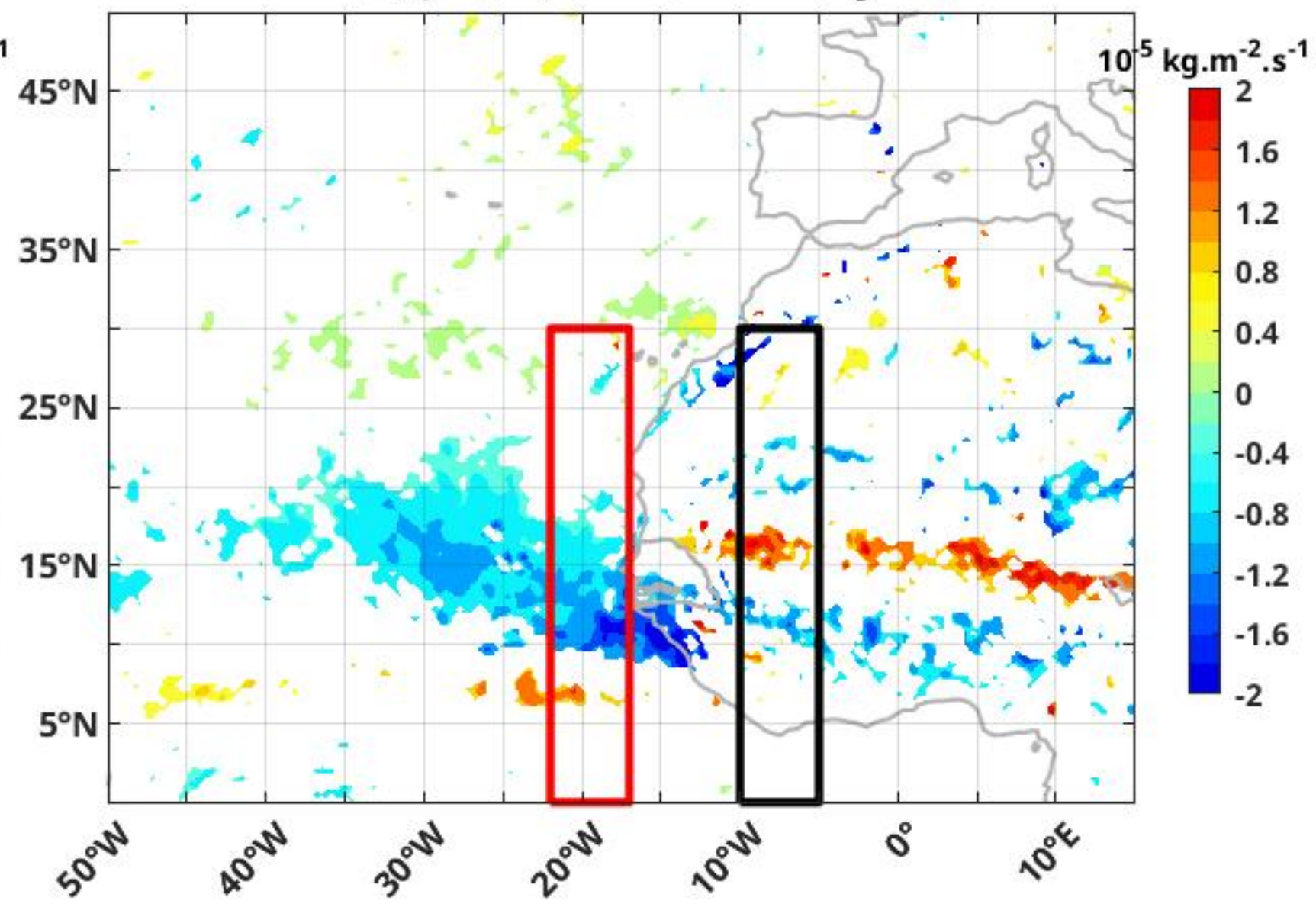


Figure 7.

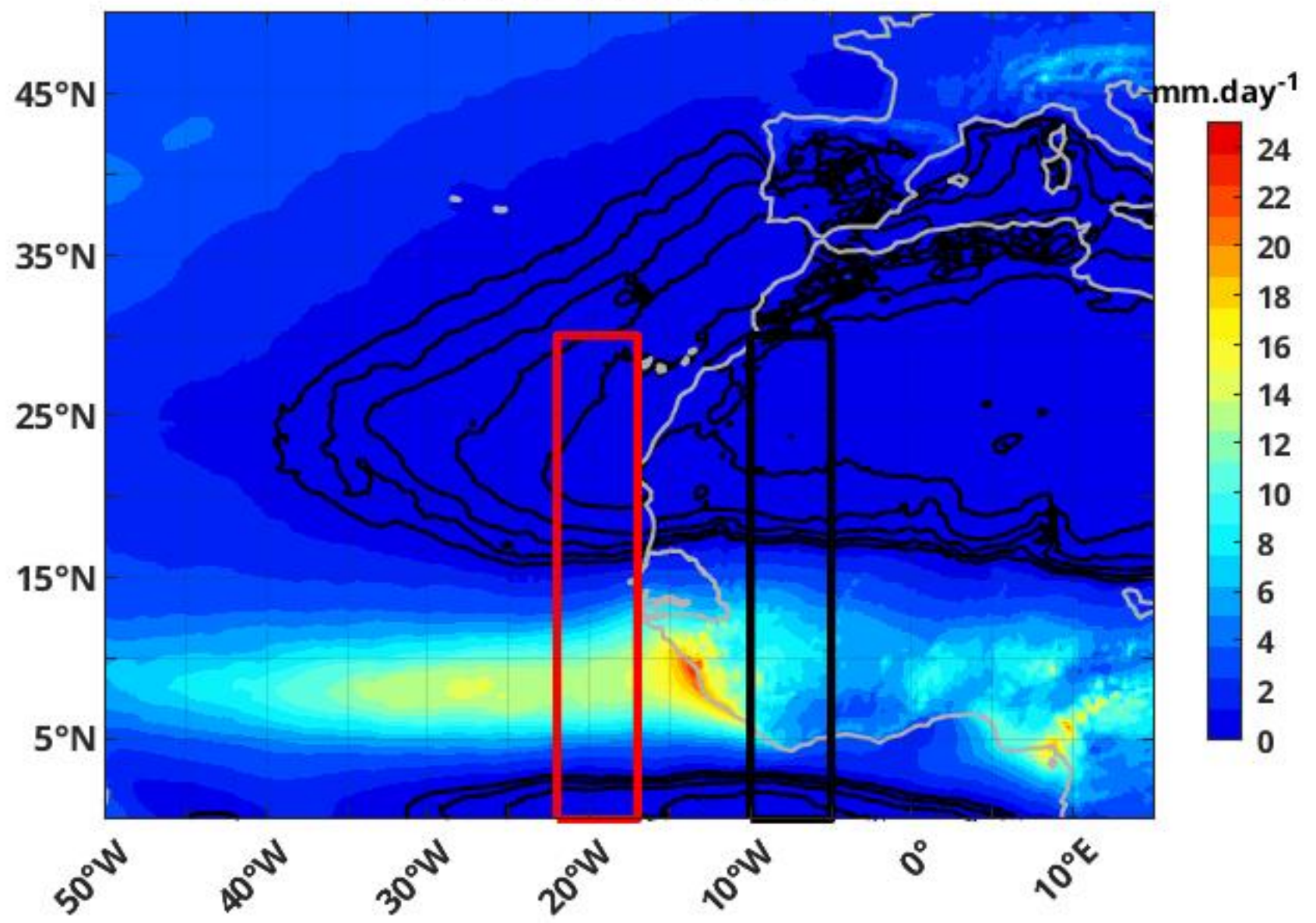
a) JAS mean HT



b) JAS HT anomaly

c) JAS mean $\nabla\cdot\text{HT}$ d) JAS $\nabla\cdot\text{HT}$ anomaly

e) JAS mean PPT



f) JAS PPT Anomaly

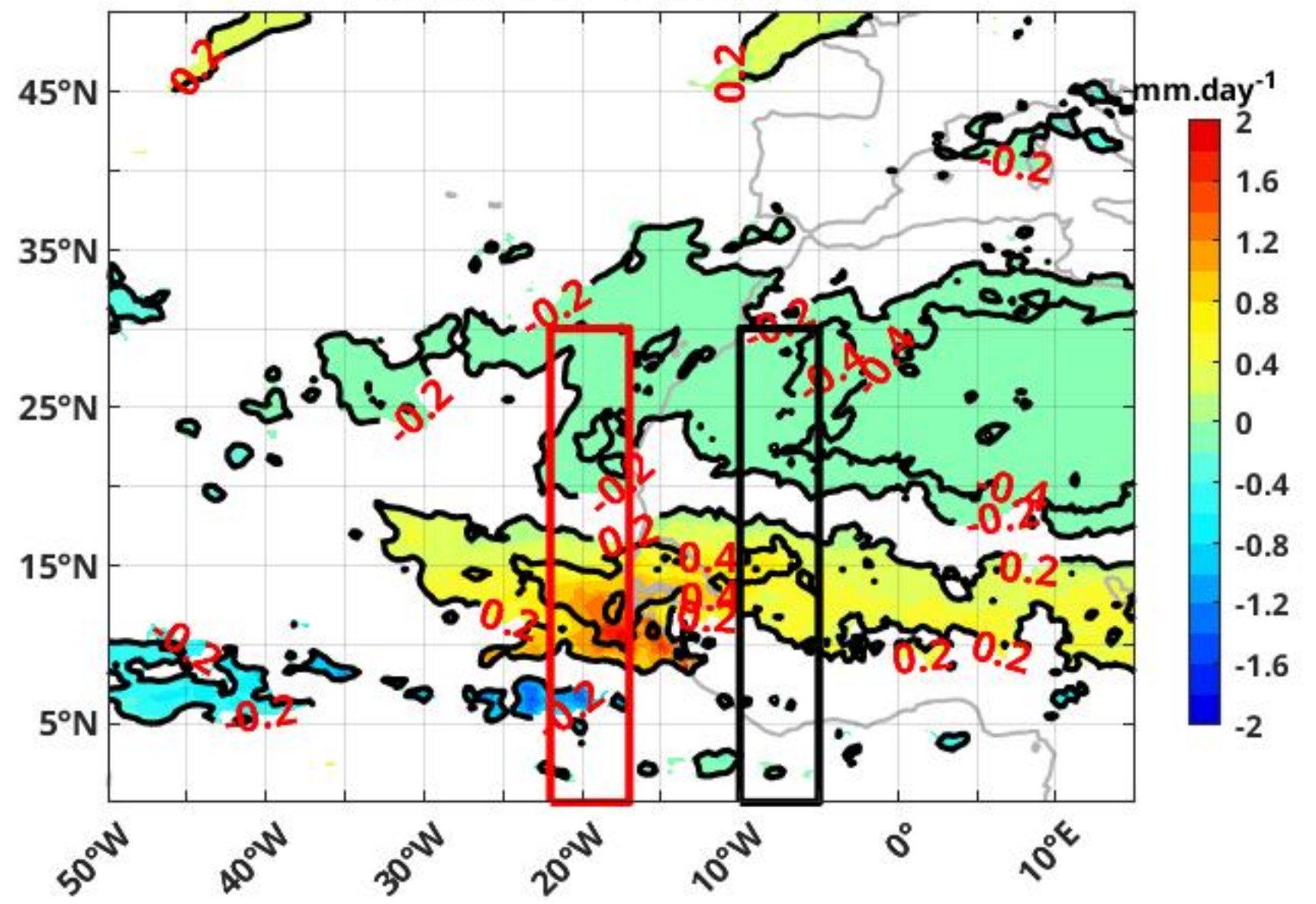
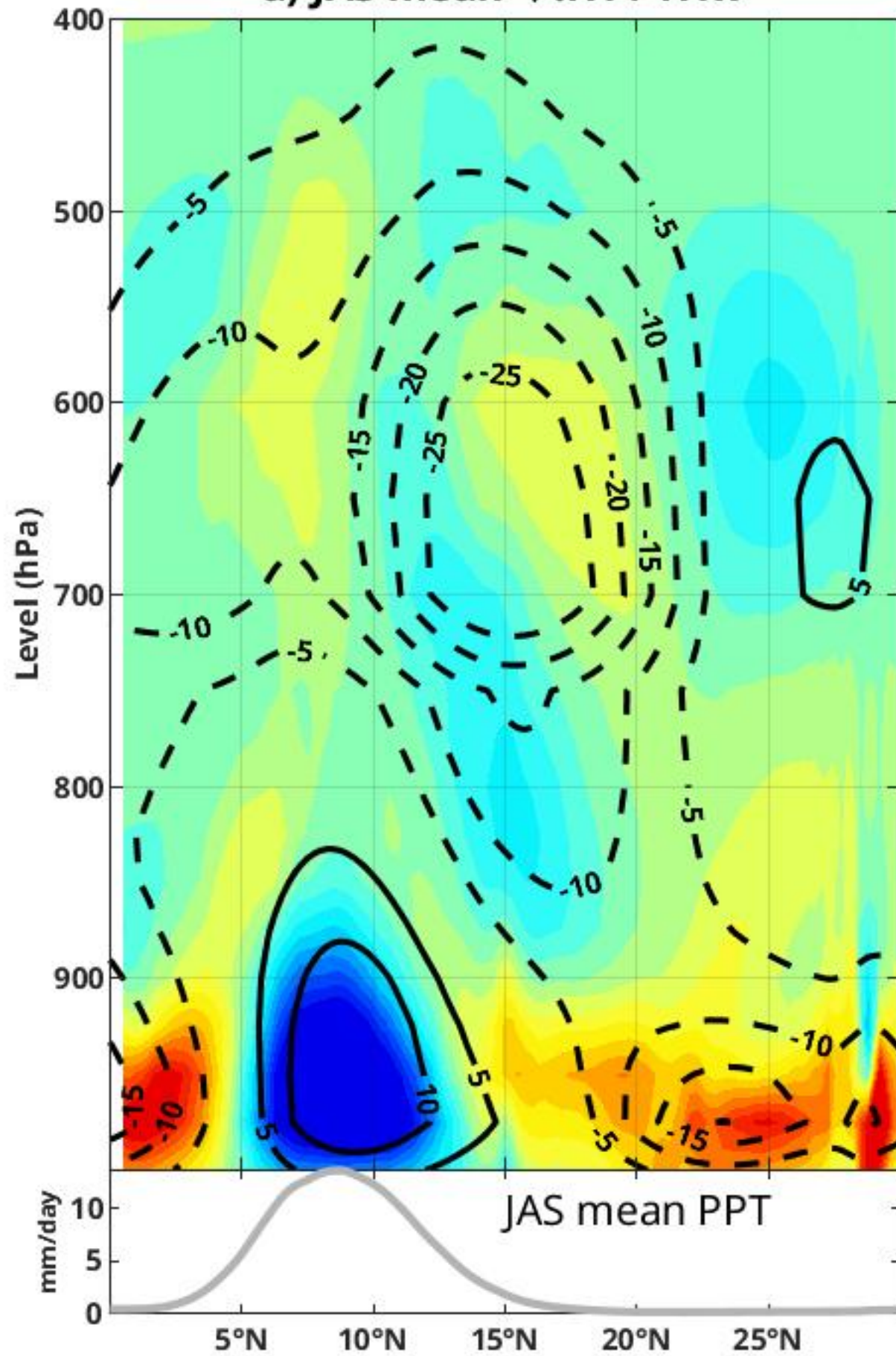
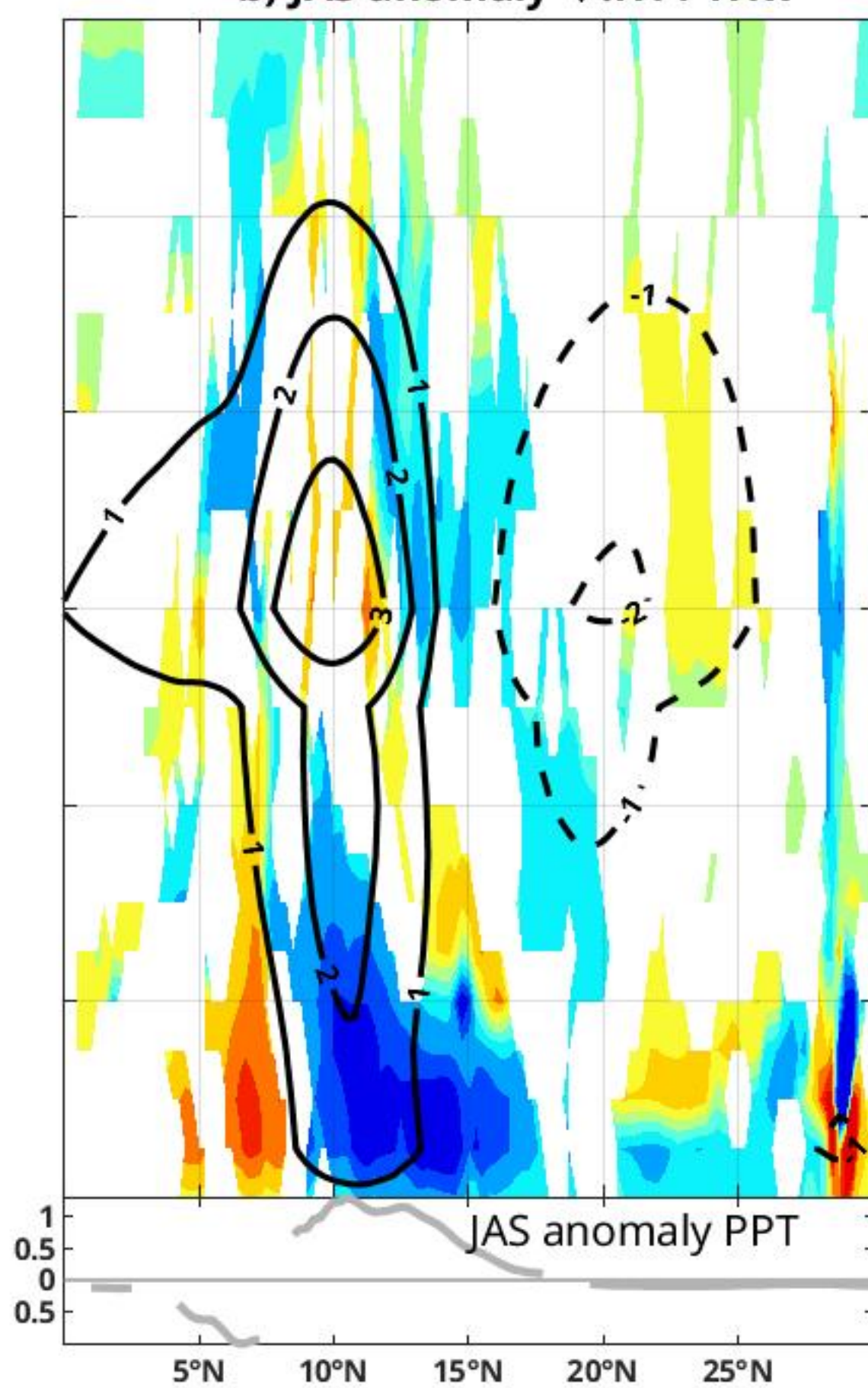
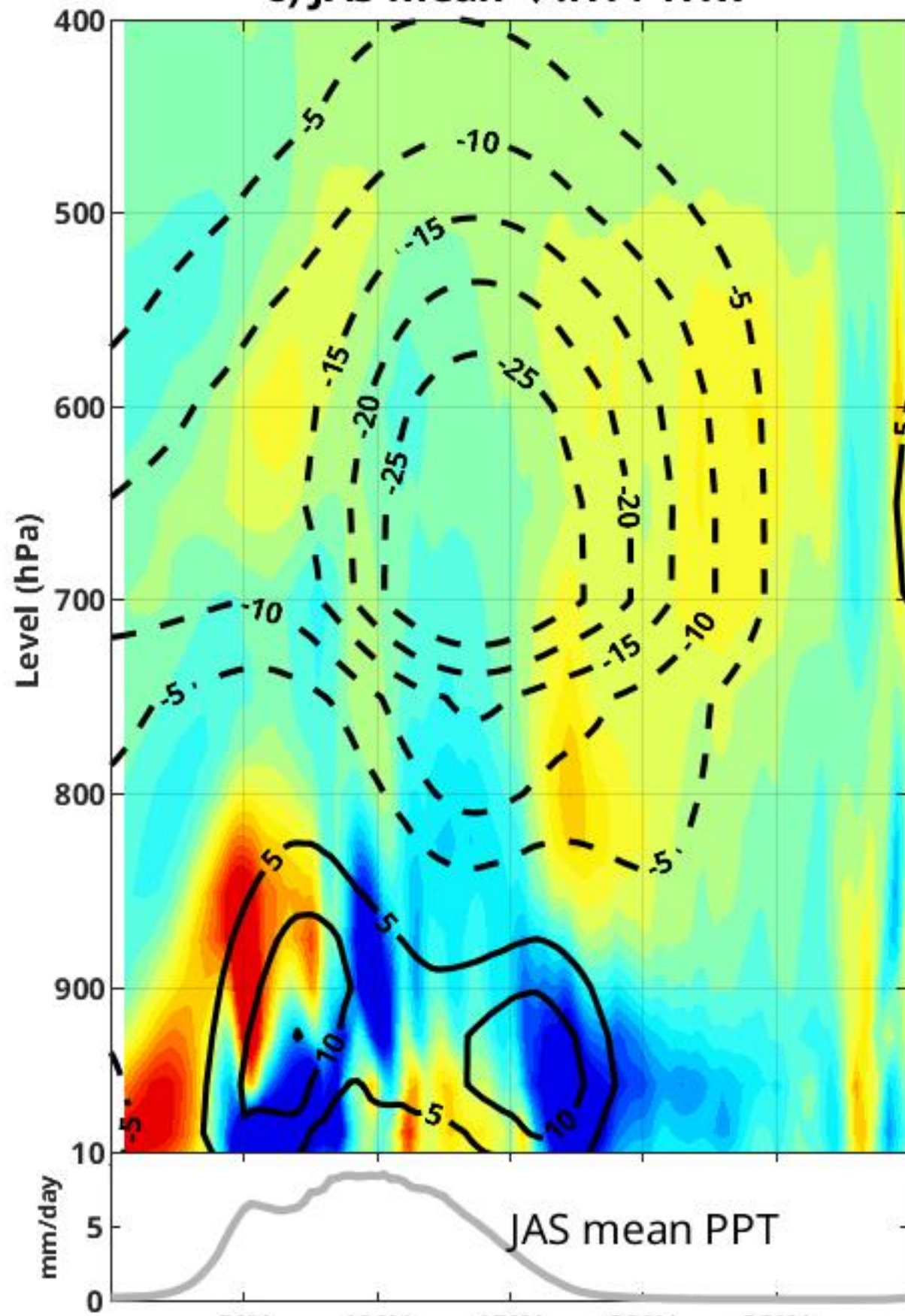
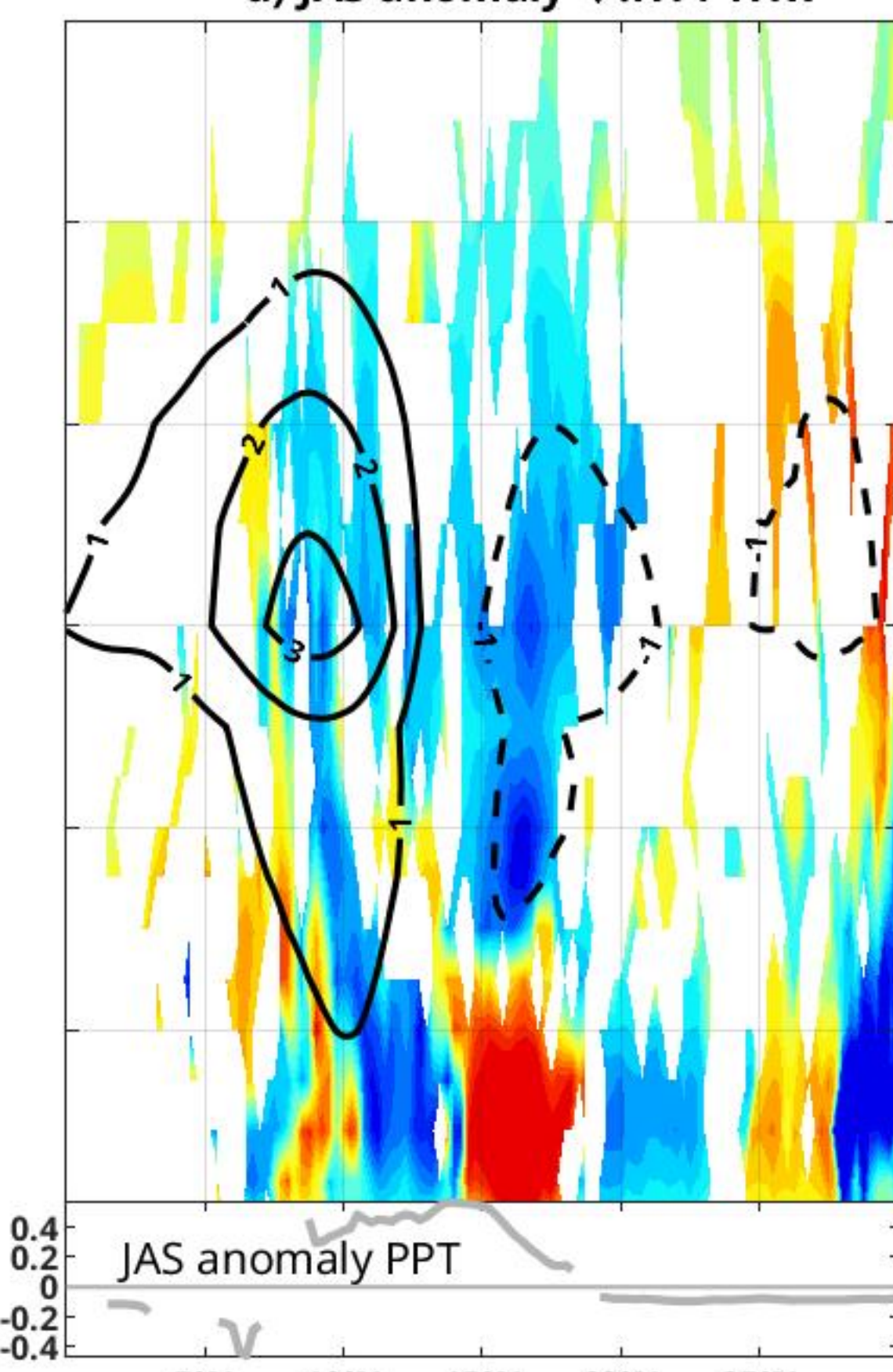


Figure 8.

a) JAS mean $\nabla \cdot \text{HT} / \text{HTx}$ b) JAS anomaly $\nabla \cdot \text{HT} / \text{HTx}$ c) JAS mean $\nabla \cdot \text{HT} / \text{HTx}$ d) JAS anomaly $\nabla \cdot \text{HT} / \text{HTx}$ 

$10^{-5} \text{ kg} \cdot \text{m}^{-2} \cdot \text{s}^{-1}$

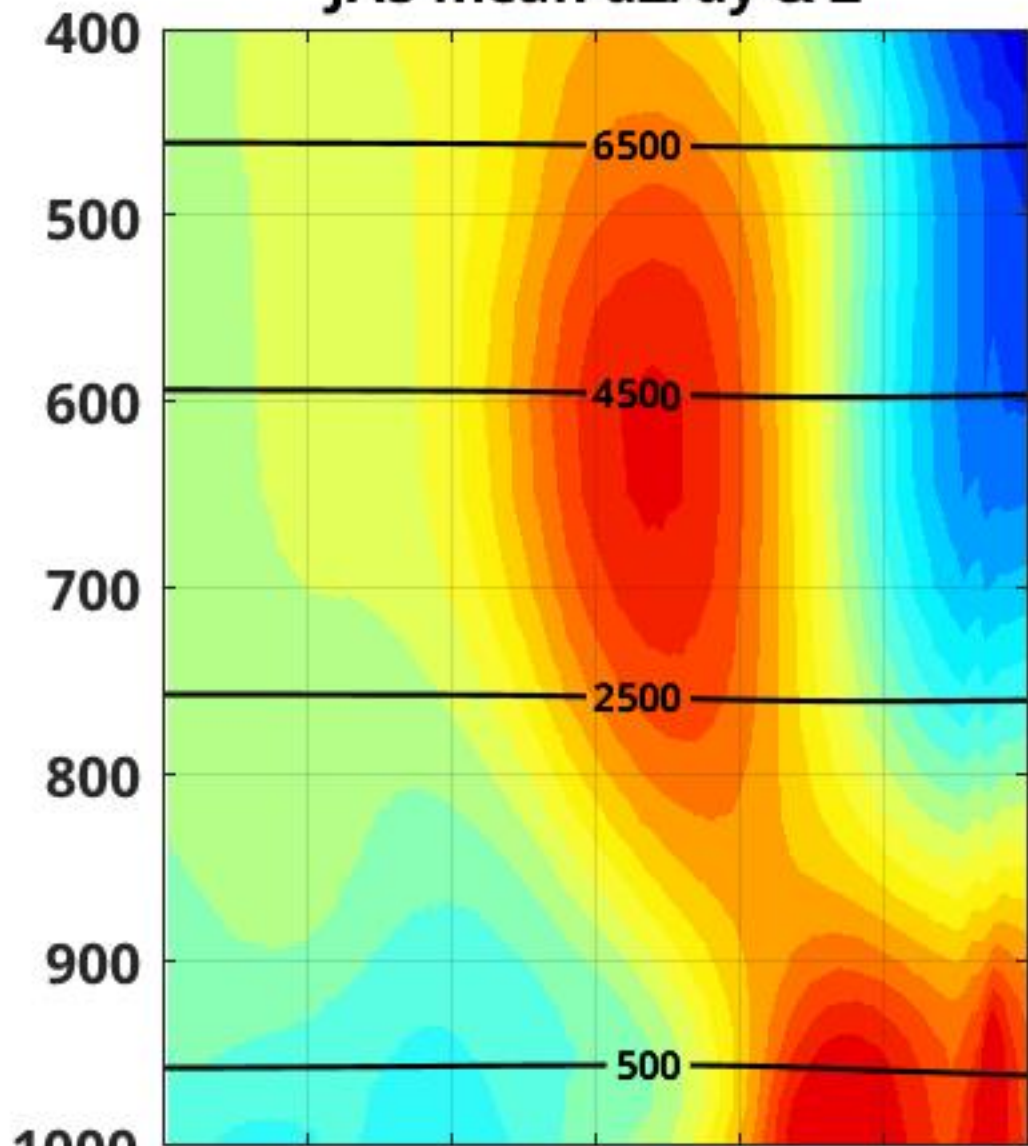
2 1.6 1.2 0.8 0.4 0 0.4 0.8 1.2 1.6 2

$10^{-6} \text{ kg} \cdot \text{m}^{-2} \cdot \text{s}^{-1}$

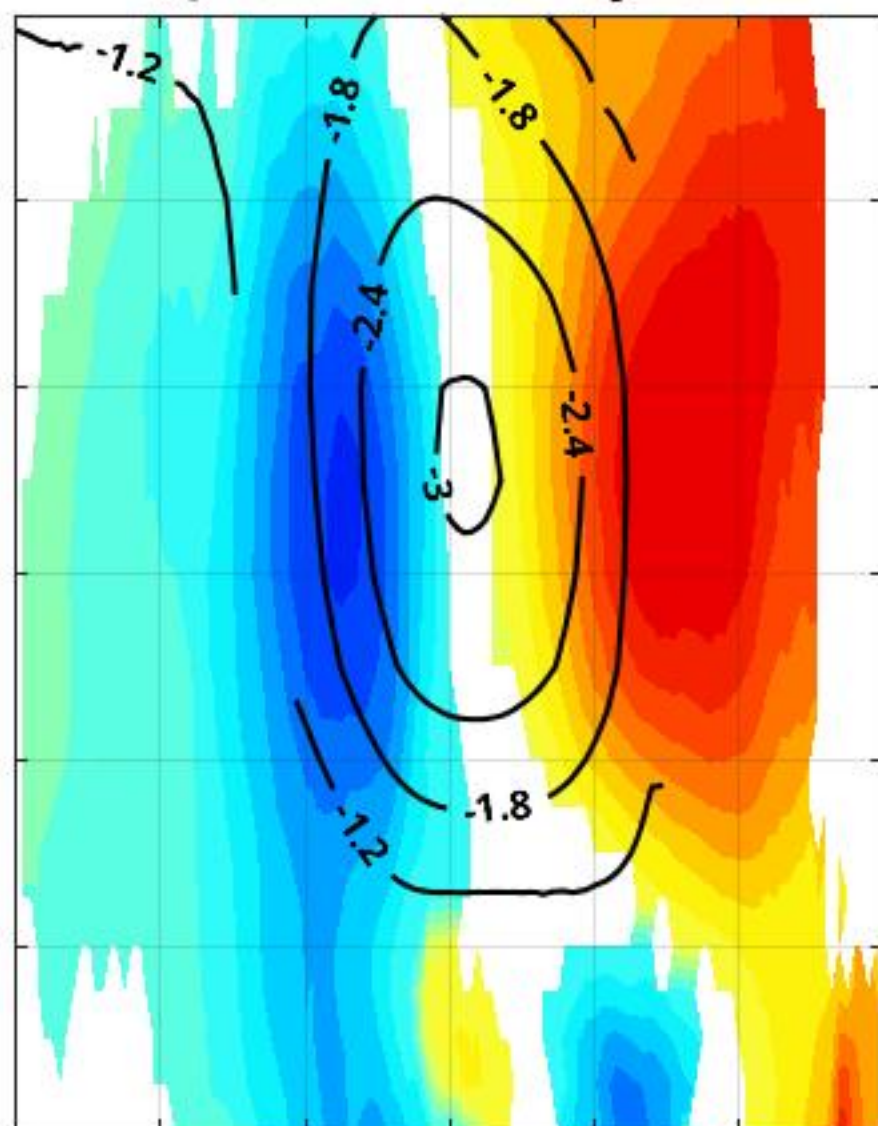
3 2.4 1.8 1.2 0.6 0 0.6 1.2 1.8 2.4 3

Figure 9.

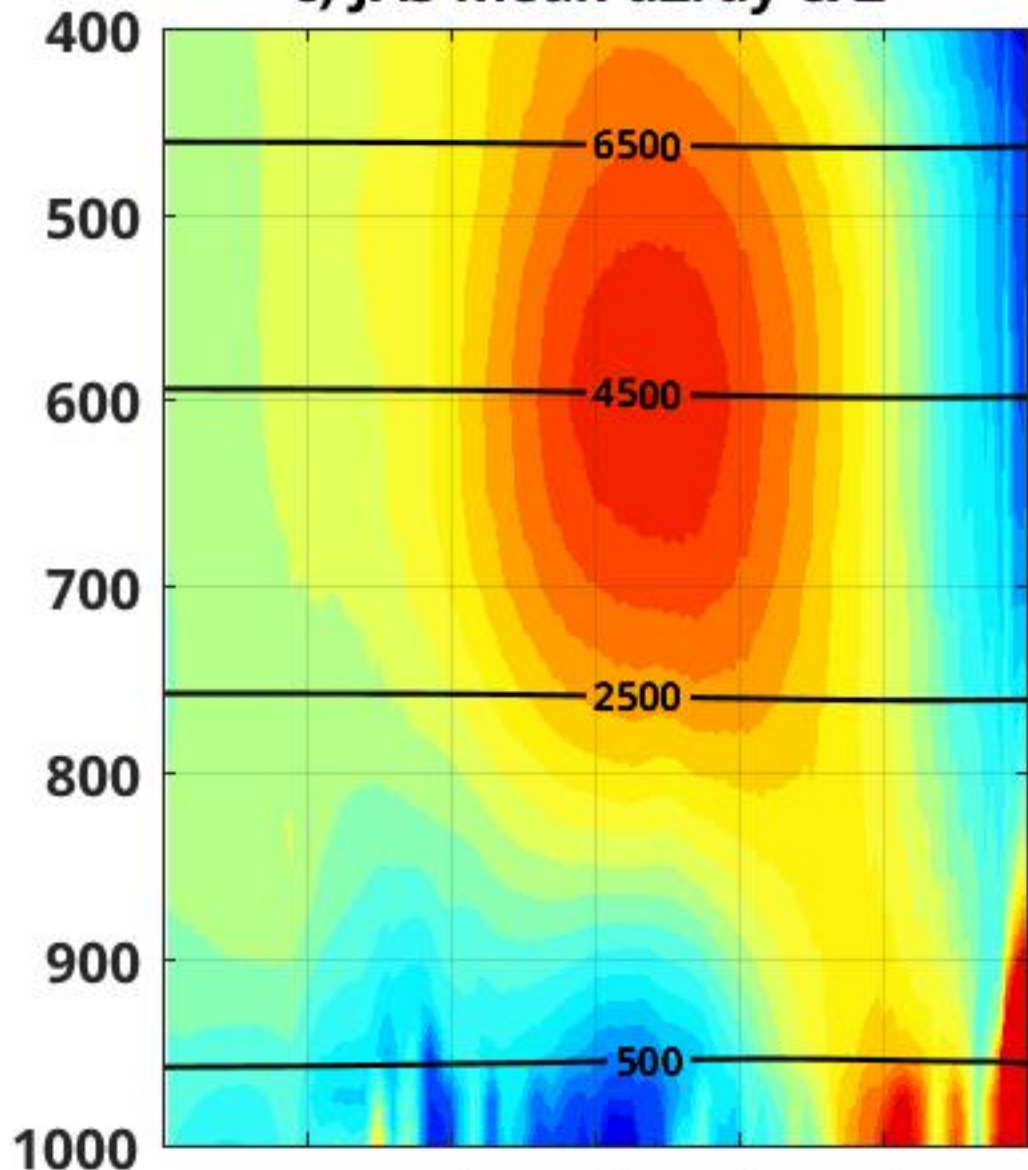
JAS mean dZ/dy & Z



b) JAS anom. dZ/dy & Z



c) JAS mean dZ/dy & Z



d) JAS anom. dZ/dy & Z

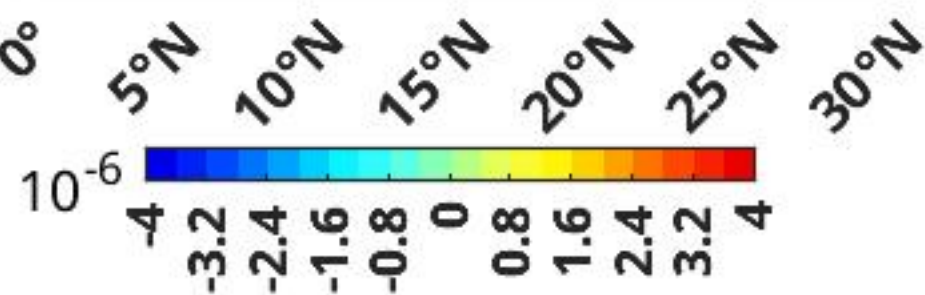
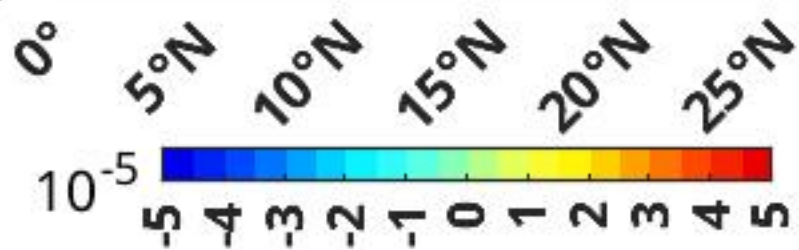
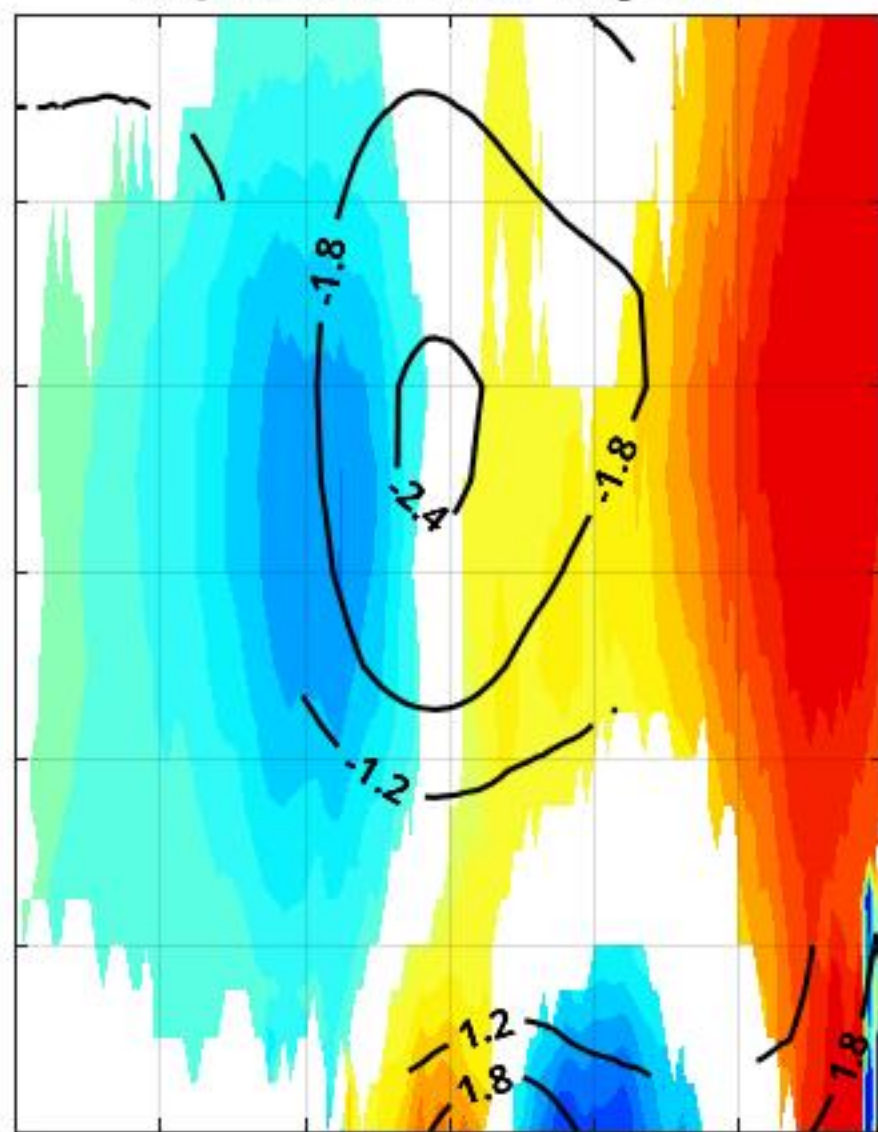


Figure A1.

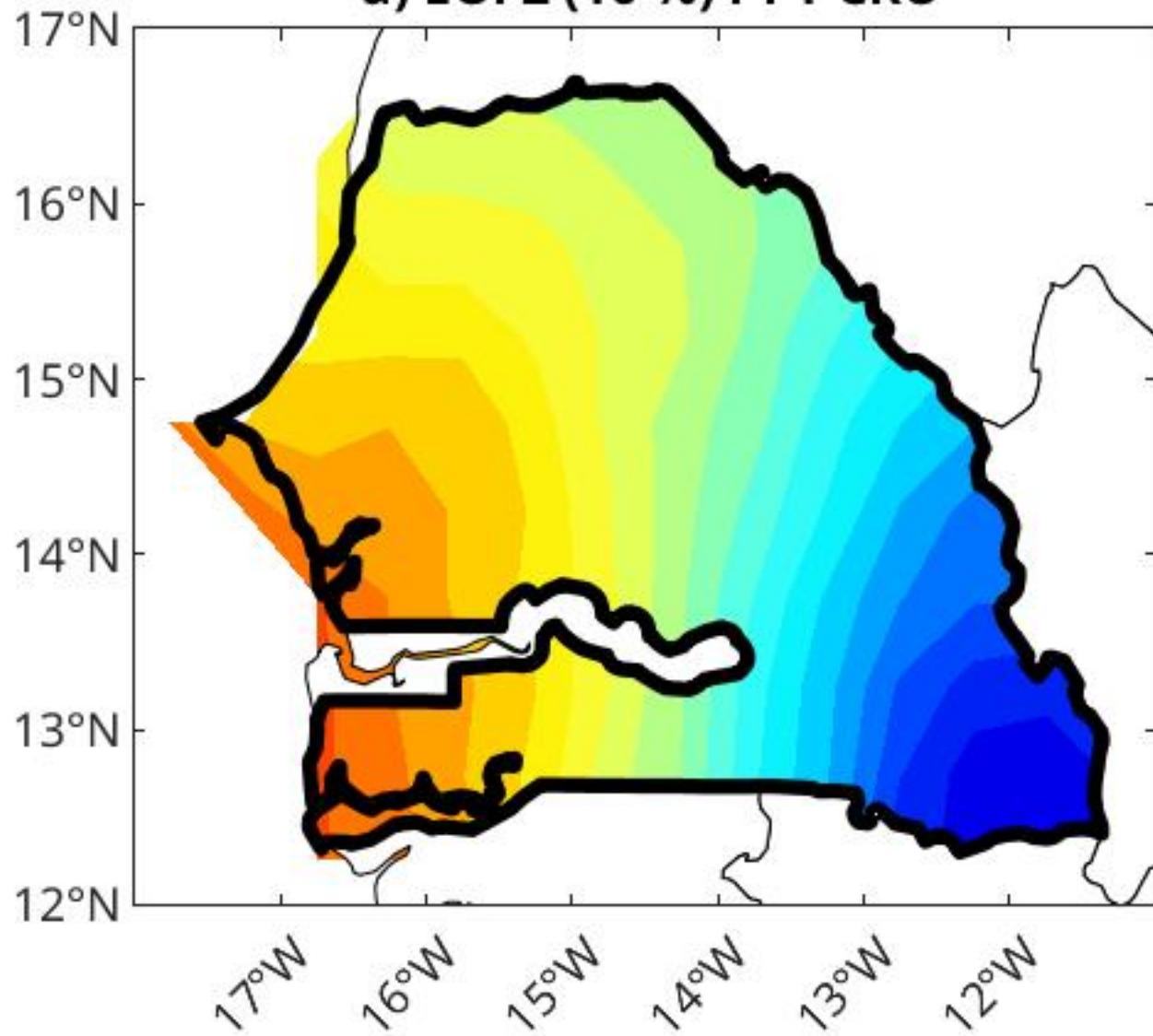
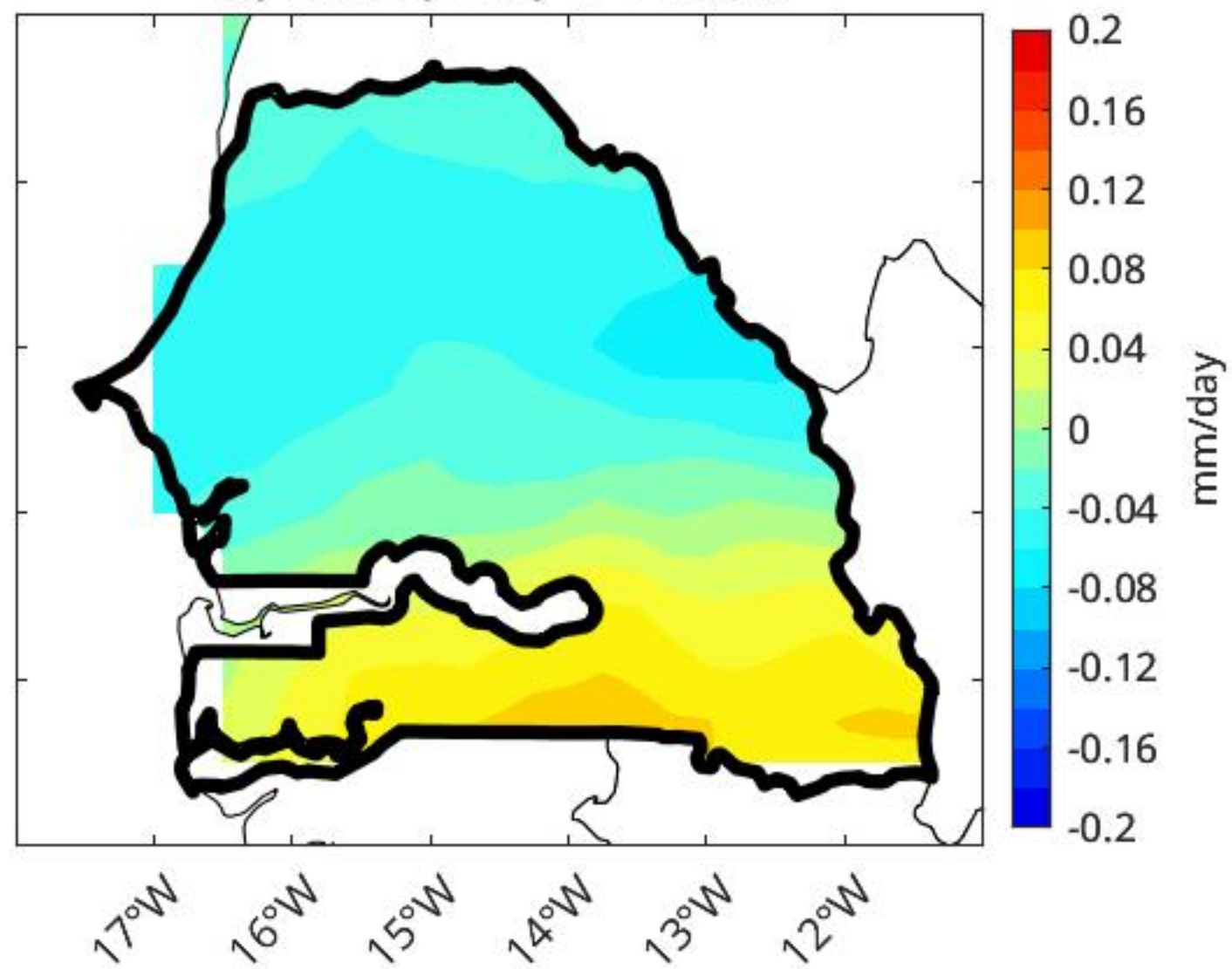
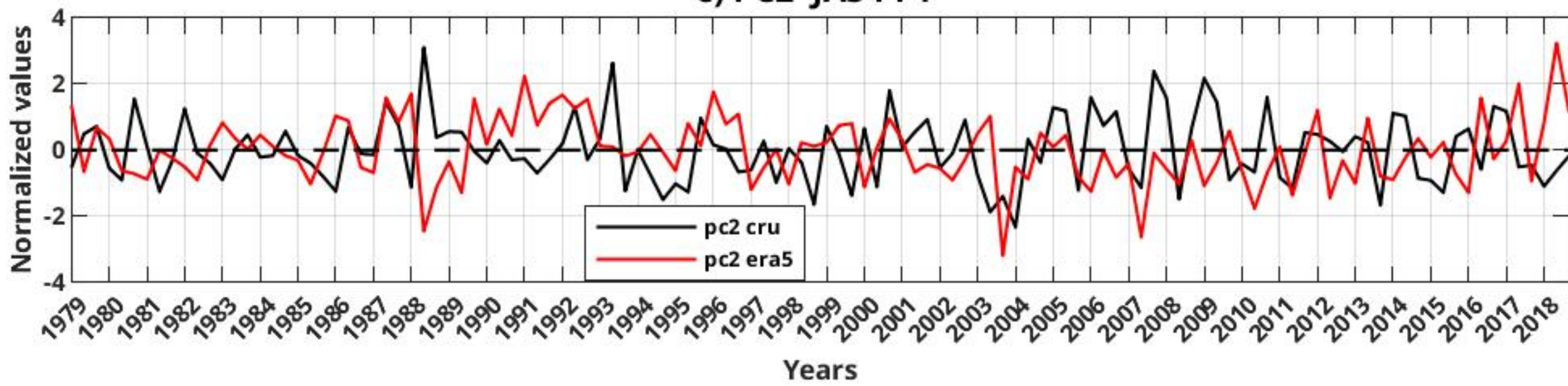
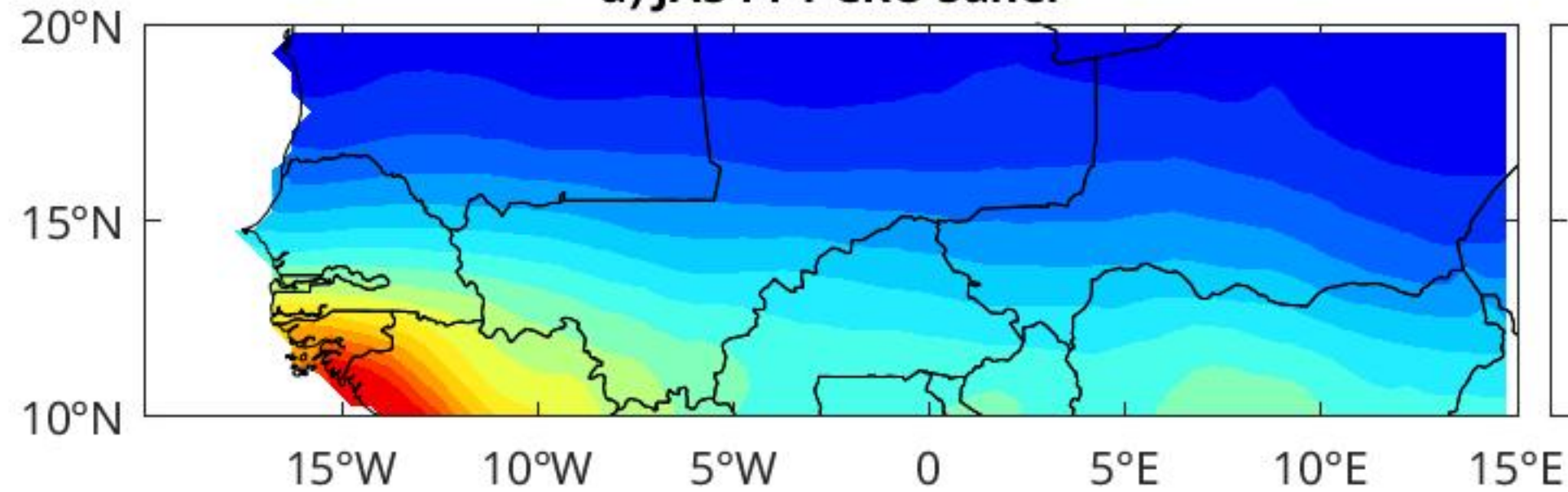
a) EOF2 (10 %) PPT CRU**b) EOF2 (11%) PPT ERA5****c) PC2 JAS PPT**

Figure A2.

a) JAS PPT CRU Sahel



b) JAS PPT ERA5 Sahel

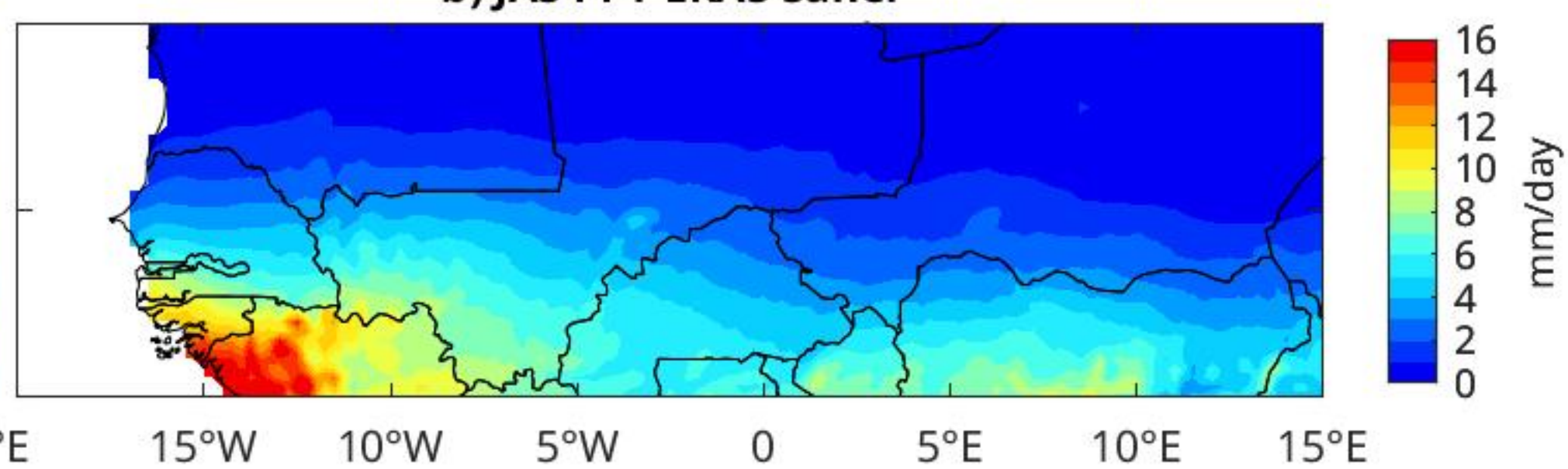
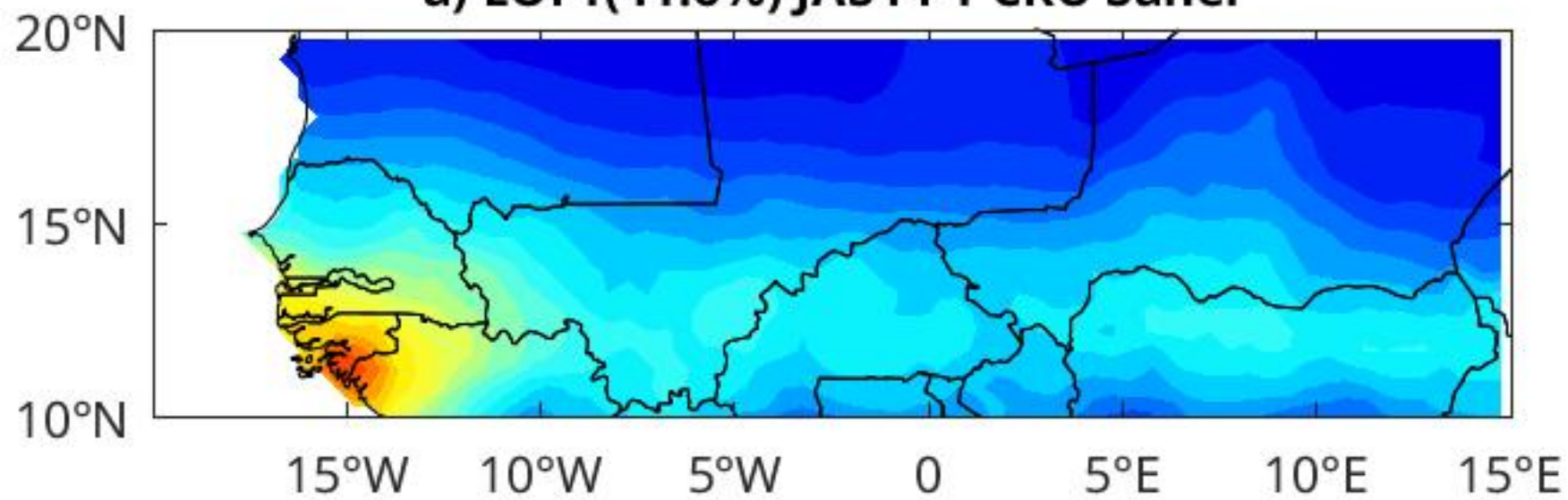
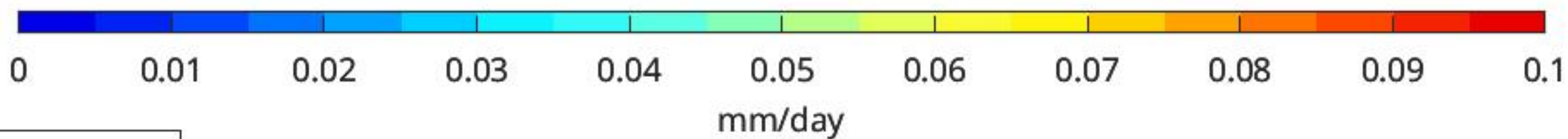
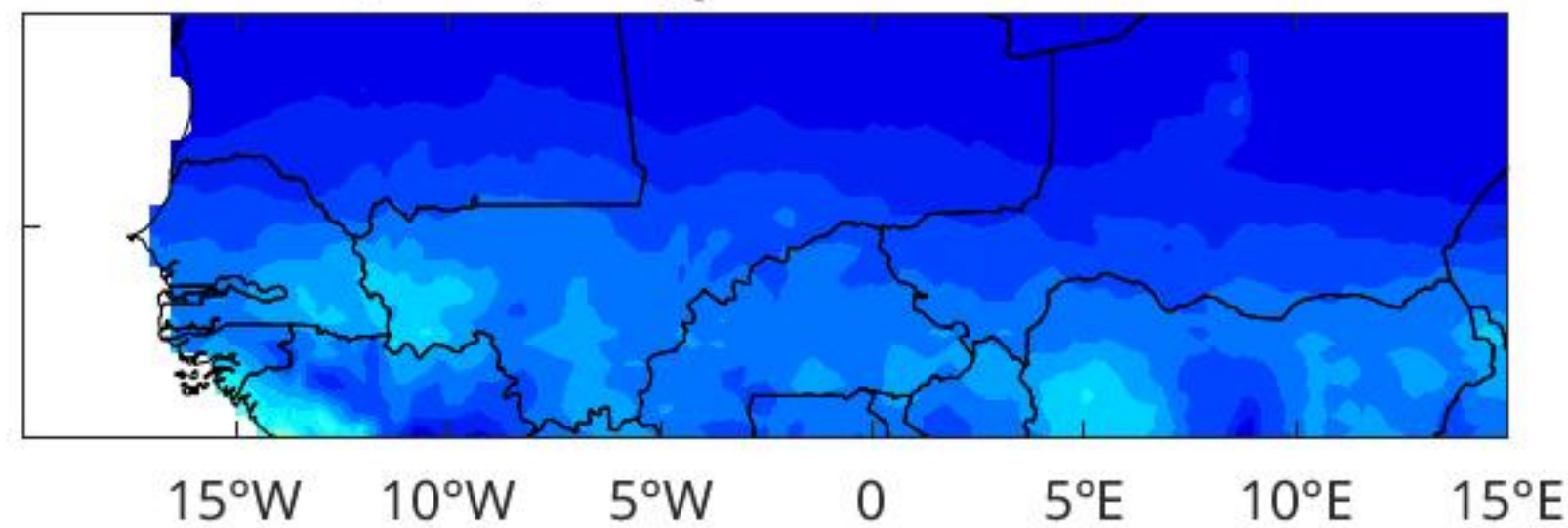


Figure A3.

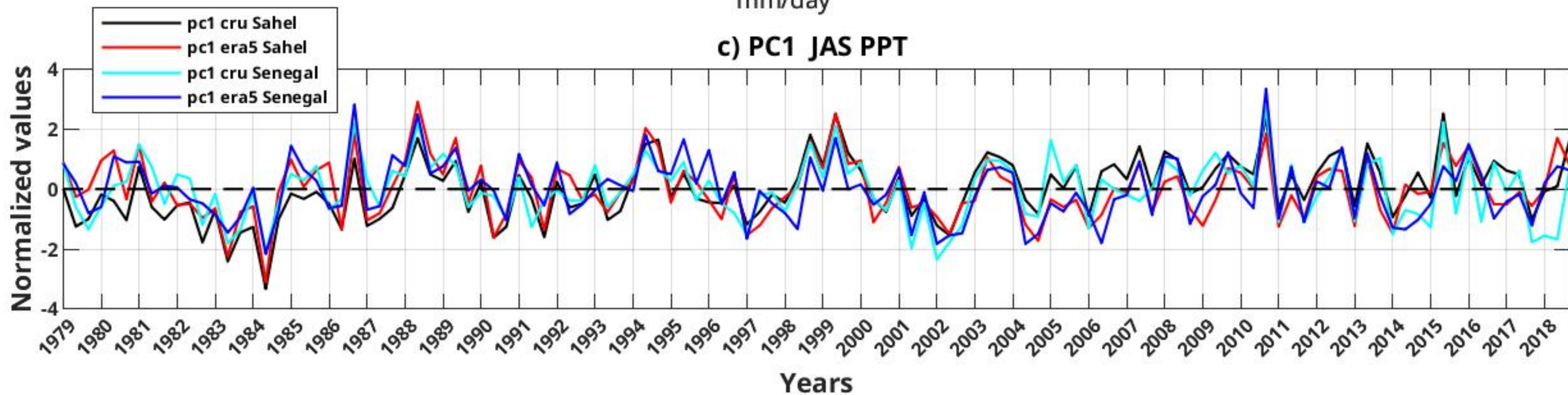
a) EOF1(41.6%) JAS PPT CRU Sahel



b) EOF1(33 %) JAS PPT ERA5 Sahel



c) PC1 JAS PPT



1 **Impact of the sea surface temperature in the**
2 **north-eastern tropical Atlantic on precipitation over**
3 **Senegal**

4 **Mamadou Thiam^{1,2}, Ludivine Oruba², Gaelle de Coetlogon², Malick Wade¹,**
5 **Bouya Diop¹, Abdou Karim Farota¹**

6 ¹Laboratoire des Sciences de l'Atmosphère et des Océans – Matériaux, Énergie et Dispositifs
7 (LSAO-MED), Université Gaston Berger, Saint-Louis, Sénégal

8 ²Laboratoire Atmosphère et Observations Spatiales (LATMOS), Sorbonne Université, Paris, France

9 **Key Points:**

- 10 • Wet summers in Senegal are preceded by La Niña events and warming in the Mediter-
11 ranean but also by warming in the Northeastern Tropical Atlantic
12 • Moisture transport convergence within a stronger West African Westerly Jet (WAWJ)
13 explains this increase in precipitation
14 • Feedback between the North Tropical Atlantic surface temperature and atmospheric
15 pressure is proposed to explain this WAWJ acceleration

Corresponding author: Mamadou Thiam, thiam.mamadou9@ugb.edu.fr

16 **Abstract**

17 This study examines 40 years of monthly precipitation data in Senegal (1979-2018)
 18 using CRU observations and ERA5 reanalyses, aiming to understand the influence of oceanic
 19 and atmospheric factors on Senegal's precipitation in July, August and September (JAS).
 20 The variability of Senegal's precipitation is first compared with that of the broader Sa-
 21 hel region: although they share a significant portion of their variance, Senegal appears
 22 more closely related to the Northeastern Tropical Atlantic (NETA) Sea Surface Temper-
 23 ature (SST). A detailed examination of this region reveals that Senegal's increased pre-
 24 cipitation is linked to the northward shift of the InterTropical Convergence Zone (ITCZ),
 25 consistent with numerous previous studies. Over the continent, this shift corresponds
 26 to a northward shift of the African Easterly Jet (AEJ) and, consequently, the Mesoscale
 27 Convective Systems responsible for most precipitation. It seems primarily driven by the
 28 northward shift of the Heat Low. Over the ocean just west of Senegal, there is a com-
 29 parable shift of the AEJ, accompanied by an increase in low-level moisture transport con-
 30 vergence within the West African Westerly Jet (WAWJ) which explains the majority of
 31 the increase in JAS precipitation in Senegal. This phenomenon is triggered by a nega-
 32 tive pressure anomaly in the NETA, located above a positive Sea Surface Temperature
 33 (SST) anomaly: we suggest that the latter is the origin of the former, forming a feed-
 34 back mechanism that potentially significantly influences Senegal's precipitation. The mech-
 35 anism involves a geostrophic adjustment of the WAWJ to the southern gradients of the
 36 SST anomaly. Further investigations utilizing daily data or regional atmospheric mod-
 37 els are necessary to validate the role of NETA SST feedback on Senegal's precipitation,
 38 with potential benefits for enhancing seasonal forecasting capabilities.

39 **Plain Language**

40 This study, spanning 40 years of monthly precipitation data in Senegal, explores
 41 the intricate relationship between oceanic and atmospheric factors shaping precipitation
 42 patterns from July to September. The increased summertime precipitation in the West-
 43 ern Sahel is primarily of continental origin, associated with the northward shift of mesoscale
 44 convective systems linked to lower pressure in the Sahara. However, over the ocean west
 45 of Senegal, there is also an increase in inland moisture transport that explains a signif-
 46 icant part of the intensified precipitation from July to September in Senegal. This trans-
 47 port is reinforced by a low-pressure system over the ocean, potentially caused by warmer
 48 sea surface temperatures between 10°N and 20°N off West Africa. This close connection
 49 between Senegal's precipitation and ocean surface temperature in the Northeastern Trop-
 50 ical Atlantic could help enhance crucial seasonal forecasts for agricultural planning, the
 51 economy, and food security in West Africa.

52 **1 Introduction**

53 The study of Sahel's rainfall variability is crucial due to its vulnerability to climate
 54 change. Accurate forecasts are vital for managing water resources, agriculture, and health
 55 (Sultan et al., 2005; Grace & Davenport, 2021). This semi-arid region, experiences most
 56 of its precipitation from July to September (JAS). During this period, a zonal rain belt
 57 spans from approximately 5°N to 15°N across West Africa, shifting southward the rest
 58 of the year (Parker & Diop-Kane, 2017). The summer rains are primarily attributed to
 59 mesoscale convective systems (MCSs), with up to 95% originating above the eastern high-
 60 lands and crossing East to West Africa within one or two days (Nicholson, 2013). These
 61 systems form due to the African Easterly Jet (AEJ)'s presence in the mid-troposphere,
 62 particularly its southern half, with strong horizontal vorticity facilitating barotropic and
 63 baroclinic instabilities (Parker & Diop-Kane, 2017).

64 This zonal band of precipitation experiences strong year-to-year and even decadal
 65 variations between 10°N and 15°N. For instance, an exceptionally severe drought occurred
 66 in the 1980s (Le Barbé & Lebel, 1997). Various mechanisms have been identified to ex-
 67 plain this extensive variability, including the land-atmosphere-ocean system and changes
 68 in atmospheric circulation patterns and weather systems behavior in West Africa dur-
 69 ing the rainy season (Zeng et al., 1999; Nicholson & Palao, 1993; Vizzy & Cook, 2001).
 70 Nevertheless, numerous studies highlight the pivotal role of global sea surface temper-
 71 ature (SST) such as the Indian Ocean warming (Hagos & Cook, 2008), which influences
 72 the African monsoon through atmospheric teleconnections through modifications in Walker
 73 cells intensity, or equatorial atmospheric Kelvin and Rossby waves (Wang, 2019). Strong
 74 correlations have indeed been observed between Sahel precipitation and remote SST at
 75 interannual timescales in the Pacific equatorial region (Janicot et al., 2001; Joly & Voldoire,
 76 2009; Diatta & Fink, 2014; Gomara et al., 2017), in the Mediterranean Sea (Rowell, 2003;
 77 Jung et al., 2006; Polo et al., 2008; Fontaine et al., 2009; Diakhate et al., 2019; Worou
 78 et al., 2020), or in the Indian Ocean (Bader & Latif, 2003; Biasutti et al., 2008; Mohino
 79 et al., 2011; Caminade & Terray, 2010).

80 Sahel rainfall variability may also be influenced by coupled regional dynamics in
 81 the Tropical Atlantic (Camberlin et al., 2001; Polo et al., 2008). At interannual timescales,
 82 the SST in the Gulf of Guinea is influenced by an equatorial ocean-atmosphere coupled
 83 mode known as the "zonal mode" or Atlantic Niño (Zebiak, 1993; Cabos et al., 2019),
 84 subsequently affecting precipitation along the Guinea Coast (Meynadier et al., 2016; Polo
 85 et al., 2008; de Coëtlogon et al., 2010, 2014) and, seemingly, in the Sahel (Caniaux et
 86 al., 2011; Steinig et al., 2018; Janicot et al., 1998; Vizzy & Cook, 2001; Losada et al., 2010).
 87 Regarding the North Tropical Atlantic, Mo et al. (2001) and Ward (1998) suggested that
 88 NETA SST does not significantly influence West African rainfall. Using a general cir-
 89 culation model, Vizzy and Cook (2001) also concluded that precipitation over West Africa
 90 is generally insensitive to NETA SST anomalies. In the other hand, Camberlin and Diop
 91 (1999) found that precipitation in Senegal is more sensitive to climatic anomalies in the
 92 northern Tropical Atlantic than in the rest of the Sahel over the period 1960-1990. More-
 93 over, Fall et al. (2006) found that precipitation over Senegal is well correlated with North
 94 Tropical Atlantic SST from January to May. The role of NETA SST in relation to Sa-
 95 hel precipitation remains therefore unclear, especially for western Sahel. However, Sa-
 96 hel precipitation in summer is strongly linked to the latitude of the intertropical conver-
 97 gence zone (Camberlin et al., 2001; Nicholson, 2013), and the latter could be tied to the
 98 zonal band of maximum SST in the Tropical Atlantic (Diakhaté et al., 2018): when the
 99 SST in the Northeastern Tropical Atlantic (NETA) is warmer than those further south,
 100 the ITCZ migrates northward, leading to positive rainfall anomalies observed in the Sa-
 101 hel (Xie & Carton, 2004; Gu & Adler, 2009; Gu, 2010; Janicot et al., 2001; Biasutti et
 102 al., 2008). It therefore appears important to clarify whether NETA SST has an impact
 103 on Sahel precipitation, carefully distinguishing between Senegal (Western Sahel) and Cen-
 104 tral Sahel.

105 The primary objective of this paper is to build a robust index of Senegal precip-
 106 itation for monitoring its variability based on observations. It then briefly revisits tele-
 107 connections between global SST and precipitation on interannual timescales with a par-
 108 ticular focus on Senegal specifically, in contrast to the broader Sahel region as commonly
 109 done in previous research. Subsequently, we delve deeper into the NETA signatures of
 110 SST, Sea Level Pressure (or SLP), wind fields, and low-level moisture transport anom-
 111 alies: we discuss their influence on Senegal's precipitation patterns and consider the po-
 112 tentiel role of a regional SST feedback mechanism on precipitation in West Africa. The
 113 paper is divided as follows: Section 2 describes the data and the methods, Section 3 presents
 114 the building of the index, Section 4 discusses the signals found in global SST, Section
 115 5 focuses on the NETA SST and near-surface dynamics, Section 6 discusses the mois-
 116 ture transport and precipitation, Section 7 proposes a mechanism for the SST influence
 117 on the WAWJ, and Section 8 concludes the study.

2 Data and methods

2.1 Data

The present study relies on the Climatic Research Unit (CRU) Time-series (TS). The CRU TS dataset was originally created and subsequently updated by the UK Natural Environment Research Council (NERC) and the US Department of Energy. In this paper, we utilized Version 4.03 of the CRU TS dataset, which spans the period from 1901 to 2018 at a high resolution of $0.5^\circ \times 0.5^\circ$. Monthly averaged precipitation data for the mainland, covering the period from 1979 to 2018, were acquired from various weather services and other sources.

CMWF Reanalysis v5 (ERA5) data are employed in this study to monitor the atmospheric dynamics associated with Senegal precipitation fluctuations. ERA5 is produced by the Copernicus Climate Change Service (C3S) and incorporates data assimilation, combining model data with observations from worldwide sources. It provides estimates for numerous atmospheric, terrestrial, and oceanic climate variables from 1979 to the present day, with a horizontal grid resolution of $0.25^\circ \times 0.25^\circ$ and 37 vertical levels ranging from 1000 to 1 hPa and we also use monthly average data. Global SST data from ERA5 are used to identify global teleconnections with precipitation. These SST data are based on the Hadley Centre Sea Ice and Sea Surface Temperature dataset version 2 (HadISST2) from 1979 to August 2007 and the Office Operational Sea Surface Temperature and Sea Ice Analysis (OSTIA) daily product from September 2007 to the present. These SST datasets closely align with the Reynolds observation product (Yang et al., 2021).

The atmospheric parameters used in this study are SLP, zonal (u) and meridional wind (v) at 10 meters above the surface, and at the available pressure levels in ERA5. Additionally, geopotential height (Z) and specific humidity (q) are also used. Wind speed ($\sqrt{u^2 + v^2}$) is treated as an additional parameter: we calculate its monthly seasonal anomalies separately from the zonal and meridional components. Linear regressions of wind speed anomalies hence indicate whether the wind anomalies correspond to a weaker (negative anomalies) or stronger (positive) wind speed in comparison to the average.

2.2 Linear statistical tools

The calculation of monthly seasonal anomalies is conducted over the 40-year period from 1979 to 2018 for all parameters. Anomalies are determined by subtracting the seasonal cycle, computed by averaging the values for each month over the 1979-2018 period. Additionally, to remove long-term periodicities (decadal and beyond), a quadratic trend computed over the 480 monthly anomalies is removed from these anomalies in all parameters.

Empirical Orthogonal Function (EOF) decomposition are performed in both the CRU and ERA5 precipitation anomalies in JAS over Senegal in section 3. The Principal Components (PCs) represent the eigenvectors of the estimated covariance matrix. Following the approach outlined in Von Storch and Zwiers (1999), the spatial patterns, also known as EOFs, correspond to the linear regression of the JAS anomalies on the PCs as described just below.

Given an independent, identically distributed sample of random parameters X_i and Y_i for $i = 1$ to $n = 120$ (i.e. 40 years times 3 months), the correlation is computed

with the following maximum likelihood estimator:

$$\hat{R} = \frac{\sum_{i=1}^n (X_i - \bar{X})(Y_i - \bar{Y})}{\sqrt{\left(\sum_{i=1}^n (X_i - \bar{X})^2\right) \left(\sum_{i=1}^n (Y_i - \bar{Y})^2\right)}} \quad (1)$$

Here, $\bar{X} = \frac{1}{n} \sum_{i=1}^n X_i$ and $\bar{Y} = \frac{1}{n} \sum_{i=1}^n Y_i$ are estimators of the variables means. Subsequently, we apply the least squares estimate of the slope of the simple linear regression, as described in Von Storch and Zwiers (1999):

$$\hat{a} = \frac{\sum_{i=1}^n (X_i - \bar{X})(Y_i - \bar{Y})}{\sqrt{\sum_{i=1}^n (X_i - \bar{X})^2}} \quad (2)$$

159 The resulting \hat{a} field represents the variation of Y associated with a fluctuation of
 160 one standard deviation of X . For example, if (X_i) represents the normalized PC1CRU
 161 index, and (Y_i) represents the SST, \hat{a} indicates the change in SST anomalies (in °C) as-
 162 sociated with a one-standard deviation increase in the precipitation index. This result-
 163 ing field is typically referred to as the SST anomaly obtained from the regression of SST
 164 on the precipitation index. Note that all descriptions in this study pertain to positive
 165 values of this index, reflecting anomalies associated with higher-than-average JAS pre-
 166 cipitation in Senegal. However, we could have chosen to describe opposite anomalies (i.e.,
 167 related to a dry summer) without altering the interpretation of our results.

168 Moreover, we employ the unbiased estimator $\sigma(X) = \sqrt{\frac{1}{n-1} \sum_{i=1}^n X_i^2}$ to calculate
 169 the standard deviation of a random variable X based on a sample of n values. By con-
 170 sidering X_i as the July anomalies, Y_i as the August anomalies and Z_i as the Septem-
 171 ber anomalies, we proceed to estimate the typical interannual anomaly (i.e., averaged
 172 over the entire JAS season) as follows:

$$\sigma_{interannual} = \sqrt{\frac{1}{N-1} \sum_{i=1}^N XYZ_i^2}$$

173 where $N = 40$ years and $XYZ_i = \frac{X_i+Y_i+Z_i}{3}$ is the yearly anomaly in JAS, whereas
 174 the intraseasonal signal, representing the typical monthly anomaly within each JAS sea-
 175 son (independently of the variations between the different JAS averages), is estimated
 176 as follows:

$$\sigma_{intraseasonal} = \sqrt{\frac{1}{3N-1} \sum_{i=1}^N (X_i - XYZ_i)^2 + (Y_i - XYZ_i)^2 + (Z_i - XYZ_i)^2}$$

177 Finally, to distinguish meaningful correlations from chance occurrences, a p-value
 178 of 0.05 (95% confidence level) is chosen, indicating a one-in-twenty probability that a cor-
 179 relation exceeds the threshold by pure coincidence. The determination of this thresh-
 180 old depends on the number of independent data points in the time series. In this study,
 181 we allocate one degree of freedom per month, having verified that the three monthly data
 182 points per year are uncorrelated in the reference time series (PC1CRU, defined in sec-
 183 tion 3). The correlation between July and August anomalies is indeed 0.16, and 0.21 be-
 184 tween August and September, both well below the significant correlation threshold of

185 0.31 with 40 degrees of freedom, ensuring the independence of the 120 monthly values.
 186 With a degree of freedom of 120, the 95% confidence level for correlation yields the thresh-
 187 old of 0.18: only linear regression values with correlations exceeding this value are de-
 188 picted in the following figures or discussed in the text as either "positive anomalies" or
 189 "negative anomalies."

190 2.3 Moisture transport and divergence

We calculate moisture transport using specific humidity (q) and horizontal winds $\mathbf{U} = (u, v)$. At each pressure level, moisture transport is computed as $q \cdot \mathbf{U}$. To integrate this calculation from p_b to p_t , we apply a weight factor to each pressure level, dP/g . This factor corresponds to the mass per unit area of the respective pressure interval (i.e., ρdz , where ρ represents the air density) using the hydrostatic approximation ($dp = -\rho g dz$):

$$\mathbf{HT} = \frac{1}{g} \int_{p_b}^{p_t} q \cdot \mathbf{U} \cdot dp \quad (3)$$

191 The result gives the integrated moisture transport between p_b and p_t in $kg \cdot m^{-1} \cdot s^{-1}$

192 The horizontal divergence of the moisture transport is calculated at each pressure
 193 level by using a centered scheme on the zonal and meridional components HT_x and HT_y
 194 as follows:

$$\nabla \cdot \mathbf{HT}(i, j) = \frac{HT_x(i+1, j) - HT_x(i-1, j)}{2 \delta x} + \frac{HT_y(i, j+1) - HT_y(i, j-1)}{2 \delta y} \quad (4)$$

195 where i and j are the indices of the gridpoints, and δx and δy are the zonal and merid-
 196 ional lengths of the gridpoints.

197 3 JAS precipitation index for Senegal

198 The highest rainfall in Senegal is observed during July, August and September (JAS),
 199 with the peak occurring in August. In the other quarters (not shown), it decreases to
 200 approximately 10-30% of this peak, consistent with prior research (Rowell et al., 1995;
 201 Sultan & Janicot, 2000; Grist & Nicholson, 2001; Lebel et al., 2003; Fall et al., 2006).
 202 JAS averages are presented for both the CRU observation-based data product (Figure
 203 1a) and ERA5 reanalyses (Figure 1b). Both datasets exhibit a clear zonal symmetry, with
 204 values increasing from north to south (Figure 1a, b), consistent with previous studies (Camberlin
 205 et al., 2001; Moron et al., 2006; Rust et al., 2013). The maximum precipitation occurs
 206 in the southern region, ranging from 8 to 12 mm/day in the southwest, while it remains
 207 below 3 mm/day in the northern part. A bias of about 1-2 mm/day is noted in ERA5
 208 reanalyses, with a maximum of 2-3 mm/day along the western coast and in the south-
 209 east (Figure 1e).

210 We first examine the interannual variability: monthly JAS anomalies were aver-
 211 aged for each year, resulting in 40 annual anomalies from 1979 to 2018, and their stan-
 212 dard deviation $\sigma_{interannual}$ (see section 2.2) plotted in Figures 1c and d. Like the aver-
 213 age, they exhibit a zonal pattern with values decreasing from south to north: regions with
 214 higher average precipitation also display larger interannual variability. The standard de-
 215 viation appears slightly smaller in ERA5 than in observations (by about 0.5 mm/day);
 216 however, the standard deviation of this bias (obtained by computing the standard de-
 217 viation of the time series differences between observations and ERA5) is comparable to
 218 or smaller than the JAS precipitation standard deviation (Figure 1f), accounting for ap-
 219 proximately only 10-25% of the mean value. Consequently, ERA5 data reasonably cap-
 220 ture the interannual variability of Senegal precipitation in JAS. Nevertheless, averaging
 221 values in JAS to a single value per year results in the loss of the intraseasonal signal con-
 222 tained within these three summer months. Since we aim to identify related signals in SST,

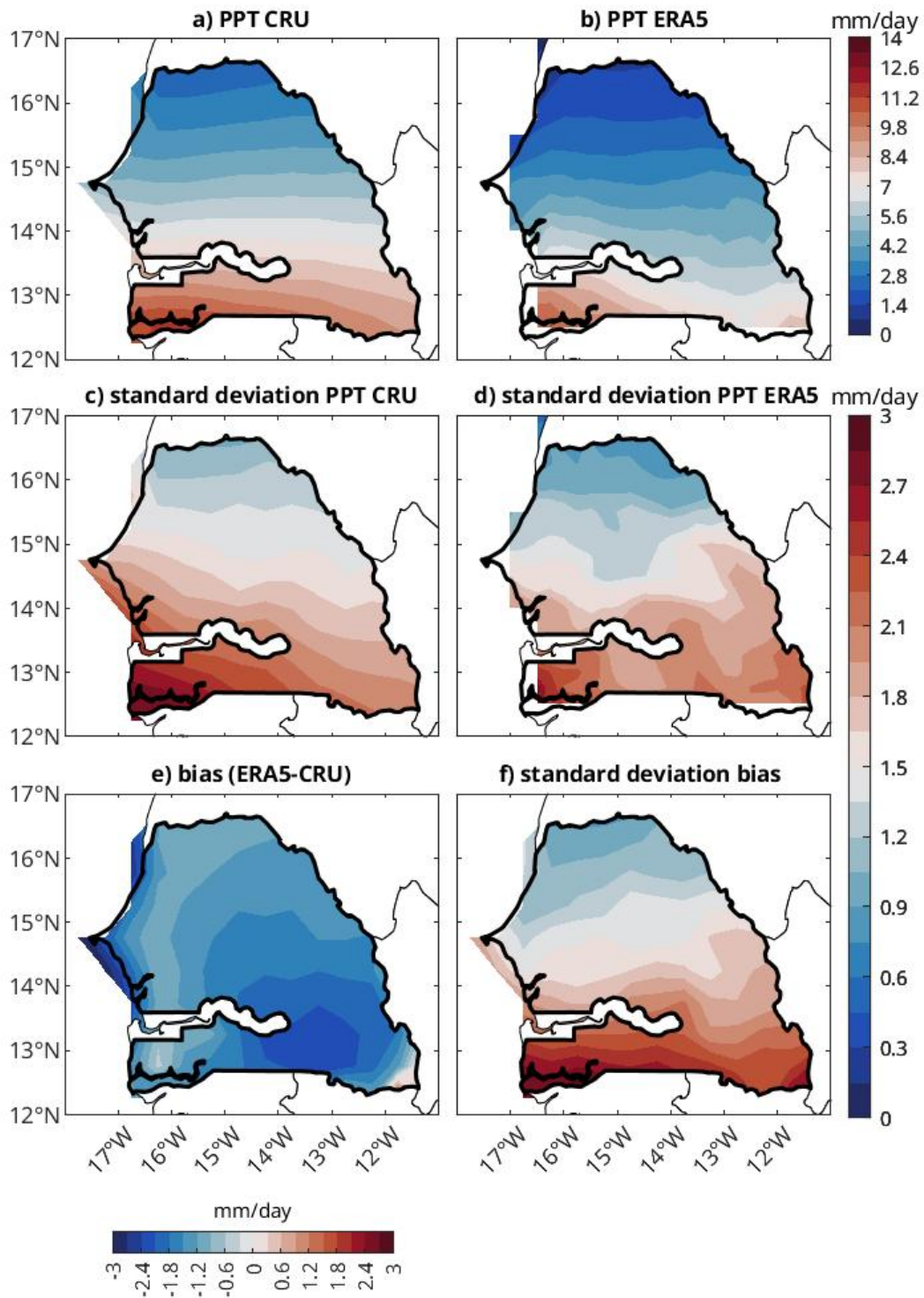


Figure 1. JAS 1979-2018 precipitation (PPT) in Senegal (mm/day): a. CRU observations, b. ERA5 reanalyses, c. standard deviation of CRU anomalies, d. standard deviation of ERA5 anomalies, e. mean bias between CRU observations and ERA5 reanalyses, f. standard deviation of the bias.

223 which has proven challenging due to the contrasting findings in previous studies, it is crucial to preserve the maximum signals. Therefore, we retain each individual July, August, and September anomaly throughout the remainder of the paper, including in the EOF decomposition.

227 The resulting first EOF of the CRU data (EOF1) accounts for 66.1% of the total variance (Figure 2a). Interestingly, the associated principal component (or PC1) time series yields a $\sigma_{intraseasonal}$ of 0.75, larger than the $\sigma_{interannual}$ of 0.66. This indicates that retaining three summer monthly values per year significantly enhances the representation of the intraseasonal (or intermonthly) variability in our analysis. The ERA5 EOF1 accounts for 48.5% of the total variance (Figure 2b). EOF1 are very similar in ERA5 and CRU: they both exhibit a monopolar structure (i.e. with values of the same sign all over Senegal) of the precipitation anomalies. With zonal symmetry, an increase in the anomaly amplitude is observed from north to south, logically reflecting the standard deviation (Figure 1c,d): it is maximum in the southwest of Senegal (in Casamance), with more than 0.1 mm/day in CRU mode, and about half of that in ERA5 mode. The time series associated with EOF1 (or PC1) for CRU and ERA5 (Figure 2c) both exhibit strong interannual and intraseasonal monthly variability in precipitation. Their correlation (0.71) is highly significant, and they also demonstrate substantial covariability within the three-month summer periods, with common extreme months (e.g., August 1984, September 1986, July 1997, July 2002, September 2010, etc.).

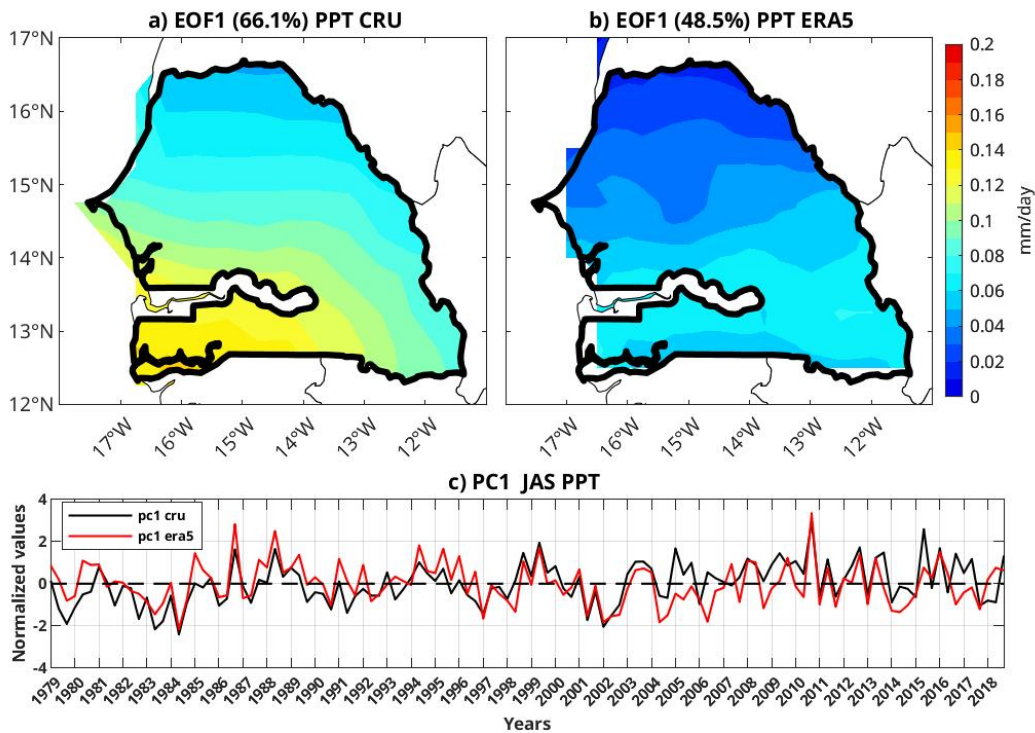


Figure 2. JAS 1979-2018, principal mode of variability (EOF1) for precipitation (PPT) anomalies (mm/day): a. CRU observations, b. ERA5 reanalyses and c. corresponding time series (black contours for CRU, red contours for ERA5).

243 The JAS mean and EOF1 precipitation for the entire Sahel region in both CRU
 244 and ERA5 datasets are not reproduced here but only in the annex (additional Figures
 245 A2 and A3), as they align with the findings of numerous previous studies, such as Quagraine
 246 et al. (2020). They exhibit similar zonal patterns, particularly covering the Senegal re-

gion, with maximum anomalies located in the west in both datasets. Although the Sahel’s first mode explains approximately 33% of the variance in ERA5 and slightly over 40% in CRU observations (see Table A1), both Senegal’s and Sahel’s modes show a high degree of correlation in both datasets, indicating shared interannual / summer monthly intraseasonal variance of more than 50% in CRU and ERA5 (see Figure A3c).

In summary, we observe that ERA5 reanalyses effectively capture months of extreme precipitation in JAS, both at regional and local scales. These findings align with the conclusions of Quagraine et al. (2020). They are also in agreement with the work of Fall et al. (2006) and Wade et al. (2015), who identified a moderate but significant correlation between seasonal rainfall in Senegal and the rest of West Africa. While precipitation patterns are generally consistent across much of the Sahel, they exhibit slight variations in the western region near the Atlantic (primarily Senegal) compared to the continental sector (Nicholson & Palao, 1993). However, when performing an EOF decomposition over the entire West Africa region - not just the Sahel - Fall et al. (2006) found that Senegal’s precipitation is more correlated with the second mode of variability of precipitation across West Africa than with the first mode, but this could only highlight the strong dependence of interannual variability modes on the selected region for analysis. Focusing on Senegal’s modes, the second mode in the CRU data accounts for approximately 10% of the total variance (see additional Figure A1 and Table A1), whereas the first mode explains two-thirds of the variance: consequently, in the subsequent analysis, we use CRU’s PC1 for JAS as a summer monthly interannual / intraseasonal index of JAS precipitation in Senegal. This index is hereafter referred to as PC1CRU. Lastly, while ERA5 precipitation does not perfectly match CRU observations, they do share a significant portion of their variance, indicating that the atmospheric dynamics in ERA5 are relevant for identifying the mechanisms leading to increased precipitation in Senegal.

4 Global SST anomalies

This section explores linear regressions of global SST anomalies on a reference index. First, we use the index characterizing precipitation variability across the entire Sahel in observations (plotted in additional Figure A3c, black). Following that, we compare these findings with the results obtained using the precipitation index specific to Senegal (PC1CRU). We present SST anomalies during the three summer months (JAS) and also the preceding months: the term ‘lag -1’ refers to the correlation between PC1CRU in JAS and SST anomalies with a 1-month lag (i.e., in JJA); ‘lag -2’ indicates a 2-month lag (MJJ), and so forth.

A wetter-than-average summer in Sahel is clearly associated with a La Niña-like signal in the eastern equatorial Pacific (red box, 170-80°W, 5°S-5°N), characterized by negative SST anomalies, reaching more than -0.4°C at lag -5 (Figure 3). This signal reflects an anticorrelation between SST anomalies in the eastern equatorial Pacific and PC1CRU Sahel. It begins to show significance in spring (lag -5, or FMA), but the maximum anticorrelation is observed at lag -3 (in AMJ): SST in this region between April and June would have a significant impact on Sahel’s summer rainfall, as discussed in numerous previous studies (Folland et al., 1986; Janicot et al., 2001; Giannini et al., 2003; Joly & Voldoire, 2009; Rodríguez-Fonseca et al., 2011; Diatta & Fink, 2014; Gomara et al., 2017; Diakhaté et al., 2020): during an El Niño event (warm waters in the equatorial Pacific), warm Pacific waters trigger a Kelvin atmospheric wave associated with increased subsidence and reduced precipitation in West Africa (Semazzi et al., 1988; Moron & Ward, 1998; Rowell, 2001; Mohino et al., 2011). Joly and Voldoire (2009) suggested that the inverse mechanism is involved during a La Niña event, leading to increased monsoon rainfall in West Africa.

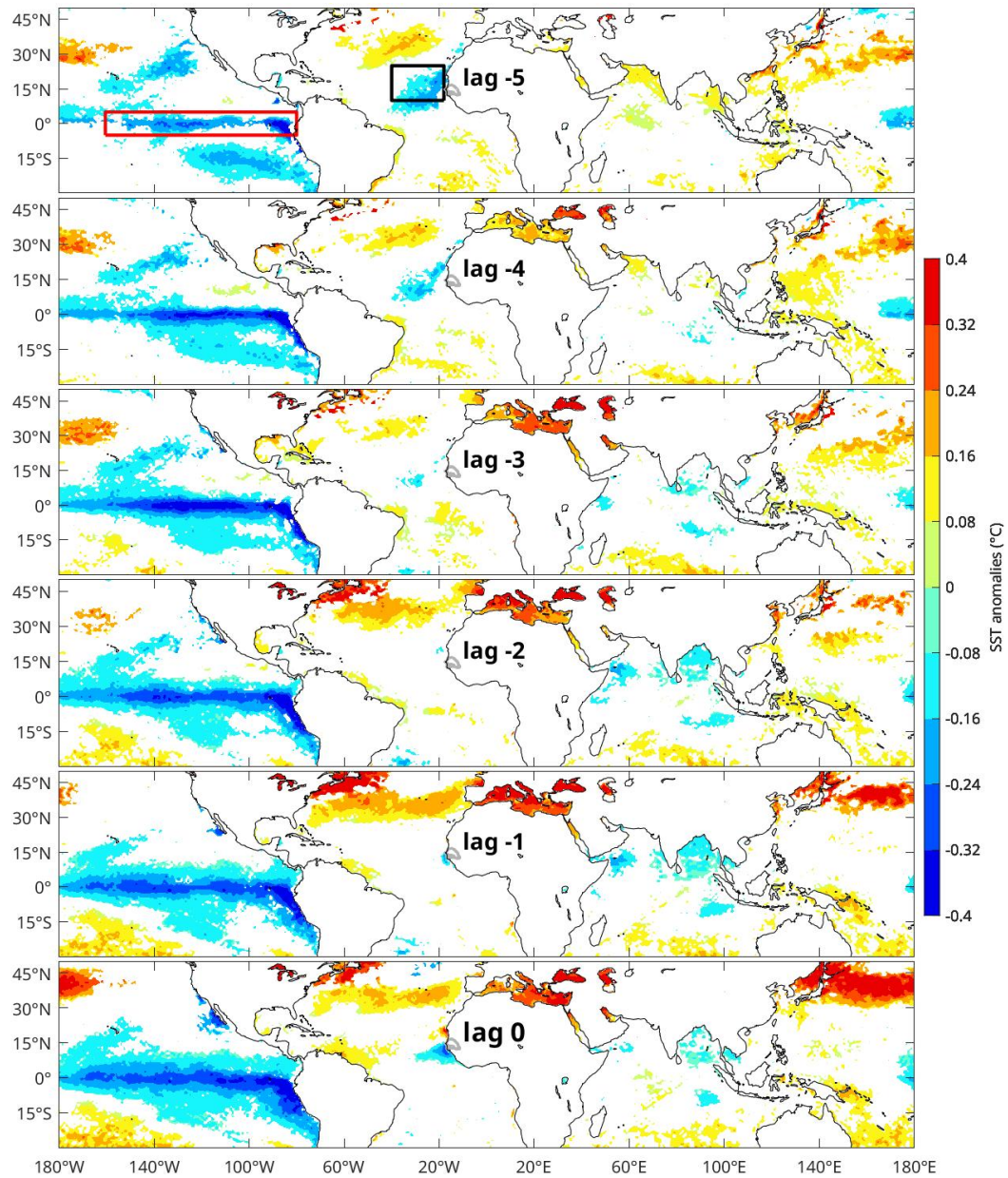


Figure 3. Linear regression of SST anomalies on PC1CRU Sahel ($^{\circ}\text{C}$) from lags -5 to 0 (indicating that SST precedes PC1CRU Sahel by 5 to 0 months). Only values significant at the 95% confidence level are plotted. The red box outlines the eastern equatorial Pacific (180°W - 80°W , 5°S - 5°N). The black box frames the Northeastern Tropical Atlantic (40°W - 17°W , 10°N - 25°N).

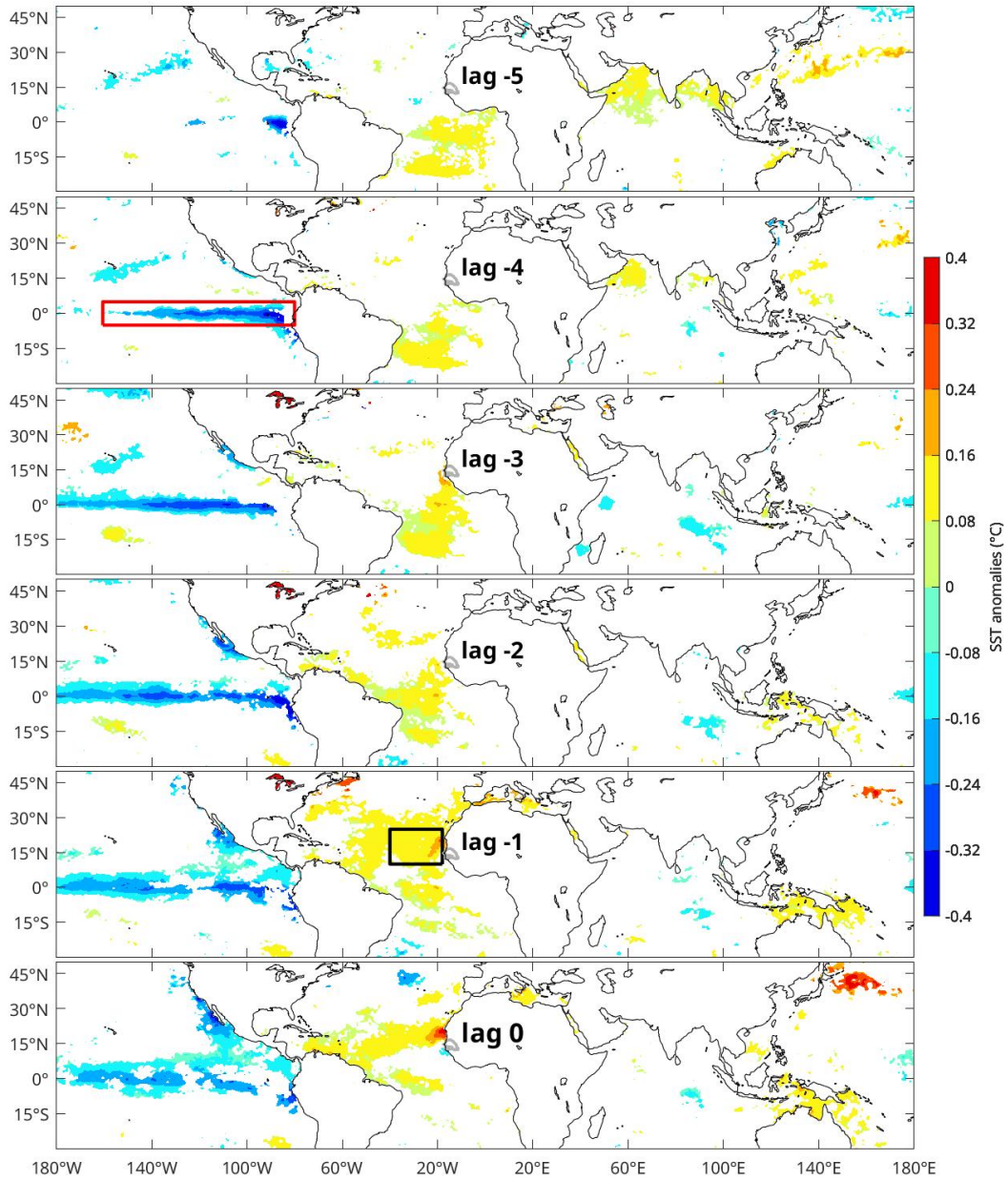


Figure 4. Identical to Figure 3 but for PC1CRU Senegal.

297 Strong significant positive SST anomalies in the Mediterranean precede a wetter-
 298 than-average summer in Sahel in the preceding months (Figure 3). This finding aligns
 299 with previous studies suggesting that increased SST leads to more rainfall through the
 300 supply of moisture over the Sahel, impacting Sahel precipitation (Rowell, 2003; Polo et
 301 al., 2008; Fontaine et al., 2009; Diakhate et al., 2019; Worou et al., 2020; Polo et al., 2008;
 302 Gaetani et al., 2010; Mohino et al., 2011; Gomara et al., 2017; Diakhate et al., 2019; Worou
 303 et al., 2020). Notably, Jung et al. (2006) identified a significant increase in Sahel rain-
 304 fall following the 2003 Mediterranean heat episode. Very strong correlations are also found
 305 in the northern Atlantic, with anomalies exceeding 0.4° in the Gulf Stream region north
 306 of 30°N (Wang et al., 2012; Y. Liu et al., 2014; Monerie et al., 2020) or in the northwest-
 307 ern Pacific: Northern Hemisphere extratropical warming indeed induces a significant in-
 308 crease in Sahel rainfall through the modification of the large-scale meridional heat dis-
 309 tribution, according to Park et al. (2015) or Suárez-Moreno et al. (2018).

310 Other significant signals are found in the Indian Ocean between lags -3 and -1, also
 311 highlighted in previous studies for the post-1970 period (Mohino et al., 2011; Fontaine
 312 et al., 2011). Although these signals appear relatively weak, they could nonetheless im-
 313 pact precipitation in the Sahel, as suggested in several studies (Bader & Latif, 2003; Bi-
 314 asutti et al., 2008; Mohino et al., 2011; Caminade & Terray, 2010). Hardly significant
 315 but large warm anomalies are found in the western tropical Pacific in the preceding months,
 316 likely as a continuation of the La Niña signal (Figure 3). However, no particular signal
 317 is found in the equatorial and subtropical South Atlantic. A signal corresponding to the
 318 'Atlantic Niño' in the eastern equatorial Atlantic is observed, as in Dommenget and Latif
 319 (2000), but approximately one year before the start of the rainy season, at lags -10 and
 320 -9 (not shown).

321 In the linear regression on PC1CRU Senegal, the vast majority of the signals iden-
 322 tified with PC1CRU Sahel are once again present but with weaker correlations and much
 323 less significant amplitudes (Figure 4). For example, the 'La Niña' signal in the eastern
 324 equatorial Pacific reaches up hardly -0.3°C at lag -3. The warm signal in the Mediter-
 325 ranean Sea is also significantly weaker and not observed until lag -1. On the other hand,
 326 a warm signal is found at lag -5 (FMA) in the equatorial Atlantic, disappearing by lag
 327 -1 (in JJA), and a warm anomaly appears around $15\text{-}20^\circ\text{S}$ from lag -5 with a peak at lag
 328 -4: Camberlin and Diop (1999) and Fall et al. (2006) have also found this predictive power
 329 of the South Subtropical Atlantic on Senegal precipitation with approximately a 5-month
 330 lead time. Moreover, significant differences are observed in the NETA (black box, 40°-
 331 20°W , $5^\circ\text{-}25^\circ\text{N}$), off the coast of Senegal and Mauritania: a positive anomaly of 0.2 to
 332 0.3°C is observed in phase with and one month before heavy rainfall in Senegal (lags 0
 333 and -1), where a negative anomaly was found instead in the regression on the Sahel in-
 334 dex (Figure 3).

335 These results indicate that despite the high correlation observed between the two
 336 principal modes of precipitation, one obtained over the entire Sahel and the other specifi-
 337 cally over Senegal, the latter appears to be less affected by remote SST anomalies com-
 338 monly discussed in the literature. Instead, it is more influenced by regional SST in the
 339 NETA region as well as the South Tropical Atlantic. The latter aspect is beyond the scope
 340 of the present study. However, in the following sections, we examine in more detail the
 341 oceanic and atmospheric signals linked to Senegal's precipitation in the NETA region.

342 5 Anomalies of SST and near-surface atmospheric circulation in the 343 Northeastern Tropical Atlantic

344 The JAS averages of SLP, SST, and surface winds from ERA5 reanalyses for the
 345 period 1979-2018 are shown in Figure 5. Over the continent, the primary characteris-
 346 tic of SLP is the "Heat Low" (Lavaysse et al., 2009), with values below 1010 hPa between
 347 15°N and 30°N (Figure 5a, black contours). Further west and slightly northward over the

348 ocean, there is a maximum SLP in the Azores region, around 35°N. The significant pres-
 349 sure gradient between these two regions results in very strong northeasterlies over the
 350 ocean along the coast, and northerlies over the Western Sahara and southern Morocco
 351 (Figure 5b). In response, the signature of a coastal upwelling can be observed north of
 352 20°N off Cap Blanc (the border between Mauritania and Western Sahara), with SST val-
 353 ues decreasing to as low as 20-22°C (Figure 5a). Furthermore, north of 15°N, SST is warmer
 354 in the west than in the east: this is likely explained by the fact that, on a seasonal scale,
 355 SST is primarily balanced between solar heating on one hand and cooling through la-
 356 tent heat fluxes on the other hand (Foltz & McPhaden, 2006), with surface winds be-
 357 ing stronger in the east compared to the west.

358 South / southeast trade winds are found south of 5°N (Figure 5b). East of 10-15°W,
 359 they turn north/northeastward while bringing moisture to West Africa ("monsoon flow").
 360 Further west, over the ocean, they converge with the northeast trade winds between 5°N
 361 and 15°N, defining the Intertropical Convergence Zone (ITCZ) where SST is maximum.
 362 The convergence of surface winds and maximum SST are indeed closely linked in the trop-
 363 ics (Fontaine & Janicot, 1996; Xie & Carton, 2004). For instance, Diakhaté et al. (2018)
 364 suggested that SST gradients significantly influence pressure gradients along the edges
 365 of the ITCZ in the Atlantic Ocean. Following the mechanism of Lindzen and Nigam (1987),
 366 a SST gradient tends to induce an opposite gradient in SLP just above through turbu-
 367 lent heat fluxes and hydrostatic adjustment. Consequently, surface winds tend to con-
 368 verge toward the center of a warm tropical SST region, favoring weak surface winds and
 369 deep atmospheric convection in the core of the ITCZ. However, east of 30°W, these winds
 370 turn eastward under the influence of the Heat Low and its extension over the ocean, form-
 371 ing the WAWJ (highlighted in red frame), which blows from the Atlantic towards the
 372 continent around 10°N (Grotsky, 2003; Pu & Cook, 2010). This low-level jet, observed
 373 below 800 hPa (Bonner, 1968; Stensrud, 1996), is known to be a significant source of mois-
 374 ture for the West African Monsoon in boreal summer (Cadet & Nnoli, 1987; Grams et
 375 al., 2010; Thorncroft et al., 2011; Pu & Cook, 2012; Lélé et al., 2015; W. Liu et al., 2020).
 376 The moisture transport into West Africa, and consequently precipitation, is thus poten-
 377 tially influenced by NETA SST through its impact on the WAWJ.

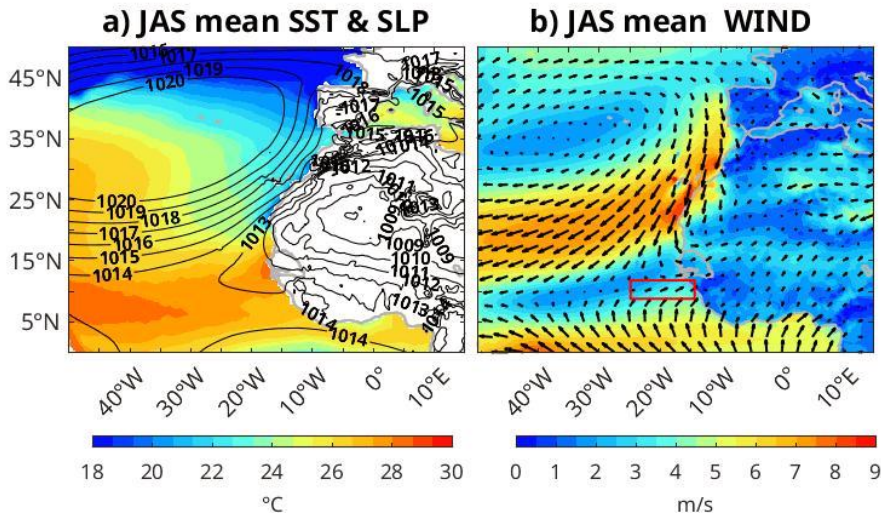


Figure 5. JAS 1979-2018 ERA5 reanalyses: a. SST (colors) and SLP (black contours). b. 10m-wind speed (colors) and direction (arrows). The red frame indicates the location of the WAWJ (25°W-14°W, 9°N-12°N).

378 Figure 6 presents the linear regression of SST, SLP and 10-meter wind on PC1CRU,
 379 with lags ranging from -2 (meaning the parameters precede PC1CRU by two months)
 380 to 0. Two months prior to a wet summer in Senegal, a significant negative SLP anomaly
 381 (exceeding -0.4 hPa) begins to emerge in the North Atlantic, reflecting a weakening of
 382 the Azores high (Figure 6, left, lag -2). This results in a weakening of the trade winds
 383 by approximately -0.3 m/s off Mauritania and Western Sahara (Figure 6, right), reduc-
 384 ing the intensity of coastal upwelling and latent heat fluxes, thereby creating a warm SST
 385 anomaly off Senegal and Cap Blanc (Figure 6, left, lags -1). At lag -1, the subtropical
 386 SLP anomaly strengthens and extends over the continent to the eastern border of Mau-
 387 ritania (around 5°W) between 20°N and 30°N, with a significant weakening of the north-
 388 easterlies to -0.3 to -0.4 m/s off Senegal and Cap Blanc (between 10°N and 25°N). In re-
 389 sponse, the warm SST anomaly off Cap Blanc reaches +0.4°C at lag 0 and extends hor-
 390 izontally southwestward between 10°N and 15°N at 50°W. This small yet significant warm-
 391 ing, owing to its extended coverage, could contribute to the formation of a negative pres-
 392 sure anomaly (exceeding -0.4 hPa) between 15°N and 25°N at lag 0 over the ocean (Fig-
 393 ure 6, left, lag 0). This negative SLP anomaly indicates the northward shift of low-pressure
 394 systems within the marine ITCZ. The most significant anomalies it generates are pri-
 395 marily located in the southern half of the anomaly, between 10°N and 20°N. In this re-
 396 gion, it decelerates surface winds in the north and intensifies them in the south (com-
 397 pare Figure 6, right, lag 0, and Figure 5b). Westerly anomalies are subsequently observed
 398 between 7°N and 12°N off the coast, signifying a strengthening of the WAWJ. Finally,
 399 over the continent, a positive pressure signal is observed around 20°N to 30°N, associ-
 400 ated with a less intense Heat Low than average. Although this signal is visible only at
 401 the 1000 hPa pressure level over the continent (not shown), its extension over the ocean
 402 is evident in the SLP anomaly near the coast around 25°N (Western Sahara).

403 A similar linear regression was conducted using the PC1CRU index calculated for
 404 the entire Sahel (not shown): no significant differences in surface wind or SLP were iden-
 405 tified, which is expected given the strong correlation between the two indices. However,
 406 disparities in NETA SST anomalies, as discussed in the previous section, still exist: Sen-
 407 egal JAS precipitation, although sharing the majority of its interannual / summer monthly
 408 intraseasonal variance with the entire Sahel, appears to be influenced by a different SST
 409 anomaly: it supports the hypothesis that a regional feedback involving NETA SST, SLP
 410 and surface winds could be at work.

411 6 Moisture transport

412 The JAS average of the low-level moisture transport (integrated between 1000 hPa
 413 and 850 hPa) is plotted in Figure 7a. Over the ocean, it closely resembles the surface
 414 wind pattern (Figure 5b): moisture transport carried along by the trade winds, controlled
 415 by the Azores and Saint Helena anticyclones, converge between 8°N and 15°N. East of
 416 30°W, at approximately 10°N, there is a notable inland-directed moisture transport, likely
 417 carried by the WAWJ, in agreement with Pu and Cook (2010, 2011), and Lélé et al. (2015).

418 The divergence of the moisture transport exhibits a zonal band of significant con-
 419 vergence along the ITCZ between 5°N and 13°N, slightly south of the wind maximum
 420 convergence (Figure 7c). This convergence aligns perfectly with the zonal band of av-
 421 erage JAS precipitation (Figure 7e). The most significant precipitation is located along
 422 the coast (Figure 7c), induced by the strong coastal convergence of moisture transport
 423 driven by the WAWJ around 10°N and further south by the southern monsoon flux (Fig-
 424 ure 7a). Indeed, given that the lower atmospheric layer is consistently close to moisture
 425 saturation in oceanic areas, near-surface convergence and precipitation are co-located
 426 most of the time (Weller et al., 2017).

427 Over the continent, there is a noticeable contrast in moisture transport patterns.
 428 To the south of 18°N, the moisture transport is south / southwestern and relatively in-

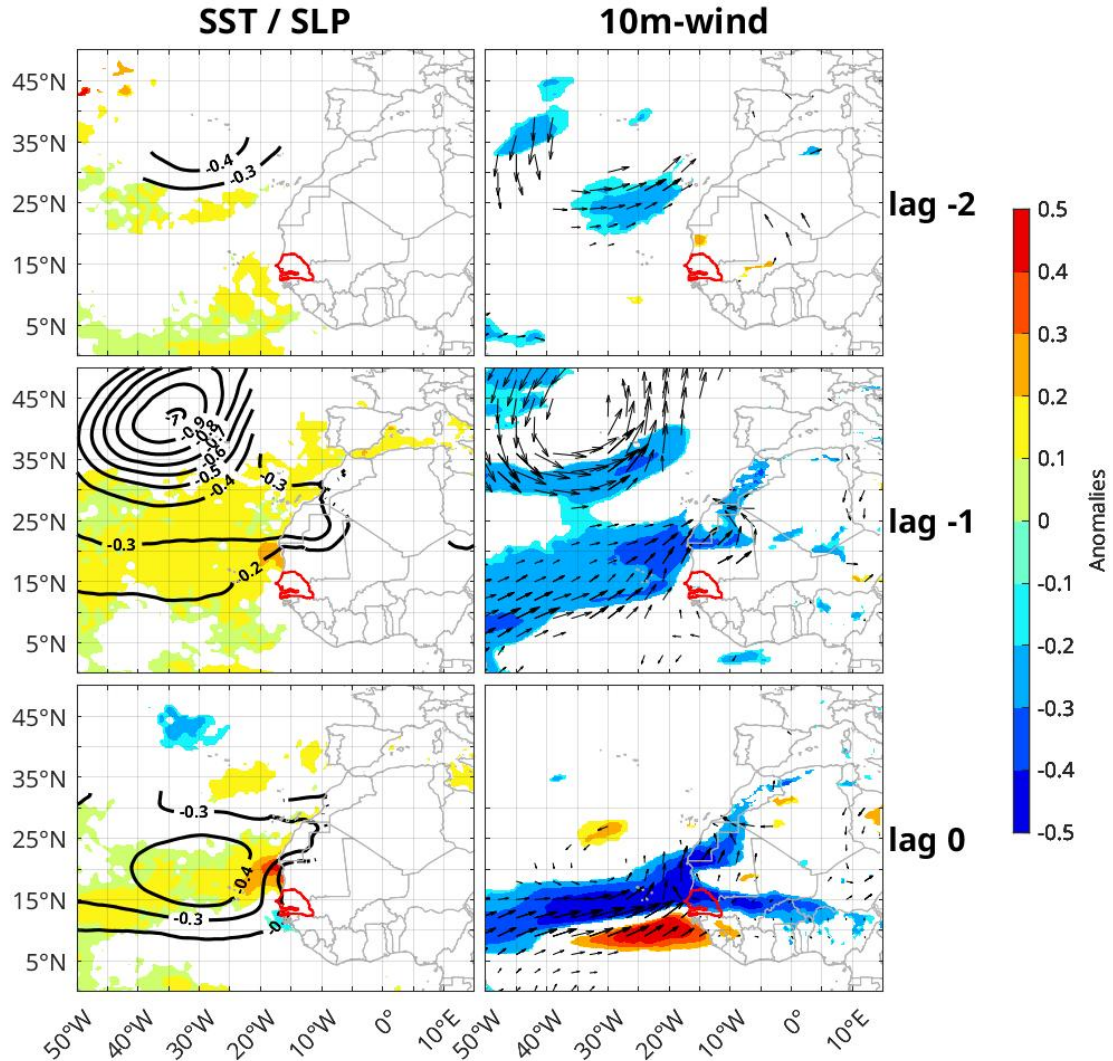


Figure 6. Linear regression of ERA5 reanalyses on PC1CRU, from lags -2 (ERA5 leads PC1CRU by 2 months) to lag 0. Left: SST (colors, °C) and SLP (black contours, hPa). Right: 10m-wind speed (colors, m/s) and direction (arrow). Only values significant at the 95% level are plotted.

429 tense. It strongly weakens north of 18°N and reaches a minimum in the core of the Heat
 430 Low (Figure 7a). This naturally leads to a notable convergence of moisture transport
 431 around 18°N, roughly corresponding to the "Intertropical Front", or "Intertropical Dis-
 432 continuity" (ITD). However, unlike over the ocean, this pronounced near-surface con-
 433 vergence does not coincide with a precipitation peak: the latter is observed further south
 434 between 5°N and 15°N (Figure 7e). Indeed, precipitation is primarily associated with the
 435 formation of MCSs south of the AEJ, as mentioned in the introduction, and is more in-
 436 fluenced by moisture transport convergence in the mid-to-high troposphere rather than
 437 in the lower troposphere.

438 A last notable feature of the mean moisture transport over the continent is a distinct
 439 weakening of the westerly flow around 10°N-10°W, where the largest mountain in
 440 Sierra Leone, the Loma Mansa, rises to almost 2000m in height (Figure 7a). More gen-
 441 erally, the high relief near the coast contributes to the amplification of precipitation on
 442 the windward side of these mountains (Figure 7e), in agreement with Kante et al. (2020).

443 The linear regressions of low-level moisture transport, its divergence, and precip-
 444 itation in JAS are presented in Figure 7 (right). Over the ocean, a wetter than usual sum-
 445 mer in Senegal is associated with a cyclonic moisture transport anomaly that clearly cor-
 446 responds to the negative SLP anomaly found previously between 10°N and 30°N (Fig-
 447 ure 7b). The induced strengthening of the WAWJ in the southern edge of this anomaly
 448 results in an increase in eastward moisture transport between approximately 6°N and
 449 12°N, while a decrease in westward transport is observed between 12°N and 16°N (Fig-
 450 ure 7b). This leads to a significant increase in the coastal convergence of moisture trans-
 451 port between 6°N and 12°N (Figure 7d), and consequently, higher oceanic and coastal
 452 precipitation, with a maximum anomaly reaching up to 2 mm/day over the ocean be-
 453 tween 8°N and 15°N (Figure 7f).

454 On the continent, there is a narrow zonal band of reduced moisture transport be-
 455 tween 12°N and 15°N (Figure 7b), bordered by opposite positive anomalies further south
 456 and in the region of the Heat Low further north. Consequently, there is a zonal band of
 457 negative divergence anomaly to the south (around 10°N) and positive to the north (around
 458 15°N) of this zonal band. The Heat Low anomaly probably explains most of the weak
 459 but highly correlated negative precipitation anomalies detected between 18°N and 25°N,
 460 as well as part of the positive precipitation anomalies between 10°N and 18°N (Figure
 461 7f, black contours). The increase in Sahel precipitation is indeed mostly controlled by
 462 the weakening of the Heat Low in its southern half, which shifts moisture transport fur-
 463 ther north (Cook, 1999). However, the convergence anomalies (Figure 7d) may also con-
 464 tribute to the increase in precipitation between 10°N and 18°N, following the inland ex-
 465 tension of the WAWJ acceleration and eastward moisture transport around 10°N.

466 These results highlight the complex nature of the atmospheric dynamics control-
 467 ling precipitation in West Africa. They lend support to investigations of the ITCZ, mois-
 468 ture transport, and precipitation, spanning the entire troposphere. Two vertical merid-
 469 ional cross-sections are conducted on either side of the coast, one over the ocean, span-
 470 ning from 22°W to 17°W, and the other to the east of Senegal, spanning from 10°W to
 471 5°W. Note that the results presented below remain consistent when the width of the sec-
 472 tions is slightly adjusted or increased by 5°. Horizontal divergence of moisture transport
 473 is calculated as in equation (4) (Figure 8, colors). Given that zonal transport (black con-
 474 tours) typically surpasses meridional transport above 850 hPa, only the former is plot-
 475 ted in the figures.

476 In the mean profile over the ocean, in the lower layer (below 850 hPa), we observe
 477 similar signals to those in Figure 7: framed by divergent moisture transports south of
 478 5°N or north of 15°N, a robust convergence coincides with the peak of eastward mois-
 479 ture transport within the WAWJ between 5°N and 13°N (Figure 8a). It also coincides
 480 with the heaviest rainfall (Figure 8a, bottom panel, gray profile). This convergence re-
 481 sults from the south and north trade winds meeting within the ITCZ, and an increase
 482 in eastward moisture transport toward the coast via the WAWJ around 10°N (Figure 8a,
 483 solid black contours). Above 850 hPa, there is an intense westward moisture transport
 484 between 750 and 550 hPa, at 12-18°N (Figure 8a, dashed black contours), indicating the
 485 presence of the AEJ. No signal is detected above 400 hPa, suggesting that moisture trans-
 486 port by the Tropical Easterly Jet, located at approximately 5°N between 100 and 200
 487 hPa, is negligible.

488 In the mean profile over the continent, above 850 hPa, a similar maximum of zonal
 489 moisture transport is found at the location of the AEJ (Figure 8c, black contours). Be-

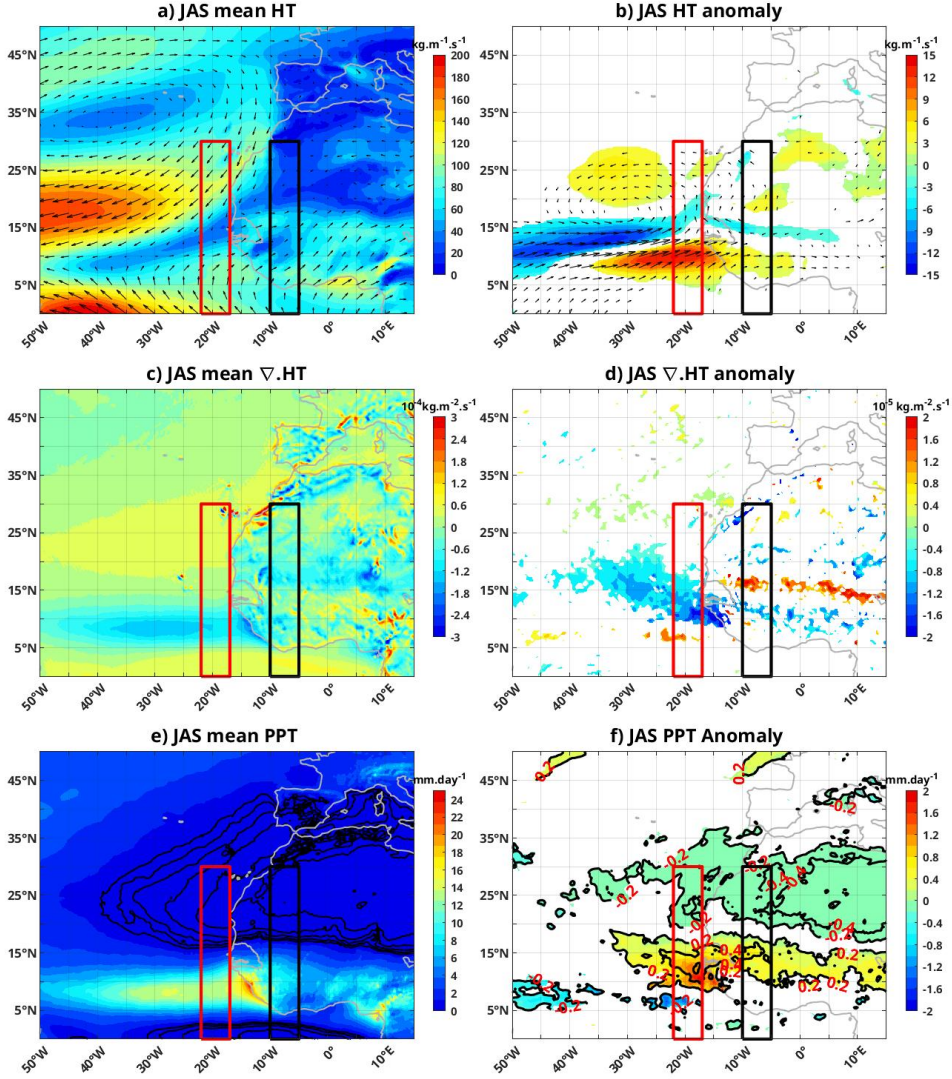


Figure 7. JAS 1978-2018 ERA5 reanalyses, average (left) and linear regression on PC1CRU index (right): a., b. magnitude (colors) and direction (arrow) of moisture transport (HT). c., d. divergence of moisture transport ($\nabla \cdot \text{HT}$). e., f. precipitation (PPT). In e., values less than 1 mm/day are outlined in black (intervals of 0.1 mm/d). In b., d. and f., only values significant at the 95% confidence level are plotted. In f., correlations are depicted using black contours with intervals of 0.2. Red and black frames indicate the location of the meridional-vertical sections plotted in Figures 8 and 9.

490 low 850 hPa, the western moisture transport extends as far north as 18°N (15°N over the
 491 ocean). A minimum in moisture transport convergence is found at 9-12°N, dividing the
 492 flow into two segments on either side of the Loma Mansa mountains as observed in Fig-
 493 ure 7a. Strong convergence takes place at the bottom of the southern branch, explain-
 494 ing the heavy precipitation south of 10°N (Figure 8c, bottom panel). A second conver-
 495 gence maximum is observed in the northern branch, in the ITD region around 18°N, but
 496 it does not correspond to strong precipitation. The latter is governed by MCSs gener-
 497 ated along the AEJ north of 17°N, as mentioned earlier, which probably explains why
 498 the precipitation peak is located around 10°N, at the latitude of the AEJ southern edge.

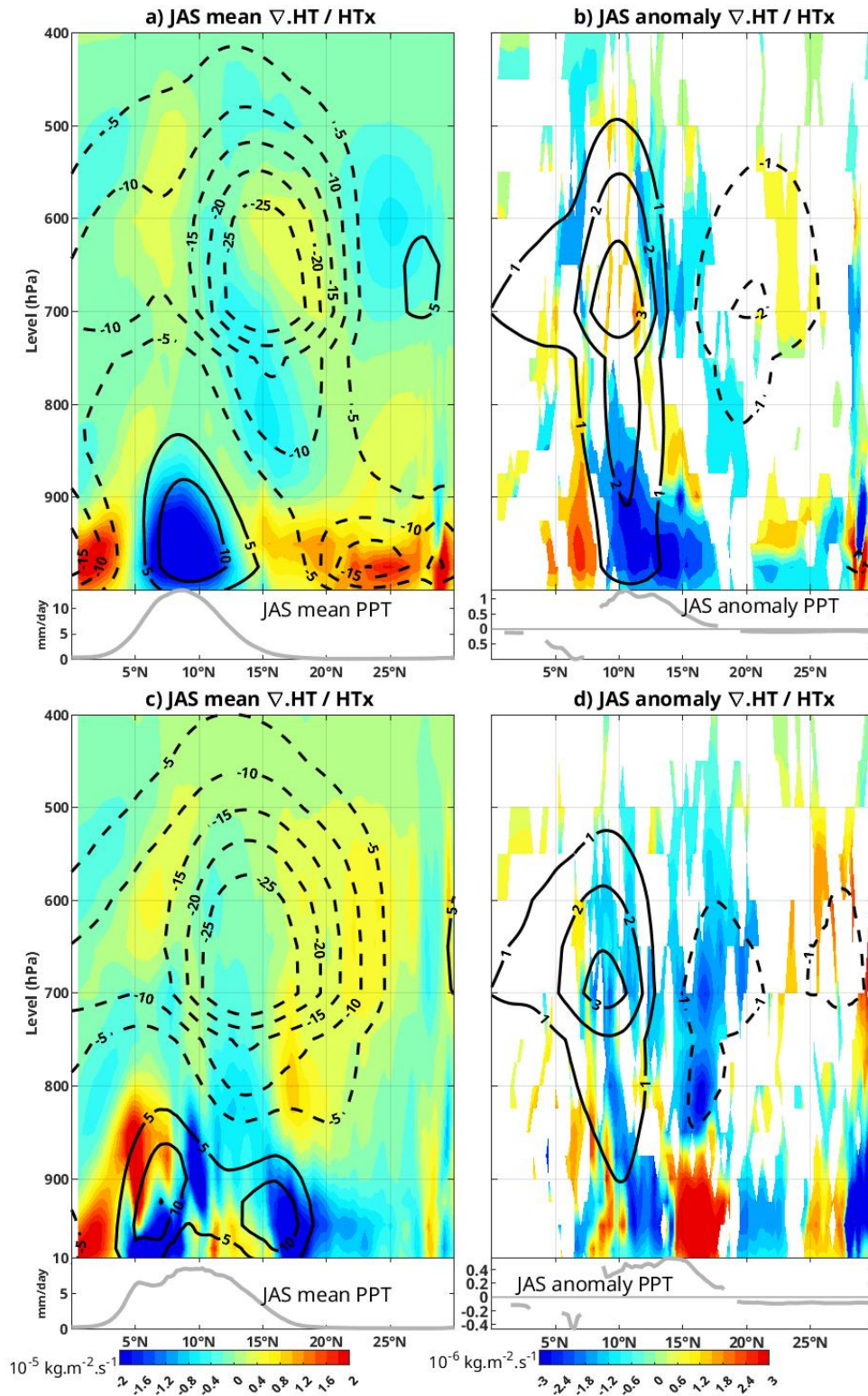


Figure 8. JAS 1978-2018 ERA5 reanalyses, average (left) and linear regressions on the PC1CRU index (right) in vertical meridional sections over the ocean (22°W-17°W, a., b.) and over the continent (10°-5°W, c., d.): Divergence of moisture transport (colors) and zonal moisture transport (black contours, solid for positive, dashed for negative), superimposed on precipitation (gray line in panels at the bottom). Only values significant at the 95% confidence level are plotted.

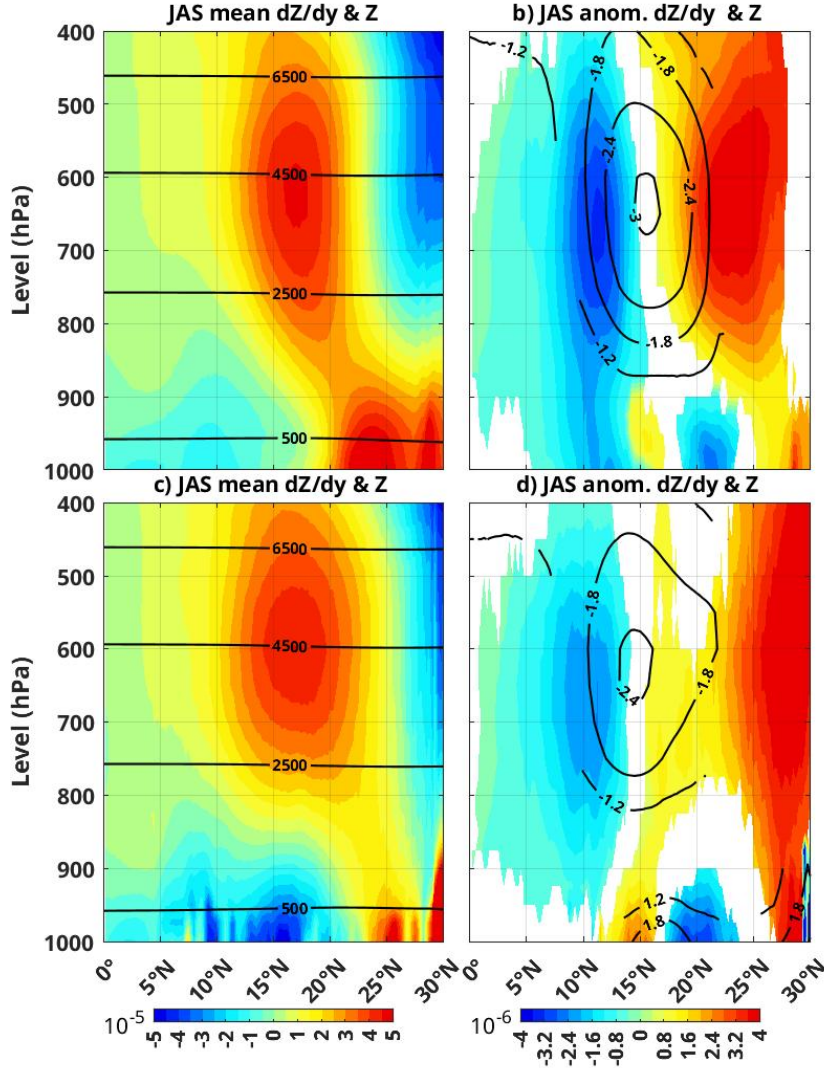


Figure 9. Same as Figure 8, but for geopotential height (black contours) and its meridional gradient (colors).

499 Over the ocean, the linear regression on PC1CRU shows an increase in low-level
 500 convergence of moisture transport between 9°N and 18°N (Figure 8b, colors), aligning
 501 with positive precipitation anomalies a few degrees north of their mean position (Fig-
 502 ure 8b, bottom panel, grey profile). The increased convergence is caused by the accel-
 503 eration of the WAWJ along its northern edge, as indicated by the positive anomaly in
 504 zonal transport between 9°N and 13°N (black contours). This anomaly extends in alti-
 505 tude up to about 500 hPa, peaking between 600 and 700 hPa: at this altitude, it indi-
 506 cates a deceleration of the AEJ on the southern edge of its mean position. At the same
 507 altitude, a negative anomaly in zonal transport is observed further north, around 20°N,
 508 indicating an acceleration of the AEJ on its northern edge: the AEJ has slightly shifted
 509 north.

510 In the linear regression over the continent, above 850 hPa, anomalies of zonal mois-
 511 ture transport resemble those over the ocean. However, the negative anomaly north of
 512 15°N is less pronounced and extends further north (Figure 8d, black contours). More-

513 over, the positive anomaly between 9°N and 12°N remains above 850 hPa without reach-
 514 ing the surface, in contrast to the situation above the ocean. Below 850 hPa, alternat-
 515 ing positive and negative divergence anomalies emerge approximately every 5°: north of
 516 15°N, they probably result from the weakening of the Heat Low in its southern half, as
 517 mentioned earlier. However, between 10°N and 15°N, the convergence anomaly rather
 518 corresponds to a continental extension of the large WAWJ acceleration found over the
 519 ocean at the same latitude: it probably contributes significantly to the heavy precipi-
 520 tation observed between 10°N and 15°N.

521 In summary, the increase in summer precipitation in Senegal is partly of continen-
 522 tal origin and controlled by the Heat Low and the AEJ. However, there are also clear
 523 signs of an influence coming from the Atlantic ocean through the WAWJ: a northward
 524 shift of the ITCZ comes with an intensification of the latter, which increases the west-
 525 ern moisture transport between 10°N and 15°N and its convergence. It results in an in-
 526 crease in precipitation at the same latitudes. The SST could play a role in this inten-
 527 sification by altering low-level meridional pressure gradients through hydrostatic adjust-
 528 ment along its southern edge, along 10-15°N: the WAWJ would then respond to the pres-
 529 sure gradient signal via geostrophic adjustment. We test the plausibility of this hypoth-
 530 esis in the next section.

531 7 Geostrophic adjustment to the NETA SST anomaly

532 In this section, the geopotential height (or Z) at different pressure levels is used to
 533 calculate a meridional gradient (dZ/dy , colors): anomalies in dZ/dy can then be assim-
 534 ilated as anomalies in meridional pressure gradient of the same sign and provide infor-
 535 mation about the geostrophic zonal wind north of 5°N (geostrophic approximation is no
 536 longer valid near the equator), through the formula: $u_g = -\frac{g}{f} \frac{\partial Z}{\partial y}$.

537 A large peak of positive dZ/dy is found at 10-20°N around 500-700 hPa over the
 538 ocean (Figure 9a), emphasizing the clear geostrophic origin of the AEJ (Cook, 1999). Neg-
 539 ative values of dZ/dy are found further north, indicating a high in the mid and upper
 540 tropospheric pressure around 20-25°N. Below 850 hPa, dZ/dy displays a negative value
 541 within the WAWJ (driving eastward geostrophic wind) south of 18°N and a positive value
 542 to the north (westward wind). The value of dZ/dy at 10°N is approximately -1 to -2×10^{-5}
 543 units, which corresponds to a geostrophic zonal wind speed of 3.8 to 7.8 m/s when mul-
 544 tiplied by $-g/f$ (with $g = 9.81 \text{ m/s}^2$, $f = 2\Omega \sin(10^\circ)$ and $\Omega = 2\pi \text{ rad / day}$), i.e.
 545 representative of the speeds typically found within the WAWJ. This is in line with Pu
 546 and Cook (2010) who show that while the jet is largely ageostrophic during its seasonal
 547 transitions, it is dominated by geostrophy on average.

548 The local negative minimum of dZ/dy around 10°N is located over an ocean region
 549 where the meridional SST gradient is positive and may reach a local maximum, as can
 550 be observed in Figure 5 (left). A positive maximum of dZ/dy is located further north
 551 around 23-25°N, over a strongly negative SST gradient in the southern front of the coastal
 552 upwelling off Cap Blanc. These alignments of dZ/dy and $dSST/dy$ extrema are in agree-
 553 ment with the theory of Lindzen and Nigam (1987) suggesting that the near-surface pres-
 554 sure gradients adjust to the SST gradients. This is also in agreement with Diakhaté et
 555 al. (2018), who suggested that the equatorial low, thus the marine ITCZ, is partially con-
 556 trolled on its edges by meridional SST gradients.

557 A similar signature of the AEJ is found in the mid-troposphere above the conti-
 558 nent, but the subtropical high is shifted north by 2 or 3 degrees (Figure 9c). Below 850
 559 hPa, negative values of dZ/dy are found to the south and positive values to the north
 560 of the Heat Low, whose center is located around 20-25°N. Large values of dZ/dy at 25°N
 561 and at 16-17°N reflect the very steep "walls" of the Heat Low, with the southernmost
 562 corresponding to the ITD.

563 Above the continent, the linear regression of Z and dZ/dy on PC1CRU shows a sig-
 564 nificant drop in pressure within the AEJ, indicating its northward shift (weakening of
 565 easterlies in the southern half of its mean position, strengthening in the north, Figure
 566 9d). The dominant signal in dZ/dy is a positive anomaly north of 15°N : as it is partic-
 567 ularly intense north of 25°N , it likely reflects the influence of the large-scale subtropi-
 568 cal atmospheric circulation and / or the Mediterranean. Extending down to the surface,
 569 this anomaly covers a positive pressure anomaly confined under 900 hPa between 15°N
 570 and 20°N , which reflects the weakening of the Heat Low in its southern half, inducing
 571 a northward shift of the pressure minimum. This is primarily what controls the north-
 572 ward shift of the MCSs path, thus partly explaining the increase in precipitation between
 573 10°N and 18°N in Senegal. However, the signal corresponding to the weakening of the
 574 AEJ on its southern edge (negative anomalies in dZ/dy around 10°N at 600-700 hPa)
 575 appears to be somewhat weaker, and does not reach the surface, suggesting it is an east-
 576 ward extension of a similar anomaly found above the ocean.

577 Above the ocean, the overall anomalies in dZ/dy are similar to those over the con-
 578 tinent, with a slight northward shift of one or two degrees (Figure 9b). Below 850 hPa,
 579 the signals north of 15°N are likely an extension over the ocean of the anomalies observed
 580 above the continent, thus controlled by the variability of the Heat Low. However, south
 581 of 15°N , the negative anomaly of dZ/dy is significant between 8°N and 14°N , whereas
 582 it is not over the continent (Figure 9d). This suggests that it is forced by the SST anomaly.
 583 With a value of approximately -2×10^{-6} units, such a dZ/dy anomaly drives a geostrophic
 584 zonal wind anomaly of about 0.7 m/s, which is of the same magnitude than the surface
 585 wind anomaly observed at the same latitudes (Figure 6, right, lag 0).

586 This highlights that the strengthening of westerlies around 10°N - 15°N , which cor-
 587 responds to an acceleration of the WAWJ on its northern side and leads to increased pre-
 588 cipitation in Senegal, is clearly a geostrophic response to near-surface pressure fluctu-
 589 ations. Since the latter is likely controlled by the SST warm anomaly between 10°N and
 590 20°N , via the mechanism theorized in Lindzen and Nigam (1987), this suggests the ex-
 591 istence of a regional feedback mechanism between SST and surface winds in the NETA.

592 8 Discussion and conclusions

593 This work documents the oceanic and atmospheric signals related to monthly pre-
 594 cipitation from July to September in Senegal, using CRU observations and ERA5 reanal-
 595 yses covering the period from 1979 to 2018 (40 years). It compares the signals related
 596 to precipitation variability in Senegal versus the entire Sahel region. Noting a significant
 597 difference in Northeast Tropical Atlantic (NETA) SST, it takes a closer look at surface
 598 signals (pressure, wind, and moisture transport) and along two vertical sections in the
 599 mid and lower troposphere. Finally, it proposes a mechanism linking NETA SST to pre-
 600 cipitation in Senegal.

601 First, monthly precipitation values in Senegal for 40 years are used. Anomalies for
 602 the months of July to September are extracted, and an EOF decomposition is performed:
 603 this yields an index, PC1CRU. This index characterizes interannual variability, but since
 604 three successive monthly values per year are retained, it also captures some intraseasonal
 605 variability in JAS. This mode is highly significant, as it explains two-thirds of the to-
 606 tal precipitation variance in Senegal, with a pattern of anomalies of the same sign across
 607 the country and a strong gradient in their amplitude, from very weak in the north to very
 608 strong in the southwest of Senegal.

609 A comparison with a similar index calculated using ERA5 reanalysis precipitation
 610 data shows good correspondence, which suggests using the SST and atmospheric param-
 611 eters from these reanalyses to explore the dynamic environment of the dominant mode,
 612 PC1CRU, in Senegal's precipitation variability. All subsequent analyses are therefore based

613 on linear regressions performed on this index. It should be noted that the results are pre-
 614 sented for a positive anomaly of PC1CRU, indicating increased precipitation, but sim-
 615 ilar discussions would apply to a negative anomaly, as the regression is linear.

616 Increased JAS precipitation in Senegal is generally preceded by cold SST anoma-
 617 lies in the eastern equatorial Pacific (La Niña event) and warm SST anomalies in the Mediter-
 618 ranean Sea. These results are in line with many previous studies, including those by Rowell
 619 (2001), Giannini et al. (2003), Mohino et al. (2011), Rodríguez-Fonseca et al. (2011), and
 620 Diakhate et al. (2019). However, we obtained much weaker correlations than in these stud-
 621 ies, especially in the East Equatorial Pacific and the Mediterranean, because we used a
 622 Senegal precipitation index instead of a Sahel one. Moreover, completely different anoma-
 623 lies are found in the NETA: this suggests that the western part of the Sahel, as Sene-
 624 gal, is more influenced by the Atlantic Ocean and less by large-scale atmospheric forc-
 625 ing and teleconnections than the entire Sahel. Therefore, the atmospheric dynamic anoma-
 626 lies in the NETA related to increased JAS precipitation in Senegal are examined.

627 The main result obtained indicates that increased JAS precipitation in Senegal is
 628 attributed to the increased convergence of low-level moisture transport, driven by an in-
 629 crease in the West African Westerly Jet (WAWJ). It also appears to be linked to the north-
 630 ward shift of the African Easterly Jet (AEJ) between 750 hPa and 550 hPa.

631 Above the continent, just east of Senegal, this northward shift of the AEJ is likely
 632 due to a northward migration of the Heat Low, in agreement with previous studies such
 633 as Diallo et al. (2013) and Sylla et al. (2013) that used regional climate models, or Grist
 634 and Nicholson (2001) and Dezfuli and Nicholson (2011) who used reanalysis data. At-
 635 mospheric teleconnections, both regional and larger scale with ENSO or Mediterranean
 636 SSTs, are also likely to play an important role. This probably leads to a northward mi-
 637 gration of the trajectories of the Mesoscale Convective Systems (MCSs) responsible for
 638 most of the summer precipitation, explaining their increase between 10°N and 15°N.

639 However, over the ocean, just west of Senegal, the same northward shift of the AEJ
 640 as over the continent is observed, but the increase in precipitation is largely explained
 641 by an increase in low-level moisture transport convergence, created by an acceleration
 642 of the WAWJ. This is controlled by a significant negative pressure anomaly located in
 643 the NETA (10°N-30°N), reflecting the northward movement of the low-pressure areas char-
 644 acterizing the marine ITCZ. This negative pressure anomaly is situated above a posi-
 645 tive SST anomaly, and the near-surface winds anomalies are compatible with a geostrophic
 646 response of the WAWJ to a reinforcement of the negative meridional pressure gradient
 647 between 10°N and 15°N. The latter could itself result from an increase in the positive SST
 648 gradient on the southern edge of the warm anomaly, following the mechanism proposed
 649 by Lindzen and Nigam (1987). The SST - surface wind feedback mechanism would then
 650 be as follows: first, the northeastern Trade Winds weaken, forcing a warming of the SST
 651 between 10°N and 25°N. Second, the SLP adjusts to the warmer SST and becomes weaker
 652 between 10°N and 25°N; its increased negative meridional gradient to the south forces
 653 a strengthening of the near-surface winds in the WAWJ region. This eventually results
 654 in an increased convergence of moisture transport and precipitation between 10°N and
 655 15°N.

656 Between these two zones (ocean and continent), Senegal likely receives the influ-
 657 ence of atmospheric teleconnections and the Mediterranean through the mode of vari-
 658 ability it shares with the Sahel, but it could also be strongly influenced by NETA SST
 659 through the previously suggested feedback mechanism. As the initial Trade Winds anomaly
 660 seems driven by an anomaly of the Azores High, hence linked to the North Atlantic Os-
 661 cillation (NAO), these results could possibly explain the link between Sahel precipita-
 662 tion and the North Atlantic, as shown for example in Paeth and Friederichs (2004). How-
 663 ever, the ocean-atmosphere feedback mechanism suggested in this study needs further
 664 exploration at shorter time scales than the monthly data presented here, as the atmo-

665 spheric response to SST fluctuations is very rapid (within hours/days). Therefore, fur-
666 ther studies using daily data or a regional atmospheric model are needed to confirm or
667 refute this potential role of NETA SST feedback on the WAWJ. This could lead to a bet-
668 ter understanding of the mechanisms driving precipitation variability in Senegal and, ul-
669 timately, to improved seasonal forecasts.

670 **9 Open Research**

671 Version 4.03 of CRU TS precipitation observation data covering the period from
672 January 1901 to December 2018 (Harris et al., 2020) is available on [https://data.ceda](https://data.ceda.ac.uk/badc/cru/data/cru_ts/cru_ts.4.03/data7)
673 [.ac.uk/badc/cru/data/cru_ts/cru_ts.4.03/data7](https://data.ceda.ac.uk/badc/cru/data/cru_ts/cru_ts.4.03/data7)

674 Monthly average ERA5 data on simple levels and pressure levels from 1940 to present
675 are also available respectively at [https://cds.climate.copernicus.eu/doi/10.24381/](https://cds.climate.copernicus.eu/doi/10.24381/cds.f17050d7)
676 [cds.f17050d7](https://cds.climate.copernicus.eu/doi/10.24381/cds.f17050d7) and at <https://cds.climate.copernicus.eu/doi/10.24381/cds.6860a573>.

677 **Acknowledgments**

678 This work was supported by the IRD (institut de Recherche pour le Développement through
679 PDI-MSD program (Programme Doctoral International- Modélisation des Systèmes Com-
680 plexes). This work was also supported by the Laboratoire Mixte International ECLAIRS2.

681 **Appendix A**

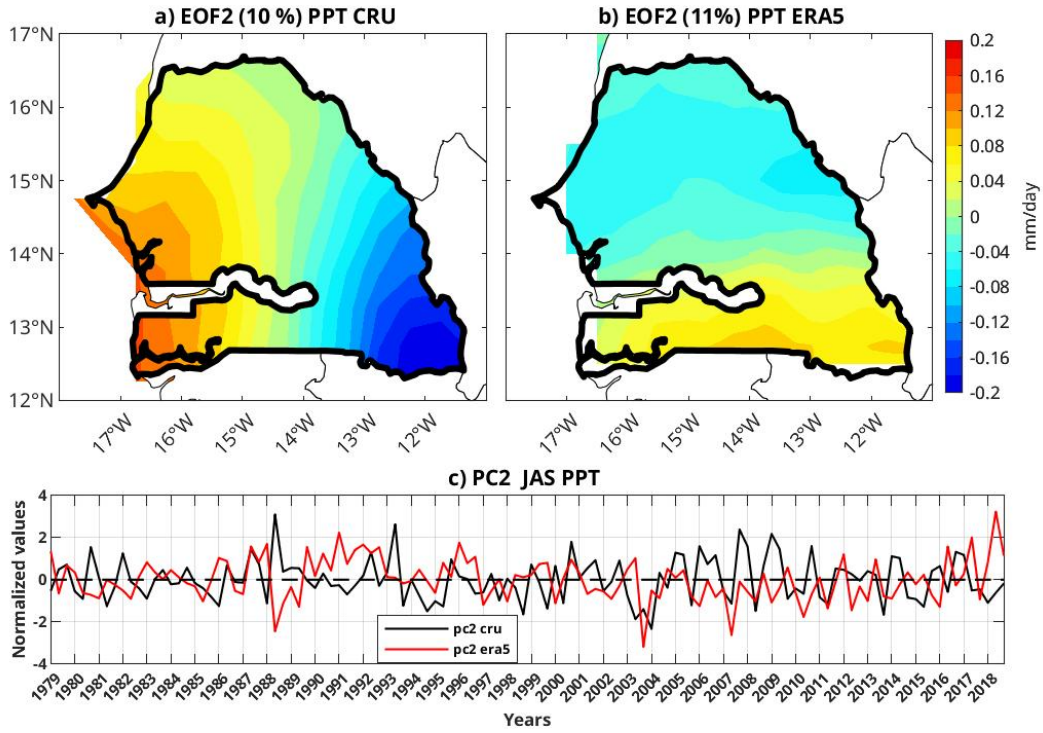


Figure A1. JAS 1979-2018 EOF2 of precipitation (mm/day): a. CRU observations, b. ERA5 reanalyses, and c. corresponding time series (black for CRU and red for ERA5).

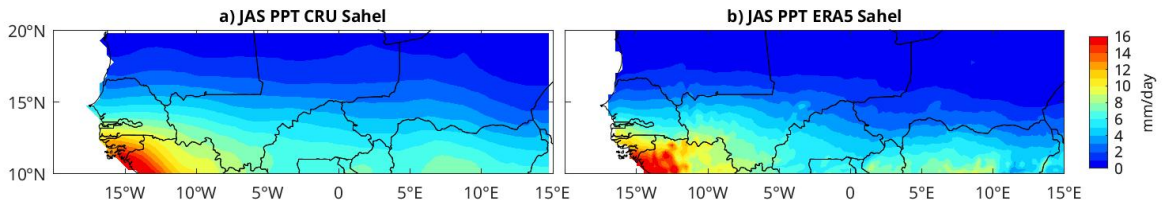


Figure A2. JAS 1978-2018 CRU (left) and ERA5 (right) precipitation.

	EOF1-Sn	EOF1-Sah	EOF2-Sn	EOF2-Sah
CRU	66.1%	41.6%	10%	9.3%
ERA5	48.5%	33%	11%	8.2%

Table A1. Percentage of total variance explained by EOF1 and EOF2 in Senegal and Sahel, using CRU or ERA5 precipitation.

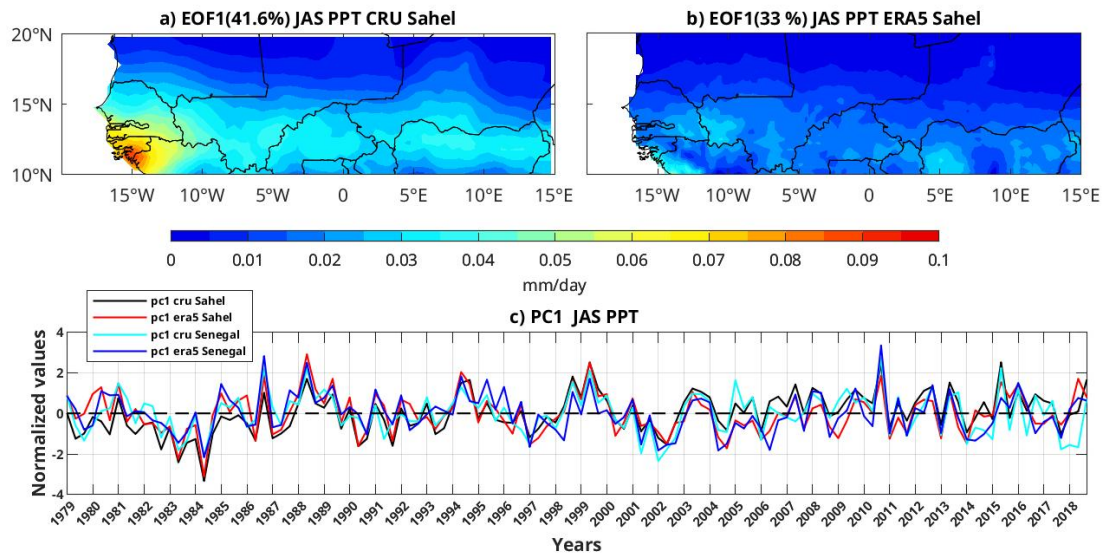


Figure A3. JAS 1979-2018 precipitation, EOF1 over the Sahel (mm/day): a. in CRU observations, b. in ERA5 reanalyses and c. their corresponding time series (CRU in black and ERA5 in red). CRU Senegal (cyan) and ERA5 Senegal (blue) time series are also plotted.

682

683

References

684

Bader, J., & Latif, M. (2003). The impact of decadal-scale indian ocean sea surface temperature anomalies on sahelian rainfall and the north atlantic oscillation. *Geophysical Research Letters*, *30*(22).

685

686

Biasutti, M., Held, I. M., Sobel, A. H., & Giannini, A. (2008). Sst forcings and sahel rainfall variability in simulations of the twentieth and twenty-first centuries. *Journal of Climate*, *21*(14), 3471–3486. doi: 10.1175/2007JCLI1896.1

687

688

Bonner, W. D. (1968). Climatology of the low level jet. *Monthly Weather Review*, *96*(12), 833–850. doi: 10.1175/1520-0493(1968)096<0833:COTLLJ>2.0.CO;2

689

690

Cabos, W., de la Vara, A., & Koseki, S. (2019). Tropical atlantic variability: Observations and modeling. *Atmosphere*, *10*(9). Retrieved from <https://www.mdpi.com/2073-4433/10/9/502>

691

692

Cadet, D. L., & Nnoli, N. O. (1987). Water vapour transport over africa and the atlantic ocean during summer 1979. *Quarterly Journal of the Royal Meteorological Society*, *113*(476), 581–602. doi: 10.1002/qj.49711347609

693

694

Camberlin, P., & Diop, M. (1999). Inter-relationships between groundnut yield in senegal, interannual rainfall variability and sea-surface temperatures. *Theoretical and Applied Climatology*, *63*(3), 163–181. doi: 10.1007/s007040050101

695

696

Camberlin, P., Janicot, S., & Poccarr, I. (2001). Seasonality and atmospheric dynamics of the teleconnection between african rainfall and tropical sea-surface temperature: Atlantic vs. enso. *International Journal of Climatology*, *21*(8), 973–1005. doi: 10.1002/joc.673

697

698

Caminade, C., & Terray, L. (2010). Twentieth century sahel rainfall variability as simulated by the arpege agcm, and future changes. *Climate Dynamics*, *35*(1432-0894).

699

700

Caniaux, G., Giordani, H., Redelsperger, J.-L., Guichard, F., Key, E., & Wade, M. (2011). Coupling between the atlantic cold tongue and the west african monsoon in boreal spring and summer. *Journal of Geophysical Research: Oceans*, *116*(C4).

701

702

Cook, K. H. (1999). Generation of the african easterly jet and its role in determining west african precipitation. *Journal of Climate*, *12*(5), 1165 - 1184.

703

704

de Coëtlogon, G., Janicot, S., & Lazar, A. (2010). Intraseasonal variability of the ocean—atmosphere coupling in the gulf of guinea during boreal spring and summer. *Quarterly Journal of the Royal Meteorological Society*, *136*, 426–441. doi: 10.1002/qj.554

705

706

de Coëtlogon, G., Leduc-Leballeur, M., Meynadier, R., Bastin, S., Diakhaté, M., Eymard, L., . . . Lazar, A. (2014). Atmospheric response to sea-surface temperature in the eastern equatorial atlantic at quasi-biweekly time-scales. *Quarterly Journal of the Royal Meteorological Society*, *140*(682). doi: 10.1002/qj.2250

707

708

Dezfuli, A. K., & Nicholson, S. E. (2011). A note on long-term variations of the african easterly jet. *International Journal of Climatology*, *31*(13), 2049–2054. doi: 10.1002/joc.2209

709

710

Diakhate, M., Rodriguez-Fonseca, B., Gomara, I., Mohino, E., Dieng, A. L., & Gaye, A. T. (2019). Oceanic forcing on interannual variability of sahel heavy and moderate daily rainfall. *Journal of Hydrometeorology*, *20*(3). doi: 10.1175/JHM-D-18-0035.1

711

712

Diakhaté, M., Lazar, A., de Coëtlogon, G., & Gaye, A. T. (2018). Do sst gradients drive the monthly climatological surface wind convergence over the tropical atlantic? *International Journal of Climatology*, *38*, e955–e965. doi: 10.1002/joc.5422

713

714

Diakhaté, M., Suárez-Moreno, R., Gómara, I., & Mohino, E. (2020). Statistical-observational analysis of skillful oceanic predictors of heavy daily precipitation events in the sahel. *Atmosphere*, *11*(6), 584. doi: 10.3390/atmos11060584

715

716

Diallo, I., Sylla, M. B., Camara, M., & Gaye, A. T. (2013). Interannual variability of rainfall over the sahel based on multiple regional climate models simulations.

717

- 738 *Theoretical and Applied Climatology*, 113(1). doi: 10.1007/s00704-012-0791-y
- 739 Diatta, S., & Fink, A. H. (2014). Statistical relationship between remote climate indices
740 and west african monsoon variability. *International Journal of Climatology*, 34(12), 3348–3367. doi: 10.1002/joc.3912
- 741
- 742 Dommenges, D., & Latif, M. (2000). Interannual to decadal variability in the tropical
743 atlantic. *Journal of Climate*, 13(4), 777–792. doi: 10.1175/1520-0442(2000)
744 013<0777:ITDVIT>2.0.CO;2
- 745 Fall, S., Semazzi, F. H. M., Dutta, D., Niyogi, S., Anyah, R. O., & Bowden, J.
746 (2006). The spatiotemporal climate variability over senegal and its relationship
747 to global climate. *International Journal of Climatology*, 26(14), 2057–2076.
748 doi: 10.1002/joc.1355
- 749 Folland, C., Palmer, T., & Parker, D. (1986). Sahel rainfall and worldwide sea tem-
750 peratures, 1901–85. *Nature*, 320(6063), 602–607. doi: 10.1038/320602a0
- 751 Foltz, G. R., & McPhaden, M. J. (2006). The role of oceanic heat advection in
752 the evolution of tropical north and south atlantic sst anomalies. *Journal of Cli-
753 mate*, 19(19), 6122–6138. doi: 10.1175/JCLI3961.1
- 754 Fontaine, B., Gaetani, M., Ullmann, A., & Roucou, P. (2011). Time evolution of
755 observed july-september sea surface temperature-sahel climate teleconnection
756 with removed quasi-global effect (1900–2008). *Journal of Geophysical Research-
757 Atmospheres*, 116, D04105. doi: 10.1029/2010JD014843
- 758 Fontaine, B., Garcia-Serrano, J., Roucou, P., Rodriguez-Fonseca, B., Losada, T.,
759 Chauvin, F., ... Janicot, S. (2009). Impacts of warm and cold situations in
760 the mediterranean basins on the west african monsoon: observed connection
761 patterns (1979–2006) and climate simulations. *Climate Dynamics*, 35(1),
762 95–114. doi: 10.1007/s00382-009-0599-3
- 763 Fontaine, B., & Janicot, S. (1996). Sea surface temperature fields associated with
764 west african rainfall anomaly types. *Journal of Climate*, 9(11), 2935–2940. doi:
765 10.1175/1520-0442(1996)009<2935:SSTFAW>2.0.CO;2
- 766 Gaetani, M., Fontaine, B., Roucou, P., & Baldi, M. (2010). Influence of the mediter-
767 ranean sea on the west african monsoon: Intraseasonal variability in numer-
768 ical simulations. *Journal of Geophysical Research: Atmospheres*, 115. doi:
769 10.1029/2010JD014436
- 770 Giannini, A., Saravanan, R., & Chang, P. (2003). Oceanic forcing of sahel rainfall on
771 interannual to interdecadal time scales. *Science*, 302(5647), 1027–1030. doi: 10
772 .1126/science.1089357
- 773 Gomara, I., Mohino, E., Losada, T., Dominguez, M., Suarez-Moreno, R., &
774 Rodriguez-Fonseca, B. (2017). Impact of dynamical regionalization on pre-
775 cipitation biases and teleconnections over west africa. *Climate Dynamics*,
776 50(11), 4481–4506. doi: 10.1007/s00382-017-3886-4
- 777 Grace, K., & Davenport, F. (2021). Correction to: Climate variability and health
778 in extremely vulnerable communities: investigating variations in surface wa-
779 ter conditions and food security in the west african sahel. *Population and
780 Environment*, 42(4), 578–578. doi: 10.1007/s11111-021-00381-x
- 781 Grams, C. M., Jones, S. C., Marsham, J. H., Parker, D. J., Haywood, J. M., &
782 Heuveline, V. (2010). The atlantic inflow to the saharan heat low: observations
783 and modelling. *Quarterly Journal of the Royal Meteorological Society*, 136,
784 125–140. doi: 10.1002/qj.429
- 785 Grist, J. P., & Nicholson, S. E. (2001). A study of the dynamic factors influenc-
786 ing the rainfall variability in the west african sahel. *Journal of Climate*, 14(7),
787 1337–1359. doi: 10.1175/1520-0442(2001)014<1337:ASOTDF>2.0.CO;2
- 788 Grodsky, S. A. (2003). Near surface westerly wind jet in the atlantic itcz. *Geophys-
789 ical Research Letters*, 30(19), 2009. doi: 10.1029/2003GL017867
- 790 Gu, G. (2010). *Summer-time rainfall variability in the tropical atlantic*
791 (S. W. Simard & M. E. Austin, Eds.). Intech Europe.
- 792 Gu, G., & Adler, R. F. (2009). Interannual variability of boreal summer rainfall in

- 793 the equatorial atlantic. *International Journal of Climatology*, 29(2), 175–184.
794 doi: 10.1002/joc.1724
- 795 Hagos, S. M., & Cook, K. H. (2008). Ocean warming and late-twentieth-century
796 sahel drought and recovery. *Journal of Climate*, 21(15), 3797–3814. doi: 10
797 .1175/2008JCLI2055.1
- 798 Harris, I., Osborn, T. J., Jones, P., & Lister, D. (2020). Version 4 of the cru ts
799 monthly high-resolution gridded multivariate climate dataset. *Scientific Data*,
800 7(1), 109. doi: 10.1038/s41597-020-0453-3
- 801 Janicot, S., Harzallah, A., Fontaine, B., & Moron, V. (1998). West african monsoon
802 dynamics and eastern equatorial atlantic and pacific sst anomalies (1970–88).
803 *Journal of Climate*, 11(8), 1874–1882. doi: 10.1175/1520-0442-11.8.1874
- 804 Janicot, S., Trzaska, S., & Pocard, I. (2001). Summer sahel-enso teleconnection and
805 decadal time scale sst variations. *Climate Dynamics*, 18(3), 303–320. doi: 10
806 .1007/s003820100172
- 807 Joly, M., & Voldoire, A. (2009). Influence of enso on the west african monsoon:
808 Temporal aspects and atmospheric processes. *Journal of Climate*, 22(12),
809 3193–3210. doi: 10.1175/2008JCLI2450.1
- 810 Jung, T., Ferranti, L., & Tompkins, A. M. (2006). Response to the summer of
811 2003 mediterranean sst anomalies over europe and africa. *Journal of Climate*,
812 19(20), 5439–5454. doi: 10.1175/JCLI3916.1
- 813 Kante, I. K., Sall, S. M., Badiane, D., Diouf, I., Dieng, A. L., Diaby, I., & Guichard,
814 F. (2020). Analysis of rainfall dynamics in conakry, republic of guinea. *Atmo-
815 spheric and Climate Sciences*, 10(1), 1. doi: 10.4236/acs.2020.101001
- 816 Lavaysse, C., Flamant, C., Janicot, S., Parker, D. J., Lafore, J.-P., Sultan, B.,
817 & Pelon, J. (2009). Seasonal evolution of the west african heat low:
818 a climatological perspective. *Climate Dynamics*, 33(2), 313–330. doi:
819 10.1007/s00382-009-0553-4
- 820 Le Barbé, L., & Lebel, T. (1997). Rainfall climatology of the hapex-sahel region dur-
821 ing the years 1950–1990. *Journal of hydrology*, 188, 43–73.
- 822 Lebel, T., Diedhiou, A., & Laurent, H. (2003). Seasonal cycle and interannual vari-
823 ability of the sahelian rainfall at hydrological scales. *Journal of Geophysical
824 Research: Atmospheres*, 108. doi: 10.1029/2001JD001580
- 825 Lindzen, R. S., & Nigam, S. (1987). On the role of sea surface temperature gradients
826 in forcing low-level winds and convergence in the tropics. *Journal of the Atmo-
827 spheric Sciences*, 44(17), 2418–2436. doi: 10.1175/1520-0469(1987)044<2418:
828 OTROSS>2.0.CO;2
- 829 Liu, W., Cook, K. H., & Vizzy, E. K. (2020). Role of the west african westerly jet in
830 the seasonal and diurnal cycles of precipitation over west africa. *Climate Dy-
831 namics*, 54(1), 843–861. doi: 10.1007/s00382-019-05035-1
- 832 Liu, Y., Chiang, J. C. H., Chou, C., & Patricola, C. M. (2014). Atmospheric tele-
833 connection mechanisms of extratropical north atlantic sst influence on sahel
834 rainfall. *Climate Dynamics*, 43, 2797 - 2811.
- 835 Losada, T., Rodríguez-Fonseca, B., Polo, I., Janicot, S., Gervois, S., Chauvin,
836 F., & Ruti, P. (2010). Tropical response to the atlantic equatorial mode:
837 Agcm multimodel approach. *Climate Dynamics*, 35(1), 45–52. doi:
838 10.1007/s00382-009-0624-6
- 839 Lélé, M. I., Leslie, L. M., & Lamb, P. J. (2015). Analysis of low-level atmospheric
840 moisture transport associated with the west african monsoon. *Journal of Cli-
841 mate*, 28(11), 4414–4430. doi: 10.1175/JCLI-D-14-00746.1
- 842 Meynadier, R., de Coëtlogon, G., Leduc-Leballeur, M., Eymard, L., & Janicot, S.
843 (2016). Seasonal influence of the sea surface temperature on the low atmo-
844 spheric circulation and precipitation in the eastern equatorial atlantic. *Climate
845 Dynamics*, 47(1432-0894).
- 846 Mo, K., Bell, G. D., & Thiaw, W. M. (2001). Impact of sea surface temper-
847 ature anomalies on the atlantic tropical storm activity and west african

- 848 rainfall. *Journal of the Atmospheric Sciences*, 58(22), 3477–3496. doi:
849 10.1175/1520-0469(2001)058<3477:IOSSTA>2.0.CO;2
- 850 Mohino, E., Rodríguez-Fonseca, B., Mechoso, C. R., Gervois, S., Ruti, P., & Chau-
851 vin, F. (2011). Impacts of the tropical pacific/indian oceans on the seasonal
852 cycle of the west african monsoon. *Journal of Climate*, 24(15), 3878–3891. doi:
853 10.1175/2011JCLI3988.1
- 854 Monerie, P.-A., Sanchez-Gomez, E., Gaetani, M., Mohino, E., & Dong, B. (2020).
855 Future evolution of the sahel precipitation zonal contrast in cesm1. *Climate*
856 *Dynamics*, 55, 2801–2821.
- 857 Moron, V., Robertson, A. W., & Ward, M. N. (2006). Seasonal predictability and
858 spatial coherence of rainfall characteristics in the tropical setting of senegal.
859 *Monthly Weather Review*, 134(11), 3248–3262. doi: 10.1175/MWR3252.1
- 860 Moron, V., & Ward, M. N. (1998). Enso teleconnections with climate variability
861 in the european and african sectors. *Weather*, 53(9), 287–295. doi: 10.1002/j
862 .1477-8696.1998.tb06403.x
- 863 Nicholson, S. E. (2013). The west african sahel: A review of recent studies on the
864 rainfall regime and its interannual variability. *International Scholarly Research*
865 *Notices*, 2013.
- 866 Nicholson, S. E., & Palao, I. (1993). A reevaluation of rainfall variability in the sahel
867 .1. characteristics of rainfall fluctuations. *International Journal of Climatology*,
868 13(4), 371–389. doi: 10.1002/joc.3370130403
- 869 Paeth, H., & Friederichs, P. (2004). Seasonality and time scales in the relationship
870 between global sst and african rainfall. *Climate Dynamics*, 23(7), 815–837.
871 doi: 10.1007/s00382-004-0466-1
- 872 Park, J.-Y., Bader, J., & Matei, D. (2015). Northern-hemispheric differential
873 warming is the key to understanding the discrepancies in the projected sahel
874 rainfall. *Nature Communications*, 6. doi: 10.1038/ncomms6985
- 875 Parker, D., & Diop-Kane, M. (2017). *Meteorology of tropical west africa: The fore-*
876 *casters' handbook*. John Wiley & Sons, Ltd.
- 877 Polo, I., Rodriguez-Fonseca, B., Losada, T., & Garcia-Serrano, J. (2008). Trop-
878 ical atlantic variability modes (1979–2002). part i: Time-evolving sst modes
879 related to west african rainfall. *Journal of Climate*, 21(24), 6457–6475. doi:
880 10.1175/2008JCLI2607.1
- 881 Pu, B., & Cook, K. H. (2010). Dynamics of the west african westerly jet. *Journal of*
882 *Climate*, 23(23), 6263–6276. doi: 10.1175/2010JCLI3648.1
- 883 Pu, B., & Cook, K. H. (2011). Role of the west african westerly jet in sahel rain-
884 fall variations. *Journal of Climate*, 25(8), 2880–2896. doi: 10.1175/JCLI-D-11
885 -00394.1
- 886 Pu, B., & Cook, K. H. (2012). Role of the west african westerly jet in sahel rain-
887 fall variations. *Journal of Climate*, 25(8), 2880–2896. doi: 10.1175/JCLI-D-11
888 -00394.1
- 889 Quagraine, K. A., Nkrumah, F., Klein, C., Klutse, N. A. B., & Quagraine, K. T.
890 (2020). West african summer monsoon precipitation variability as represented
891 by reanalysis datasets. *Climate*, 8(10), 111. doi: 10.3390/cli8100111
- 892 Rodríguez-Fonseca, B., Janicot, S., Mohino, E., Losada, T., Bader, J., Caminade,
893 C., . . . Voltaire, A. (2011). Interannual and decadal sst-forced responses of
894 the west african monsoon. *Atmospheric Science Letters*, 12(1), 67–74. doi:
895 10.1002/asl.308
- 896 Rowell, D. P. (2001). Teleconnections between the tropical pacific and the sahel.
897 *Quarterly Journal of the Royal Meteorological Society*, 127(575), 1683–1706.
898 doi: 10.1002/qj.49712757512
- 899 Rowell, D. P. (2003). The impact of mediterranean ssts on the sahelian rainfall
900 season. *Journal of Climate*, 16(5), 849–862. doi: 10.1175/1520-0442(2003)
901 016<0849:TIOMSO>2.0.CO;2
- 902 Rowell, D. P., Folland, C., Maskell, K., & Ward, M. (1995). Variability of summer

- 903 rainfall over tropical north-africa (1906-92) - observations and modeling. *Quar-*
 904 *terly Journal of the Royal Meteorological Society*, 121(523), 669–704. doi: 10
 905 .1002/qj.49712152311
- 906 Rust, H. W., Vrac, M., Sultan, B., & Lengaigne, M. (2013). Mapping weather-
 907 type influence on senegal precipitation based on a spatial-temporal sta-
 908 tistical model. *Journal of Climate*, 26(20), 8189–8209. doi: 10.1175/
 909 JCLI-D-12-00302.1
- 910 Semazzi, F., Mehta, V., & Sud, Y. (1988). An investigation of the relationship be-
 911 tween sub-saharan rainfall and global sea surface temperatures. *Atmosphere-*
 912 *Ocean*, 26(1), 118–138. doi: 10.1080/07055900.1988.9649293
- 913 Steinig, S., Harlass, J., Park, W., & Latif, M. (2018). Sahel rainfall strength and
 914 onset improvements due to more realistic atlantic cold tongue development in
 915 a climate model. *Scientific Reports*, 8(2569).
- 916 Stensrud, D. J. (1996). Importance of low-level jets to climate: A review. *Journal*
 917 *of Climate*, 9(8), 1698–1711. doi: 10.1175/1520-0442(1996)009<1698:IOLLJT>2
 918 .0.CO;2
- 919 Sultan, B., & Janicot, S. (2000). Abrupt shift of the itcz over west africa and intra-
 920 seasonal variability. *Geophysical Research Letters*, 27(20), 3353–3356. doi: 10
 921 .1029/1999GL011285
- 922 Sultan, B., Labadi, K., Guégan, J.-F., & Janicot, S. (2005). Climate drives the
 923 meningitis epidemics onset in west africa. *PLOS Medicine*, 2(1), e6. doi: 10
 924 .1371/journal.pmed.0020006
- 925 Suárez-Moreno, R., Rodríguez-Fonseca, B., Barroso, J. , & Fink, A. (2018). Inter-
 926 decadal changes in the leading ocean forcing of sahelian rainfall interannual
 927 variability: Atmospheric dynamics and role of multidecadal sst background.
 928 *Journal of Climate*. doi: 10.1175/JCLI-D-17-0367.1
- 929 Sylla, M. B., Giorgi, F., Coppola, E., & Mariotti, L. (2013). Uncertainties in daily
 930 rainfall over africa: assessment of gridded observation products and evaluation
 931 of a regional climate model simulation. *International Journal of Climatology*,
 932 33(7), 1805–1817. doi: 10.1002/joc.3551
- 933 Thorncroft, C. D., Nguyen, H., Zhang, C., & Peyrillé, P. (2011). Annual cycle of
 934 the west african monsoon: regional circulations and associated water vapour
 935 transport: Annual cycle of west african monsoon. *Quarterly Journal of the*
 936 *Royal Meteorological Society*, 137(654), 129–147. doi: 10.1002/qj.728
- 937 Vizy, E. K., & Cook, K. H. (2001). Mechanisms by which gulf of guinea and eastern
 938 north atlantic sea surface temperature anomalies can influence african rainfall.
 939 *Journal of Climate*, 14(5), 795–821. doi: 10.1175/1520-0442(2001)014<0795:
 940 MBWGOG>2.0.CO;2
- 941 Von Storch, H., & Zwiers, F. W. (1999). *Statistical analysis in climate research*.
 942 Cambridge University Press. doi: 10.1017/CBO9780511612336
- 943 Wade, M., Mignot, J., Lazar, A., Gaye, A. T., & Carre, M. (2015). On the spatial
 944 coherence of rainfall over the saloum delta (senegal) from seasonal to decadal
 945 time scales. *Frontiers in Earth Science*, 3. doi: 10.3389/feart.2015.00030
- 946 Wang, C. (2019). Three-ocean interactions and climate variability: a review and per-
 947 spective. *Climate Dynamics*, 53, 5119-5136.
- 948 Wang, C., Dong, S., Evan, A. T., Foltz, G. R., & Lee, S.-K. (2012). Multidecadal
 949 covariability of north atlantic sea surface temperature, african dust, sahel
 950 rainfall, and atlantic hurricanes. *Journal of Climate*, 25(15), 5404 - 5415.
- 951 Ward, M. N. (1998). Diagnosis and short-lead time prediction of summer rainfall
 952 in tropical north africa at interannual and multidecadal timescales. *Journal of*
 953 *Climate*, 11(12), 3167–3191. doi: 10.1175/1520-0442(1998)011<3167:DASLTP>2
 954 .0.CO;2
- 955 Weller, E., Shelton, K., Reeder, M. J., & Jakob, C. (2017). Precipitation associated
 956 with convergence lines. *Journal of Climate*, 30(9), 3169 - 3183.
- 957 Worou, K., Goosse, H., Fichfet, T., Guichard, F., & Diakhate, M. (2020). In-

- 958 terannual variability of rainfall in the guinean coast region and its links with
959 sea surface temperature changes over the twentieth century for the different
960 seasons. *Climate Dynamics*, 55(3), 449–470. doi: 10.1007/s00382-020-05276-5
- 961 Xie, S.-P., & Carton, J. (2004). Tropical atlantic variability: Patterns, mechanisms,
962 and impacts. *Earth Clim*, 147. doi: 10.1029/147GM07
- 963 Yang, C., Leonelli, F. E., Marullo, S., Artale, V., Beggs, H., Nardelli, B. B., ...
964 Pisano, A. (2021). Sea surface temperature intercomparison in the framework
965 of the copernicus climate change service (c3s). *Journal of Climate*, 34(13),
966 5257–5283. doi: 10.1175/JCLI-D-20-0793.1
- 967 Zebiak, S. (1993, 08). Air–sea interaction in the equatorial atlantic region. *Jour-*
968 *nal of Climate*, 6, 1567-1586. doi: 10.1175/1520-0442(1993)006<1567:AIITEA>2
969 .O.CO;2
- 970 Zeng, N., Neelin, J. D., Lau, K.-M., & Tucker, C. J. (1999). Enhancement of in-
971 terdecadal climate variability in the sahel by vegetation interaction. *Science*,
972 286(5444), 1537-1540. Retrieved from [https://www.science.org/doi/abs/10](https://www.science.org/doi/abs/10.1126/science.286.5444.1537)
973 .1126/science.286.5444.1537 doi: 10.1126/science.286.5444.1537